

GLIDING ROBOTIC FISH: DESIGN, COLLABORATIVE ESTIMATION, AND  
APPLICATION TO UNDERWATER SENSING

By

Osama Nasr Ennasr

A DISSERTATION

Submitted to  
Michigan State University  
in partial fulfillment of the requirements  
for the degree of

Electrical Engineering – Doctor of Philosophy

2020

## **ABSTRACT**

### **GLIDING ROBOTIC FISH: DESIGN, COLLABORATIVE ESTIMATION, AND APPLICATION TO UNDERWATER SENSING**

By

Osama Nasr Ennasr

Autonomous underwater robots have received significant attention over the past two decades due to the increasing demand for environmental sustainability. Recently, gliding robotic fish has emerged as a promising mobile sensing platform in versatile aquatic environments. Such robots, inspired by underwater gliders and robotic fish, combine buoyancy-driven gliding and fin-actuated swimming to realize both energy-efficient locomotion and high maneuverability. In this dissertation, we first discuss the design improvements for the second-generation gliding robotic fish “Grace 2”. These improvements have transformed the robots to underwater sensing platforms that can be modified to fit the requirements of a specific application with relative ease.

We focus on the application of detecting and tracking live fish underwater, which is an important part of fishery research, as it helps scientists understand habitat use, migratory patterns, and spawning behavior of fishes. The gliding robotic fish has demonstrated its ability to detect special acoustic signals emulating tagged fish through a series of trials in Higgins Lake, Michigan. These tests have also validated a gliding-based strategy for navigating to a GPS waypoint, and offered insight into the limitations of the current design. Additional improvements are proposed to allow these robots to glide at larger depths and perform more interesting working patterns underwater.

Motivated by the problem of tracking real fish, we consider the case where multiple robots localize and track a moving target without the need for a centralized node. We present theoretical treatment on how a network of robots can infer the location of an emitter (or target), and then track it, through a time-difference-of-arrival (TDOA) localization scheme in a fully distributed manner. In particular, we utilize a networked extended Kalman filter to estimate the target’s location in a distributed manner, and establish that successful localization can be achieved under fixed and time-varying undirected communication topologies if every agent is part of a network with a minimum

of 4 connected, non-coplanar agents. We further propose a movement control strategy based on the norm of the estimation covariance matrices, with a tuning parameter to balance the trade-off between estimation performance and the total distance traveled by the robots.

Finally, motivated by the distributed localization problem, we investigate a more general problem of distributed estimation by a network of sensors. Specifically, we consider the class of consensus-based distributed linear filters (CBDLF) where each sensor updates its estimate in two steps: a consensus step dictated by a weighted and directed communication graph, followed by a local Luenberger filtering step. We show that the sub-optimal filtering gains that minimize an upper bound of a quadratic filtering cost are related to the convergence of a set of coupled Riccati equations. Then we show that the convergence of these coupled Riccati equations depends on the notion of squared detectability for the networked system, and proceed to provide necessary conditions that link the convergence of the coupled Riccati equations to the network topology and consensus weights of the communication graph.

Dedicated to my parents  
Nasr & Hana  
for all the effort they put in to make this happen.

## ACKNOWLEDGEMENTS

First, I would like to express my warmest gratitude to my advisor, the director of Smart Microsystems Lab at Michigan State University, Prof. Xiaobo Tan. During my junior year at Michigan State University, Prof. Tan gave me the opportunity of exploring academic research as an undergraduate research assistant, and provided me with continuous motivation and support throughout my Ph.D. journey in the field of underwater robotics. Now, upon the completion of my Ph.D. training, with the experience and knowledge I gained over the past years, I am excitedly looking forward to starting a new chapter of my research career with the Department of Defense and the Geospatial Research Lab of the Engineering Research and Development Center. I owe much of my development to Prof. Tan, and genuinely thank him for his invaluable mentoring and guidance throughout my career and personal life.

I want to thank my academic committee members, Prof. Khalil, Prof. Mukherjee, and Prof. Bopardikar at Michigan State University for their insightful comments in the area of control and robotics. I also thank our collaborators at the U.S. Geological Survey for their kindness and generosity in facilitating the experiments for this project. Specifically, I would like to thank Dr. Chris Holbrook for all his effort and insight in advancing our robots for acoustic telemetry.

In Smart Microsystems Lab, I owe many people a debt of gratitude. The research in gliding robotic fish needs diverse expertise and extensive collaboration. Specifically, I would like to give special thanks to John Thon, without whom this work would have been impossible. The countless hours we spent together improving and debugging our robots have allowed me to navigate all the personal and professional challenges that I had to deal with over the years. I would also like to thank Demetris Coleman and Ryan Johnson for their help in advancing the electrical design of our robots, as well as my fellow researchers in our lab, Mohammed Al-Rubaiai, Maria Castano, Jason Greenberg, Pratap Solanki, and Thassy Pinto for their help and support throughout my Ph.D. journey.

I would also like to thank the other students in Smart Microsystems Lab and the faculty, students

and post-docs in my department, whose comments and discussions have helped my research. Thanks also to all of the administrators and staff members in the ECE department who have helped me over the years.

I also want to acknowledge the support from the funding agencies that made this work possible: the National Science Foundation (IIS 1319602, CCF 1331852, ECCS 1446793, IIS 1715714, IIS 1848945), the Great Lakes Fishery Commission (2014\_Tan\_44058), the United States Geological Survey Innovation Center for Earth Sciences, and the Department of Defense Science Mathematics and Research for Transformation Scholarship.

Most of all, I want to thank my mother, Hana Khreishi, my father, Nasr Ennasr, and my siblings, Haitham, Nadia, and Areej, for their unconditional love in both good times and bad times. I could not have finished my Ph.D. program without their understanding, support, and encouragement.

## TABLE OF CONTENTS

<b>LIST OF TABLES . . . . .</b>	<b>ix</b>
<b>LIST OF FIGURES . . . . .</b>	<b>x</b>
<b>CHAPTER 1 INTRODUCTION . . . . .</b>	<b>1</b>
1.1 Acoustic Telemetry in Aquatic Environments . . . . .	1
1.2 Beyond Presence-Absence Information . . . . .	4
1.3 Overview of Contributions . . . . .	6
1.3.1 Improvements to Gliding Robotic Fish . . . . .	6
1.3.2 Application to Acoustic Telemetry . . . . .	7
1.3.3 Distributed Localization and Tracking of a Moving Target . . . . .	7
1.3.4 Distributed Estimation of Linear Time-Invariant Systems . . . . .	8
1.4 Dissertation Organization . . . . .	9
<b>CHAPTER 2 DESIGN IMPROVEMENTS FOR GLIDING ROBOTIC FISH . . . . .</b>	<b>11</b>
2.1 Overview of Gliding Robotic Fish . . . . .	12
2.2 Design Improvements . . . . .	14
2.2.1 Mechanical Improvements . . . . .	14
2.2.2 Electrical and System Improvements . . . . .	16
2.3 Motion and Navigation . . . . .	18
2.3.1 Swimming-based Navigation . . . . .	20
2.3.2 Gliding-based Navigation . . . . .	21
2.4 Summary & Future Work . . . . .	23
<b>CHAPTER 3 CHARACTERIZATION OF ACOUSTIC DETECTION USING A GLIDING ROBOTIC FISH AS A MOBILE RECEIVER PLATFORM . . . . .</b>	<b>26</b>
3.1 Methods . . . . .	27
3.1.1 Mobile Receiver . . . . .	27
3.1.2 Field Tests . . . . .	29
3.1.3 Mobile Detection Range Tests . . . . .	30
3.1.4 Data Analysis . . . . .	33
3.2 Results . . . . .	38
3.3 Discussion . . . . .	39
3.4 Summary and Future Work . . . . .	45
<b>CHAPTER 4 TIME-DIFFERENCE-OF-ARRIVAL (TDOA)-BASED DISTRIBUTED TARGET LOCALIZATION BY A ROBOTIC NETWORK . . . . .</b>	<b>46</b>
4.1 Problem Setup . . . . .	48
4.2 Distributed Estimation . . . . .	50
4.2.1 Decentralized Estimation . . . . .	50
4.2.2 Distributed Estimation . . . . .	55
4.3 Target Tracking with Coordinated Robotic Network Movement . . . . .	60

4.3.1	Optimal Formation . . . . .	60
4.4	Simulation Results . . . . .	63
4.5	Summary and Future Work . . . . .	70
<b>CHAPTER 5 NECESSARY CONDITIONS FOR THE CONVERGENCE OF THE DISTRIBUTED KALMAN FILTER AND ITS COUPLED RICCATI EQUATIONS . . . . .</b>		<b>72</b>
5.1	Problem Setup . . . . .	74
5.2	Necessary Conditions . . . . .	75
5.3	Numerical Examples . . . . .	81
5.3.1	Example 1 . . . . .	81
5.3.2	Example 2 . . . . .	84
5.4	Summary and Future Work . . . . .	85
<b>CHAPTER 6 SUMMARY AND FUTURE WORK . . . . .</b>		<b>87</b>
6.1	Summary . . . . .	87
6.2	Future Work . . . . .	88
<b>APPENDICES . . . . .</b>		<b>90</b>
APPENDIX A	STOCHASTIC STABILITY FOR DISTRIBUTED TDOA-BASED LOCALIZATION OF A MOVING TARGET . . .	91
APPENDIX B	SUPPLEMENTAL RESULTS FOR TDOA-BASED DISTRIBUTED LOCALIZATION AND TRACKING OF A MOVING TARGET . . . . .	102
APPENDIX C	SUPPLEMENTAL RESULTS FOR THE DISTRIBUTED KALMAN FILTER . . . . .	109
<b>BIBLIOGRAPHY . . . . .</b>		<b>113</b>

## LIST OF TABLES

<b>Table 2.1: Reported parameters of first-generation gliding robotic fish “Grace” in [1]. .</b>	<b>13</b>
<b>Table 2.2: Mechanical specifications for Grace 2. . . . .</b>	<b>16</b>
<b>Table 2.3: Selected components for Grace 2.5. . . . .</b>	<b>19</b>
<b>Table 3.1: Summary of mobile range detection trials with GRACE at Higgins Lake in 2016, 2017, and 2018. Mean heading reflects the bearing from the first GPS measurement toward the last GPS measurement in each run. Wind speed and direction (heading; note that this is the direction the wind vectors are following, not “blowing from” as is customary) are coarse-scale regional estimates based on the NCEP’s Global Forecast System, as described in methods. . . . .</b>	<b>34</b>
<b>Table 3.2: Summary of parametric coefficients (linear terms) and smoothing terms from GAM used to determine if detection range was related to distance from transmitter (Tag Distance, in meters), direction of robot travel relative to transmitter (toward or away), robot depth (Depth, in meters from water surface), or robot pitch (Pitch, in degrees from horizontal). Included for each parametric coefficient is the estimate, standard error (SE), test statistic (Z), and p-value for the null hypothesis that the corresponding parameter is zero. Included for each smoothing term is the estimated degrees of freedom (EDF), test statistic (<math>\chi^2</math>), and approximate p-value for the null hypothesis that the smoothing term is zero. Bold faced p-values are significant at significance level of 0.05. . . . .</b>	<b>38</b>
<b>Table 3.3: Speed of the robot relative to ground from the field trials. . . . .</b>	<b>38</b>

## LIST OF FIGURES

<b>Figure 1.1:</b> Acoustic tag surgically implanted into fish (Source: Great Lakes Fishery Commission).	<b>2</b>
<b>Figure 1.2:</b> Example of OceanServer Iver2 propelled AUV used in acoustic telemetry [18].	<b>3</b>
<b>Figure 1.3:</b> Exampe of a Liquid Robotics wave glider AUV used in acoustic telemetry [17].	<b>4</b>
<b>Figure 1.4:</b> Acoustic receivers deployed across the Great Lakes (Source: Great Lakes Acoustic Telemetry Observation System).	<b>5</b>
<b>Figure 2.1:</b> The SLOCUM AUV [3].	<b>11</b>
<b>Figure 2.2:</b> Robotic fish from Smart Microsystems Lab at Michigan State University.	<b>12</b>
<b>Figure 2.3:</b> First-generation prototype of Gliding Robotic Fish "Grace" from [1].	<b>13</b>
<b>Figure 2.4:</b> Second-generation (Grace 2) prototypes of gliding robotic fish.	<b>14</b>
<b>Figure 2.5:</b> Side view of the Grace 2.5 design with the interface open depicting (a) 3D printed interface, (b) electronics board, (c) water-proof switching connector, (d) water inlets, (e) gliding mechanism, (f) quick-disconnect system, (g) adjustable balance weights, and (h) batteries.	<b>15</b>
<b>Figure 2.6:</b> A gliding robotic fish modified to carry (a) a propeller, through the introduction of (b) an auxiliary port.	<b>17</b>
<b>Figure 2.7:</b> Schematics of working patterns: (a) gliding in sagittal plane, and (b) spiraling in 3D space.	<b>19</b>
<b>Figure 2.8:</b> A gliding robotic fish prototype performing a spiral during experiments in MSU swimming pools.	<b>20</b>
<b>Figure 2.9:</b> Yaw and bearing angles.	<b>21</b>
<b>Figure 2.10:</b> Tail bias vs. angle difference $\alpha$ .	<b>22</b>
<b>Figure 2.11:</b> Flapping amplitude vs. angle difference $\alpha$ .	<b>22</b>
<b>Figure 2.12:</b> Tail deflection $\delta$ vs. angle difference $\alpha$ .	<b>23</b>

<b>Figure 2.13:</b> Front view for components for next-generation design depicting individually sealed for (a) electronics, (b) battery packs, (c) movable mass, and (d) buoyancy control tank. . . . .	<b>24</b>
<b>Figure 3.1:</b> Grace 2 carrying a forward-facing acoustic receiver. . . . .	<b>27</b>
<b>Figure 3.2:</b> Grace 2 at Higgins Lake, Michigan, 3 November 2017. . . . .	<b>28</b>
<b>Figure 3.3:</b> A gliding robotic fish prototype during field experiments in Higgins Lake. .	<b>28</b>
<b>Figure 3.4:</b> A gliding robotic fish prototype during field experiments in Higgins Lake. .	<b>29</b>
<b>Figure 3.5:</b> Lake tests (Panel A) Map of Higgins Lake, Michigan showing regions (red rectangles) where gliding robotic fish GRACE was tested 11 Nov 2016 (panel B), 03 Nov 2017 (panel C), and 14-15 June 2018 (panels D-F) with stationary transmitter locations (green circles), stationary receiver locations (yellow circles), and GPS locations (pink/red circles) recorded by the gliding robotic fish during each run. GPS points are shaded along a gradient from start (pink) to end (red) of each run. . . . .	<b>31</b>
<b>Figure 3.6:</b> Depth, pitch, and temperature profiles of gliding robotic fish Grace 2 during a 10-minute segment of run 2018-1 in Higgins Lake, with depths recorded by the on-board sensors (open symbols) and estimated depths at the time of test tag signal transmissions (red symbols). Horizontal broken lines show depth (panel A) and temperature (panel C) of stationary transmitter at site T6. . . . .	<b>36</b>
<b>Figure 3.7:</b> Depth profiles of gliding robotic fish Grace 2 during a selected 100– to 300–m segment of each run (panels A-D) in Higgins Lake, with locations of test tag transmissions that were detected (closed symbols) or not detected (open symbols) by the on-board receiver. . . . .	<b>37</b>
<b>Figure 3.8:</b> Estimated efficiencies (proportion of coded signals detected) of detecting an acoustic transmitter on acoustic receivers affixed to stationary moorings (red symbols; red shaded regions are GAM-based 95% confidence regions) and gliding robotic fish Grace 2 (black line; grey shaded regions are GAM-based 95% confidence regions) in Higgins Lake, Michigan during field tests in 2016 (panel A), 2017 (panel B), and 2018 (panels C-E). Vertical grey bars show distances between robot and the transmitter when each coded signal was detected (1) or not detected (0). . . . .	<b>40</b>
<b>Figure 3.9:</b> Partial effects of robot depth and pitch on detection probability. Estimated partial effects of robot depth and pitch on the log odds of detection probability when the robot is moving away from (panels A, B) or toward (panels C, D) a stationary transmitter in Higgins Lake, Michigan. . . . .	<b>41</b>

<b>Figure 3.10:</b> Estimated efficiencies (proportion of coded bursts detected) of detecting an acoustic transmitter on acoustic receivers affixed to gliding robotic fish Grace 2 in Higgins Lake, Michigan, during field tests in which evidence (GAM model results) suggested that detection range was influenced most by depth when the robot was moving away from the transmitter (panel C) and pitch when the robot was moving toward the transmitter (panel A, B, D).	42
<b>Figure 4.1:</b> Network of 3 agents monitoring the target with agent 1 as the reference node.	52
<b>Figure 4.2:</b> Network of 4 agents monitoring the target with agent 1 as the reference node.	52
<b>Figure 4.3:</b> The 4 possible configurations for node 1 to be connected to the network using the minimum number of edges.	59
<b>Figure 4.4:</b> Illustration of the simplified model of a propelled underwater robot with steering control, with a view on the sagittal plane. The robot has similar yaw control in the horizontal plane.	64
<b>Figure 4.5:</b> The fixed communication topology among a network of 8 agents. It is clear that no agent in the network has a sufficient number of neighbors (and therefore TDOA measurements) to estimate the process on its own.	65
<b>Figure 4.6:</b> Initial setup for simulation environment with a fixed communication topology. The big circle represents the moving target, while the small circles (overlapping one another at the origin) represent the initial estimates of the target's location for each robot. The ellipsoids represent the mobile robots, while the thin lines connecting them represent the communication links.	66
<b>Figure 4.7:</b> Simulation results of the robots for the two extreme values of $\underline{b}$ under a fixed communication topology where (a) the robots are constantly moving with target ( $\underline{b} = 0$ ), and (b) the robots are staying put ( $\underline{b} = \infty$ ).	66
<b>Figure 4.8:</b> Comparison of the Mean Squared Estimation Error (MSEE) of for each agent in the network for different values of $\underline{b}$ under a fixed communication topology.	67
<b>Figure 4.9:</b> Comparison of average covariance norms for different $\underline{b}$ values under a fixed communication topology.	68
<b>Figure 4.10:</b> Comparison of the collective distance traveled by the entire network for different $\underline{b}$ values under a fixed communication topology.	68

<b>Figure 4.11: Initial setup for distance-based communication links. . . . .</b>	<b>69</b>
<b>Figure 4.12: Final setup for distance-based communication links. . . . .</b>	<b>69</b>
<b>Figure 4.13: Mean Squared Estimation Error (MSEE) under a time-varying communication graph with continuous tracking (<math>\underline{b} = 0</math>) . . . . .</b>	<b>70</b>
<b>Figure 5.1: The minimal communication links required to satisfy the detectability requirement of all <math>(A, O_i)</math> pairs for Example 1. . . . .</b>	<b>82</b>
<b>Figure 5.2: Comparison of the norms of the covariance matrices under the consensus-then-filter distributed Kalman filter for Example 1. <math>W_g</math> represents the network that satisfies <math>(1/r_\sigma(A_i^u))^2</math>. . . . .</b>	<b>83</b>
<b>Figure 5.3: Comparison of the norms of the covariance matrices under the consensus-then-filter distributed Kalman filter for Example 2. <math>W_g</math> represents the network that satisfies <math>(1/r_\sigma(A_i^u))^2</math>. . . . .</b>	<b>85</b>

# CHAPTER 1

## INTRODUCTION

There is growing interest in monitoring aquatic environments, due to the emerging problems of environmental pollution and expanding demand for sustainable development. Such pollution involves various types of contaminants, including industrial waste, chemicals, and bacteria, to name a few. The pollution could happen in different aquatic environments, such as ponds, rivers, lakes, and even the ocean. For that reason, underwater robots are increasingly drawing attention in aquatic sensing. The past decade or so has seen great progress in the use of robotic technology in aquatic environmental sensing.

In this dissertation, we focus on the application of these robots to localization and tracking of acoustically tagged aquatic animals. For the remainder of this introduction, we discuss the existing methods for acoustic telemetry in aquatic environments, and conduct a brief survey of the technologies used in that field. We then present the contributions of this research to advancing acoustic telemetry. Specifically, we discuss the design improvements to gliding robotic fish that facilitated carrying out acoustic telemetry experiments, and theoretical work on how networks of robots can collectively localize and track a moving target or estimate the state of a dynamical system.

### 1.1 Acoustic Telemetry in Aquatic Environments

Tracking of aquatic animals presents an important problem in fishery research and is paramount to improving our understanding of aquatic ecosystems. Acoustic telemetry is often used by researchers to collect information about aquatic animals, and study their migration, habitat use, and survival. Acoustic telemetry systems consist of two main components: transmitters which broadcast a series of sound pulses (or pings) into the surrounding water, and receivers that listen to such pings and record the time and corresponding ID of any detection. Animals can be tagged with acoustic transmitters (see Fig. 1.1) and their movements can be tracked by stationary networks



**Figure 1.1: Acoustic tag surgically implanted into fish (Source: Great Lakes Fishery Commission).**

of hydrophones or acoustic receivers that can identify acoustic-tagged animals in their vicinity [4, 5, 6, 7].

Recent improvements in acoustic telemetry technology have advanced studies of long-term spatiotemporal ecology and behavior of aquatic organisms [8, 9]. In particular, fish movement tracking information obtained via acoustic telemetry has provided insight far superior than what can be obtained by direct observations or traditional survey methods (i.e., trawls, gill nets). Observations from such networks have already been used to improve control and assessment of invasive species, gain new insights into spawning behavior and habitat requirements of fish, and describe movements of high-valued stocks [8, 7]. In the future, telemetry promises to address many critical uncertainties in fishery research and aquatic ecosystems. However, logistical and economic constraints may preclude use of receiver networks to fill gaps in understanding of animal movements, especially in large systems and extreme environments.

Due to the limited detection range of these receivers, such acoustic telemetry systems are limited to fixed areas. Autonomous underwater vehicles (AUVs) are becoming more common telemetry assets as receivers can be self-contained and attached as a payload, or they can be integrated for real-time detection while simultaneously measuring physical and biological properties of the aquatic environment [10, 11]. For example, buoyancy-driven gliders with integrated or externally mounted



**Figure 1.2: Example of OceanServer Iver2 propelled AUV used in acoustic telemetry [18].**

receivers have been used to study sturgeon and shark habitats [12, 13, 14], stereo-hydrophone acoustic receiver systems have been integrated into propelled AUVs to track and follow leopard sharks [15], and receivers and hydrophones have also been externally mounted and integrated into a propeller-driven AUV [16] and a wave glider for real-time detections of tagged marine life [17]. Figs. 1.2–1.3 show examples of different AUVs equipped with acoustic receivers.

Each of these vehicles has its unique advantages and disadvantages. Propelled AUVs (e.g., REMUS-100 [16], and OceanServer Iver2 [18]) can overcome large currents and surface waves, and are capable of traveling at higher speeds than other unmanned vehicles. The main drawback for these vehicles is the power requirement needed for the propellers, limiting deployment duration in the field. Another popular class of AUVs is wave gliders, where a surface float that utilizes wave energy to move forward is attached to an underwater sub via a tether [11]. The energy-efficient nature of wave gliders, such as the Liquid Robotics Wave Glider used in [17], allows them to be deployed for months at a time. Moreover, accurate positioning of the surface float is readily available through GPS, along with reliable communication for the duration of the mission. The main limitation of wave gliders is that any underwater instrumentation needs to be tethered to the surface float, limiting the depth at which such instrumentation can be deployed, and introducing tether dynamics



**Figure 1.3: Exemple of a Liquid Robotics wave glider AUV used in acoustic telemetry [17].**

that should be considered for accurate representation of the underwater environment. Underwater gliders are another class of energy-efficient AUVs that travel by changing their buoyancy and center of gravity. Underwater gliders, such as the Slocum glider [3], have been widely used in a variety of underwater applications [12, 10]. Like wave gliders, the energy efficient nature of these robots makes them ideal for long-duration missions. However, unlike wave gliders, there is no tether involved with these robots, allowing for sampling of water environment at different depths up to the depth rating of the vehicle. The biggest challenges with these robots involve underwater localization and communication since RF signals do not penetrate water effectively. These vehicles often record data while underwater, and surface occasionally to download or offload this data.

## **1.2 Beyond Presence-Absence Information**

In addition to carrying acoustic receiver into areas that are not covered by stationary receivers, AUVs can also carry a variety of environmental sensors. Measurements from these sensors can further help characterize the interaction between aquatic animals and their environment. These sensors allow researchers to monitor the external environment of fishes, allowing them to address

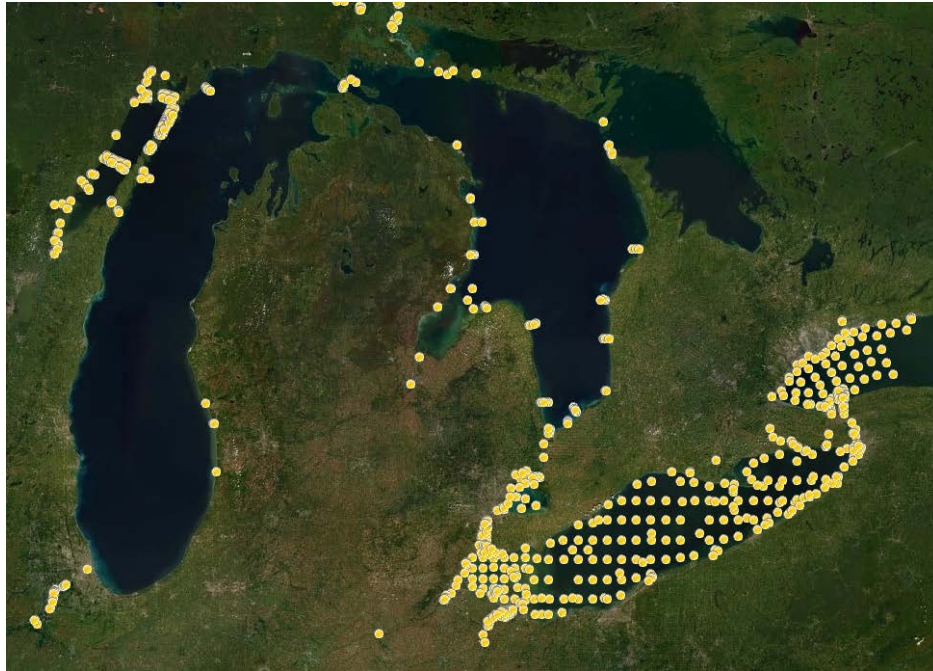


**Figure 1.4: Acoustic receivers deployed across the Great Lakes (Source: Great Lakes Acoustic Telemetry Observation System).**

biological questions that were previously difficult (or impossible) to answer.

Acoustic receivers provide information about the location of tagged fish. When a signal is identified, the tag's unique ID code is saved with the date and time. The data from any single receiver provide a record of each visit to that location by a tagged fish. Researchers often deploy many receivers over large regions to understand the movement patterns of tagged fish (see Fig. 1.4). Consequently, the fish positioning resolution is defined by the detection range of individual receivers, which is usually on the order of 100 – 1000 m.

Fine-scale fish positioning (at the resolution of a few meters to tens of meters) can be achieved with a network of receivers using time-difference-of-arrival (TDOA) methods. When the same signal is detected by multiple receivers, it is possible to infer the location of the tag from the differences in detection times. Such methods can provide a more detailed understanding of fish behavior. Networks of AUVs equipped with acoustic receivers hold great potential in understanding aquatic ecosystems, and advancing the field of acoustic telemetry. To effectively utilize such networks, algorithms should rely on distributed processing of information and cooperation between

the robots to achieve specific tasks.

### **1.3 Overview of Contributions**

The contributions of this research reside mainly in improving the design of the gliding robotic fish, investigating its applicability to acoustic telemetry, and theoretical treatment of distributed localization and estimation using robotic networks. The details are as follows.

#### **1.3.1 Improvements to Gliding Robotic Fish**

Given the ever-changing and unpredictable nature of the environments in which they operate, robots employed for underwater missions need to be both highly energy-efficient and maneuverable [19]. Gliding robotic fish, a new type of underwater robots, has emerged as a promising mobile sensing platform for monitoring aquatic environment. Such a robot combines the advantages of both underwater gliders and robotic fish and features long operation duration along with high maneuverability. This makes the gliding robotic fish well suited for a variety of underwater sensing applications.

While the first-generation design of these robots was successfully used in sampling harmful oil and algae bloom [20, 21], some aspects of the design needed to be re-addressed. The design of the gliding robotic fish was improved to increase the serviceability of the robots by incorporating a resealable design. This facilitated the rapid testing of different electrical designs, and allowed regular inspection and maintenance to be performed on these robots. The computational power, data storage capacity, and battery capacity of these robots were also dramatically improved to facilitate carrying out longer missions. The new design also allows for a larger and replaceable sensor payload that can be customized to fit different applications.

Additional improvements to the design are proposed, which would allow for further modularity of the system and reduction of the manufacturing and fabrication costs.

### **1.3.2 Application to Acoustic Telemetry**

Gliding robotic fish can be modified to carry an acoustic receivers to detect, and potentially track, tagged fish in areas where it would be difficult to install stationary receivers. The successful development of gliding robotic fish has allowed for the investigation of the robot's capability in detecting and tracking tagged fish.

A series of field trials have been conducted in Higgins Lake, Michigan, to evaluate the use of these robots as mobile receiver platforms for detecting acoustic signals in a challenging environment. A self-contained acoustic receiver was attached to the a gliding robotic fish prototype, and the detection efficiency of the mobile receiver was compared to that of stationary receivers. Further trials were conducted to study the factors that affect the detection efficiency of the mobile receiver, such as depth underwater, robot heading relative to transmitter, and pitch angle of the robot.

While the detection ranges for this mobile receiver varied between trials, the results obtained from these trials showed that the detection efficiency of the mobile receiver is comparable to that of stationary receivers at distances up to 600 m. Furthermore, the results show that the detection efficiency of the mobile receiver degrades significantly if the mobile receiver is facing away from the tag. The results also indicate that the depth and pitch of the robot also affect the detection efficiency of the mobile receiver. However, the impact of these variables is less paramount than that of the distance between the receiver and transmitter, or that of their alignment.

These trials suggest that such mobile receivers can be utilized for active tracking of tagged animals. However, care must be taken when designing tracking controller in order to maximize the alignment between the receiver and the transmitter. The trials have also offered insight into the limitations of the current design, and additional work is proposed to further characterize the performance of such mobile receivers.

### **1.3.3 Distributed Localization and Tracking of a Moving Target**

Motivated by the problem of tracking live fish through acoustic signals by a robotic network, analytical work is completed on distributed target localization and tracking using a network of

mobile agents. Time-difference-of-arrival (TDOA)-based algorithms are widely used for precise localization of a target, examples of which extend beyond acoustic telemetry in fishery research [22], to wireless ranging radar systems and cellular positioning systems [23]. However, much of the work on TDOA-based localization in the literature adopts a centralized approach, in which a reference node is chosen and the times of arrival (TOA) of the emitted signal for all other nodes in the network are subtracted from the reference node's TOA, generating TDOA measurements at fusion hub.

Due to power and bandwidth constraints in robotic networks, centralized information processing is often infeasible, particularly for large-scale and unreliable networks. Moreover, some sensors cannot transmit their measurements to the reference node due to their limited communication ranges. This has motivated us to investigate a completely distributed approach for localization of a moving target. It is shown that source localization is not possible (centrally, and therefore distributively) when the total number of TDOA measurement is insufficient. Then, we demonstrate that the target's position can be successfully estimated in a distributed manner if and only if every agent is part of a connected network that collectively has a sufficient number of TDOA measurements, even if each agent has an insufficient number of measurements.

Estimation of the target's location is achieved without relying on a centralized node, and without requiring all agents in the network to be communicating with one another. Necessary and sufficient conditions on the underlying bidirectional communication graph are derived to ensure successful localization of the target. Moreover, tracking of the moving target is examined through a coordinated moving strategy that can be tuned to emphasize estimation performance or energy conservation, depending on the application.

### **1.3.4 Distributed Estimation of Linear Time-Invariant Systems**

The problem of distributed localization of a moving target has motivated the analysis of a more general application of networked systems: the distributed estimation problem. Specifically, we examine the problem of estimating the state of a linear time-invariant system that is monitored by

a network of sensors. It is assumed that the interactions between the sensing sites are dictated by a weighted directed graph. Under this distributed approach, each sensor site only has access to its information and to that of the sensors in its neighborhood. While the analytical results obtained here do not directly apply to the distributed localization problem, these results serve as a building block for later investigation of time-varying dynamical systems monitored by sensor networks.

This distributed filtering problem has received significant attention over the past years, and different ideas have been proposed to effectively deal with this problem[24, 25, 26, 27, 28, 29]. We focus on single-time-scale algorithms in which data fusion occurs once per time step of plant dynamics due to bandwidth and power constraints presented in networked applications. In particular, we consider the class of consensus-based distributed linear filters (CBDLF) where each sensor updates its estimate in two steps: a consensus step dictated by a weighted and directed communication graph, followed by a local Luenberger filtering step.

We then present sub-optimal filtering gains that minimize an upper bound of a quadratic filtering cost, and show that these filtering gains are related to the convergence of a set of coupled Riccati equations. While it has been shown that the convergence of these coupled Riccati equations is related to the feasibility of a set of linear matrix inequalities (LMIs) [30], these conditions do not, in general, shed light on the network conditions required to satisfy such LMIs. The work presented in this dissertation utilizes some of the results developed in the Markovian jump linear systems (MJLS) literature to connect the convergence properties of these coupled Riccati equations to certain conditions on the network topology and consensus weights.

## **1.4 Dissertation Organization**

The remainder of this dissertation is organized as follows. In Chapter 2, the design concept for the gliding robotic fish is revisited, and the design improvements that the new generation of gliding robotic fish has seen are highlighted. Then, the capability of this robot in advancing acoustic telemetry in fishery research is presented in Chapter 3 through a series of field trials that were carried out in Higgins Lake, Michigan. In Chapter 4, a detailed discussion on localization of a moving

target using time-difference-of-arrival (TDOA) measurements by a network of agents is presented. This is motivated by the problem of tracking real fish, where multiple robots need to localize and track a moving target, without the need for a centralized node to collect all measurements and propagate an estimate of the target's position back to the network. This problem is expanded on in Chapter 5, where we consider the more general problem of distributed estimation of a dynamical system monitored by a network of sensors. Finally, concluding remarks are provided in Chapter 6.

## CHAPTER 2

### DESIGN IMPROVEMENTS FOR GLIDING ROBOTIC FISH

The design concept of a gliding robotic fish comes from energy-efficient underwater gliders and highly maneuverable robotic fish. On the one hand, underwater gliders are known for their great energy-efficiency and long-duration operation in oceanographic applications [31]. An underwater glider utilizes its buoyancy to enable motion without any additional propulsion and adjusts its center of gravity to achieve certain attitude, which results in glide and thus horizontal travel. Since energy is needed only for buoyancy and center-of-gravity adjustment when switching the glide profile, underwater gliders are very energy-efficient, as proven by the great success of the Seaglider [2] and SLOCUM [3] (Figure 2.1). The maneuverability of underwater gliders, however, is quite limited. The large size (1–2 m long), heavy weight (50 kg and above), and high cost [31] of these vehicles also impede their adoption in the application of networked sensing and in versatile environments like ponds and inland lakes.

On the other hand, over the past two decades, there has been significant interest in developing robots that propel and maneuver themselves like real fish do. Often called robotic fish (Figure 2.2), they accomplish swimming by deforming their body and using fin-like attachments [32]. In many designs, a fish-like flapping tail is used to provide propulsion force and a biased tail angle is applied



**Figure 2.1: The SLOCUM AUV [3].**



**Figure 2.2: Robotic fish from Smart Microsystems Lab at Michigan State University.**

to realize turning. Due to the similarity to real fish and the fact that the rotation of the tail fin is usually enabled by a motor that is easy to control and fast in response, robotic fish typically have high maneuverability (i.e., small turning radius). However, as the forward propelling force is generated from the flapping motion of the fins, such robots require constant actuation for swimming and cannot work for extended periods of time without battery recharge.

## **2.1 Overview of Gliding Robotic Fish**

Inspired by the design and merits of both underwater gliders and robotic fish, a new type of underwater robots, gliding robotic fish, has emerged as an underwater sensing platform [1]. A gliding robotic fish combines both mechanisms of gliding and swimming, featuring energy efficiency and high maneuverability at the same time. Such a robot would realize most of its locomotion through gliding like underwater gliders, by utilizing its buoyancy to enable motion without any additional propulsion, while it can adjust its center of gravity to achieve a certain attitude. It would use actively controlled fins to achieve high maneuverability, during turning and orientation maintenance. Of course, fins can also provide additional propulsive power during locomotion if needed.

Table 2.1 lists some of the aspects reported in [1] for an experimental prototype of the gliding robotic fish (Fig. 2.3). The smaller dimension of Grace compared to traditional underwater gliders proved to be valuable in relatively shallow water environment, such as lakes, rivers, and ponds,

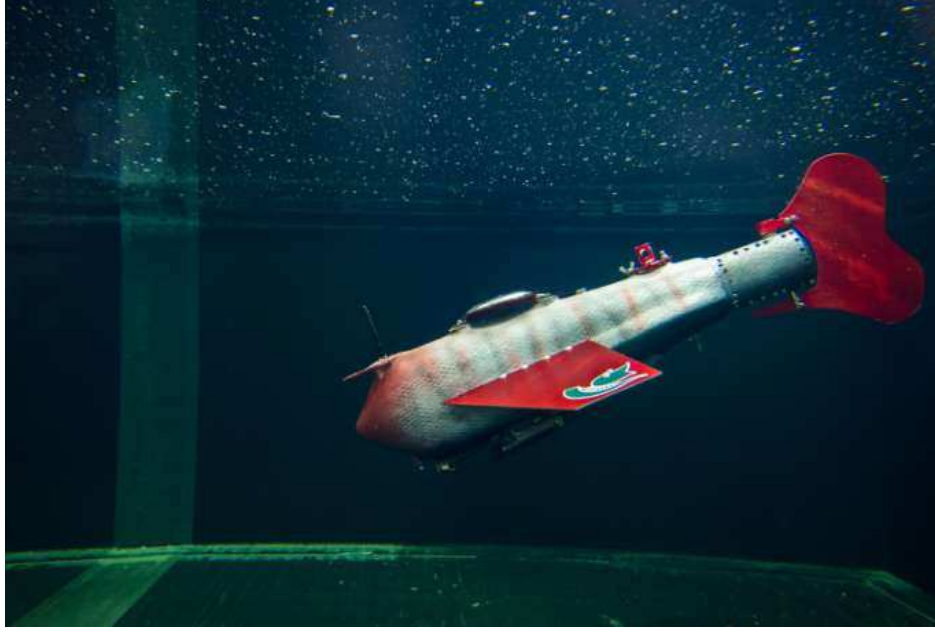


**Figure 2.3: First-generation prototype of Gliding Robotic Fish "Grace" from [1].**

**Table 2.1: Reported parameters of first-generation gliding robotic fish "Grace" in [1].**

<i>Parameter</i>	<i>Description</i>
Hull dimensions (L x W x H)	65 x 15 x 18 cm
Tail to nose length	90 cm
Wingspan	75 cm
Weight	9 kg
Payload	Turner Design Cyclops 7F sensor (crude oil or blue green algae sensor) Temperature sensor

where larger gliders are not quite suitable due to their large size and high cost. This prototype was successfully deployed for oil spill detection in Kalamazoo river, Michigan, and for monitoring algae bloom in Wintergreen lake, MI [20, 21].

However, there were several aspects of the first-generation design that needed improvement. First, the hull design of Grace in [1] was completely sealed, which made servicing the robot prohibitive, as accessing the internal electronics would require destroying the robot's shell. Second, the payload carrying capabilities of the first-generation design were limited to one or two small components, and would need external attachments (e.g., external weight, foam blocks) to accom-



**Figure 2.4: Second-generation (Grace 2) prototypes of gliding robotic fish.**

modate the buoyancy of the payload. Finally, the battery capacity of the original design limited its application to the order of several hours to one day.

## **2.2 Design Improvements**

The second-generation gliding robotic fish, which we refer to as “Grace 2”, has seen several electrical and mechanical enhancements to improve its applicability and prolong its operational time. In this section, we discuss these design improvements that were implemented on two new prototypes (see Fig. 2.4). Some of these improvements were done incrementally over the period of this study, which we subversion as 2.0, 2.1, and 2.5. We will use the term “Grace 2” when we discuss fundamental changes to the design when compared to first-generation prototype in [1], while we use “Grace 2.x” when discussing improvements that were accommodated in that specific subversion.

### **2.2.1 Mechanical Improvements**

The new mechanical design for Grace 2 addressed the issues of serviceability and payload carrying capacity<sup>1</sup>. To address the issue of serviceability, a 3D printed interface was introduced between the

---

<sup>1</sup>While the development of the Grace 2 robots involved several people, the majority of the fabrication and mechanical work on these robots was completed by John Thon from the Smart Microsystems Lab at Michigan State University. The majority of the electrical improvements was

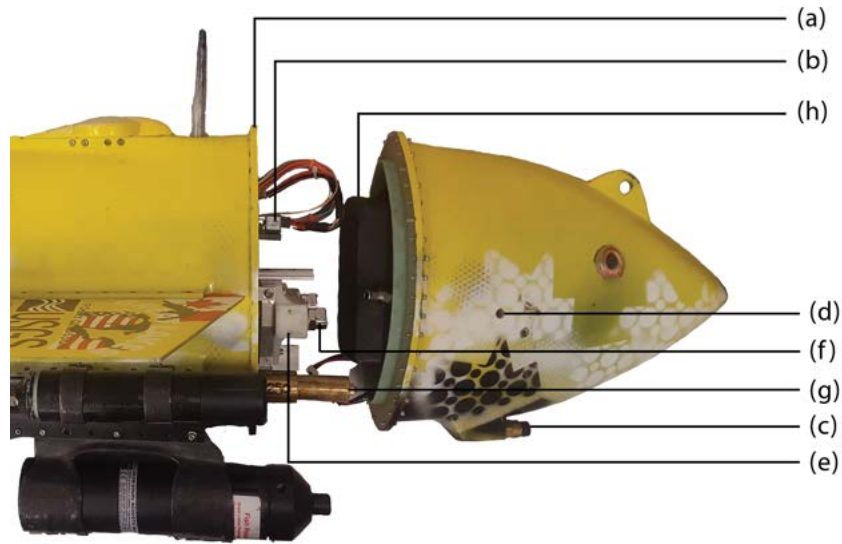


**Figure 2.5: Side view of the Grace 2.5 design with the interface open depicting (a) 3D printed interface, (b) electronics board, (c) water-proof switching connector, (d) water inlets, (e) gliding mechanism, (f) quick-disconnect system, (g) adjustable balance weights, and (h) batteries.**

nose of the robot and the rest of its body. This interface, when bolted together, formed a water-tight seal by compressing a custom O-ring at the interface. To maximize the use of space, batteries were stored in the robot's nose, and a water-proof connector was introduced to operate as a switch for the system.

Two measures were taken to allow for larger, and possibly variable, payload carrying capacity. First, a larger buoyancy-control tank, with a volume of approximately 190 mL, was utilized for the second-generation robots. To deal with the serviceable nature of the robot, a 3D printed piece was designed to fit the buoyancy-control tank and held water-tight quick disconnects that mated with the water inlets from the nose. The movable mass and the buoyancy tank were fixed together to form what we refer to as the “gliding mechanism”, which could slide in and out of the robot's main body for maintenance and inspection. The second measure allowed for variable weights to be attached to the bottom of the gliding mechanism. These weights are typically adjusted and moved around before deployment in order to accommodate the buoyancy and weight distribution of the payloads.

---

completed by the author.

**Table 2.2: Mechanical specifications for Grace 2.**

<i>Component</i>	<i>Description</i>
Hull dimensions (L x W x H)	103 x 20 x 30 cm
Tail to nose length	140 cm
Wingspan	60 cm
Weight	20 kg
Robot hull material	Carbon fiber with 3D printed interface
Buoyancy Control	190 mL
Pitch Control	+ 40°, -25°
Payload	Dissolved Oxygen and Temperature sensor Photosynthetically Active Radiation sensor Freshwater Blue Green Algae sensor Chlorophyll sensor Acoustic receiver

Fig. 2.5 depicts a side view of a Grace 2 prototype and its different components.

The need for larger buoyancy control, payload carrying capacity, and battery capacity required a larger body hull that can accommodate all these components. Table 2.2 lists the mechanical specifications of the Grace 2.

### **2.2.2 Electrical and System Improvements**

The serviceable nature of the new design allowed us to rapidly prototype and test out different electrical systems and components to improve the robot's functionality. The Grace 2 design implemented a changeable sensor harness that could be replaced to accommodate a different set of sensors, and a connector was introduced between each of the shell components and the on-board electronics.

The initial electrical design for Grace 2.0 utilized an architecture similar to the first-generation Grace, with the exception of introducing a second microcontroller (MCU) dedicated to reading and communicating with the sensor bundle. The power system for the Grace 2.0 design used linear regulators to regulate battery voltages to 3.3V and 5V, which provided power to the electronics and the sensors. However, due to the relatively high power demand of the sensors along with the big difference between the battery voltage and the regulated voltages, the linear regulators became

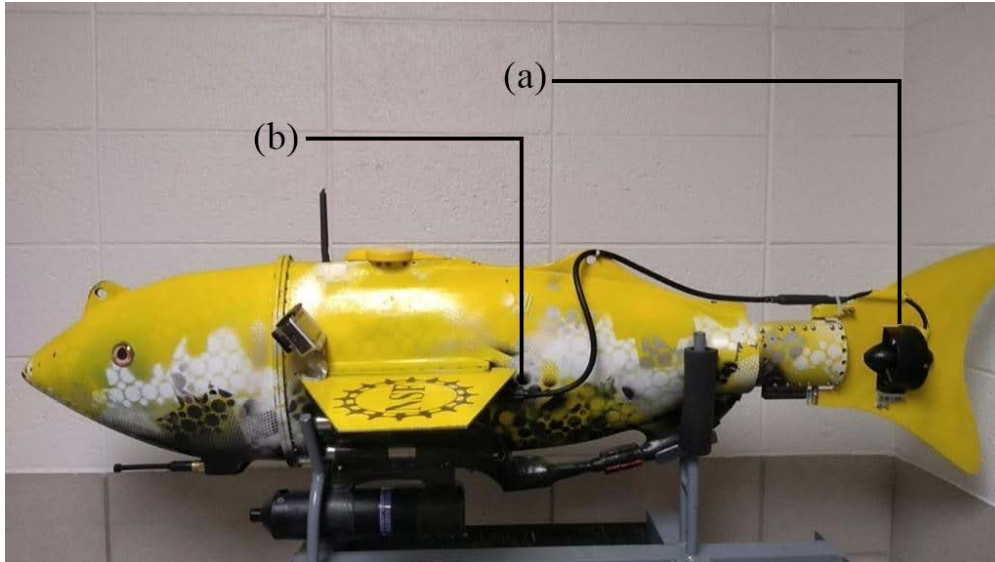


**Figure 2.6: A gliding robotic fish modified to carry (a) a propeller, through the introduction of (b) an auxiliary port.**

very hot in a very short period of time, causing the electronics to behave erratically and the entire system to shut off. The electrical design for Grace 2.1 used a new power system architecture, in which the linear regulators were replaced with switching regulators. The introduction of these regulators drastically improved the stability of the electronics and allowed us to perform meaningful experiments (which we present later in Chapter 3). Additionally, the wiring harness inside the robot was simplified to only two connectors, one for the shell components (namely, the GPS, tail servo, and pressure sensor), and one for the sensor bundle. The Grace 2.1 design relied on the same dual-MCU architecture used in Grace 2.0, in which one MCU was dedicated to reading and communicating with the set of environmental sensors, while another MCU was responsible for controlling the actuators, reading essential sensors (i.e., depth, GPS, and IMU), and communicating with a base station.

The design in Grace 2.0 and 2.1 did not implement on-board storage of the data. Instead, the robot periodically sent essential data (i.e., UTC time, GPS position, and IMU info) to a laptop over the wireless XBee channel. When the robot performed a dive, all these parameters along with the robot depth were temporarily stored in memory until the next time the robot surfaces, at which time the data was sent over the wireless channel.

The dual MCU architecture was somewhat limiting since all tasks needed to be implemented on this embedded structure. Furthermore, the lack of on-board storage also limited the applicability of these robot. Therefore, a new revision of the electronics was introduced in Grace 2.5 in which a Raspberry Pi (RPi) computer was included to handle high-level tasks (e.g. communicating with the base station, mission control, data storage). The RPi computer freed the MCUs to perform low-level tasks only, such as reading sensor value and controlling actuators. Internal storage onto an 8 GB mirco-SD card was also integrated with the latest design, and the robot logged all data at 5 s intervals. The introduction of the RPi computer also allowed for rapid testing of different ideas without needing to open the robot and adjusting the low-level microcontroller code. It also provided the capability of implementing an sophisticated algorithms and systems, such as the Robot Operating System (ROS). Finally, the Grace 2.5 design was modified to support an additional “auxiliary module” through an additional water-proof connector that can be used to connect another sensor or actuator, such as a propeller (see Fig. 2.6). The components used in the final design of Grace 2.5 are listed in Table 2.3.

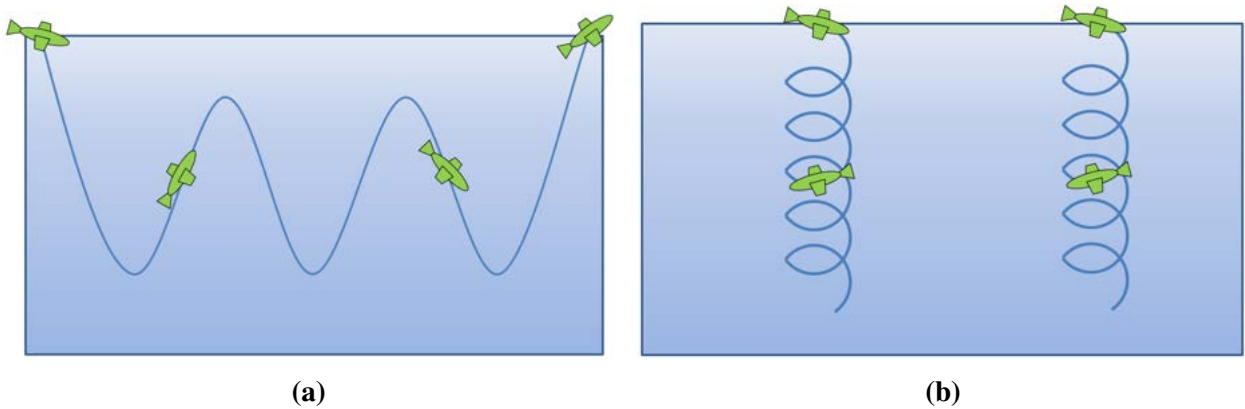
## **2.3 Motion and Navigation**

For gliding robotic fish, there could be various interesting motions generated by integrating the gliding and swimming mechanisms. Two main steady-state motion profiles are typically used as the regular working patterns for navigation and water sampling. One is gliding in the sagittal plane, and the other is spiraling in the 3D space.

Gliding is also the common operating mode for traditional underwater gliders (Fig. 2.7(a)). In the zig-zag trajectory, the gliding robotic fish only consumes energy during the transition between descending and ascending, which makes the gliding robotic fish highly energy-efficient. The other motion, spiral in the 3D space, allows for sampling water columns using gliding robotic fish (Fig. 2.7(b)). A water column is a conceptual narrow volume (like a narrow cylinder) of water stretching vertically from the surface to the bottom. Water column sampling is a routine surveying method in environmental studies. This motion is achieved by incorporating the steady gliding with

**Table 2.3: Selected components for Grace 2.5.**

<i>Component name</i>	<i>Component model</i>
Processors	Raspberry Pi Zero-W (2x) Microchip dsPIC30F6014A
Battery	(3x) Batteryspace High Power Polymer Li-Ion, 18.5v @ 185 Wh (Approximately 5 days of continuous actuation with 1400 dive cycles at 5 minute intervals)
Data Storage	8GB micro SD
Mass actuator	Actuonix L16-P Miniature Linear Actuator with Feedback
Buoyancy-control actuator	ServoCity 6" Stroke 180 lb Thrust Heavy Duty Linear Actuator
Tail servo motor	ServoCity HS-7980TH
Pressure sensor	Honeywell 40PC100G2A
GPS Unit	GPS 18x LVC
Wireless module	XBee-Pro 900HP RP-SMA
Wireless antenna	900MHz Duck Antenna RP-SMA
IMU	VectorNav VN100S
Dissolved Oxygen and Temperature sensor	In-Situ RDO PRO-X
Photosynthetically Active Radiation sensor	LI-COR LI-192SA
Chlorophyll sensor	Turner Designs Cyclops-7 Submersible sensors-C
Algae sensor	Turner Designs Cyclops-7 Submersible sensors-P
Sensor bundle connector	SubConn MCIL16-F/M
Aux port connector	SubConn MCBH6-F
Switch/charge connector	SubConn MCBH4-F

**Figure 2.7: Schematics of working patterns: (a) gliding in sagittal plane, and (b) spiraling in 3D space.**



**Figure 2.8: A gliding robotic fish prototype performing a spiral during experiments in MSU swimming pools.**

a deflected tail. The non-zero angled tail fin will introduce a turning moment to the steady gliding robot and lead to a 3D spiraling motion. With the actively-controlled tail, the gliding robotic fish is capable of spiral motions with tight turning radius. If needed, a gradually changing tail angle will form spiral-in or spiral-out 3D trajectories that can be used to orient the robot at a certain angle while gliding.

When performing field tests with these robots (such as the tests we describe in Chapter 3), a fundamental task is to navigate to a given GPS waypoint. We discuss two navigation schemes that were implemented on these robots.

### **2.3.1 Swimming-based Navigation**

The first navigation mode relies on continuously flapping the tail to propel the fish forward. The tail bias and amplitude are updated to drive the robot to the desired location. The task is simplified by assuming that the robot's yaw angle,  $\psi$ , is a good measure of the robot's heading, which can be measured directly from the on-board IMU. The bearing angle,  $\gamma$ , to the GPS target location is then calculated. Figure 2.9 depicts the yaw and bearing angles.

A proportional controller with saturation is then used to compute the bias and amplitude based

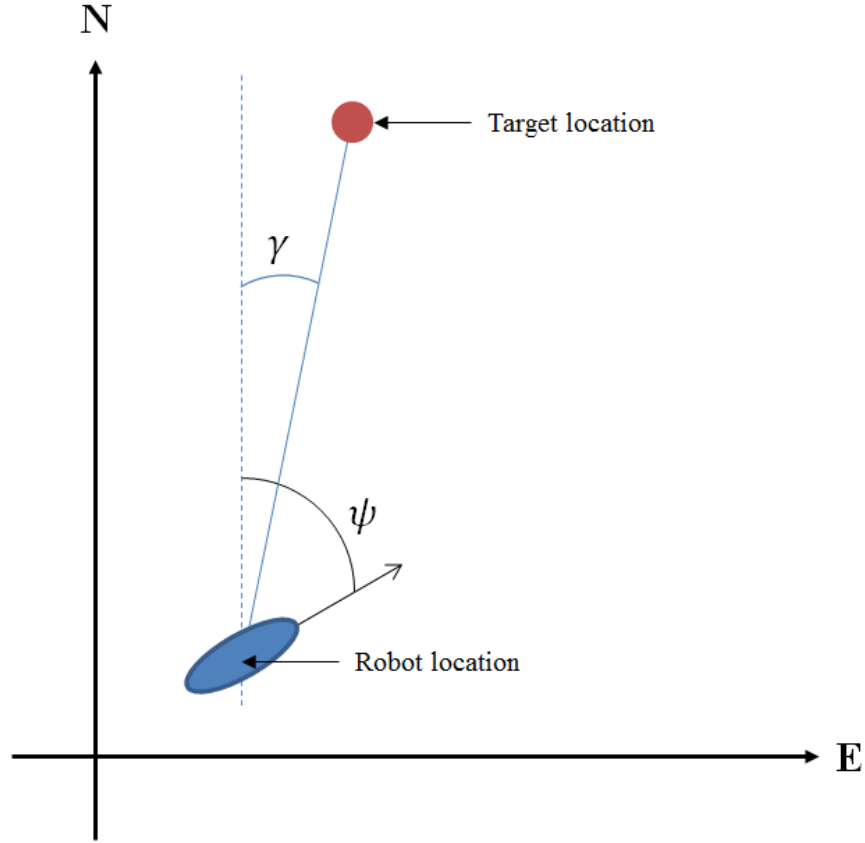


**Figure 2.9: Yaw and bearing angles.**

on the difference between the robot's heading  $\psi$  and the bearing angle to target location  $\gamma$

$$\alpha = \psi - \gamma \quad (2.1)$$

Figs. 2.10 and 2.11 show the bias and amplitude of the tail flapping as a function of the difference  $\alpha$ . The outputted tail angles from this computed bias and amplitude will always fall within the limits of the servo motor, which are set to  $\pm 45^\circ$ .

### 2.3.2 Gliding-based Navigation

Swimming based navigation offers the benefit of a continuous GPS signal while swimming on the surface. This simplifies the navigation task and makes swimming a viable strategy for accurate navigation to target. However, due to the continuous flapping of the tail, swimming is generally less efficient than gliding and should, therefore, be only used for navigation over a short distance.

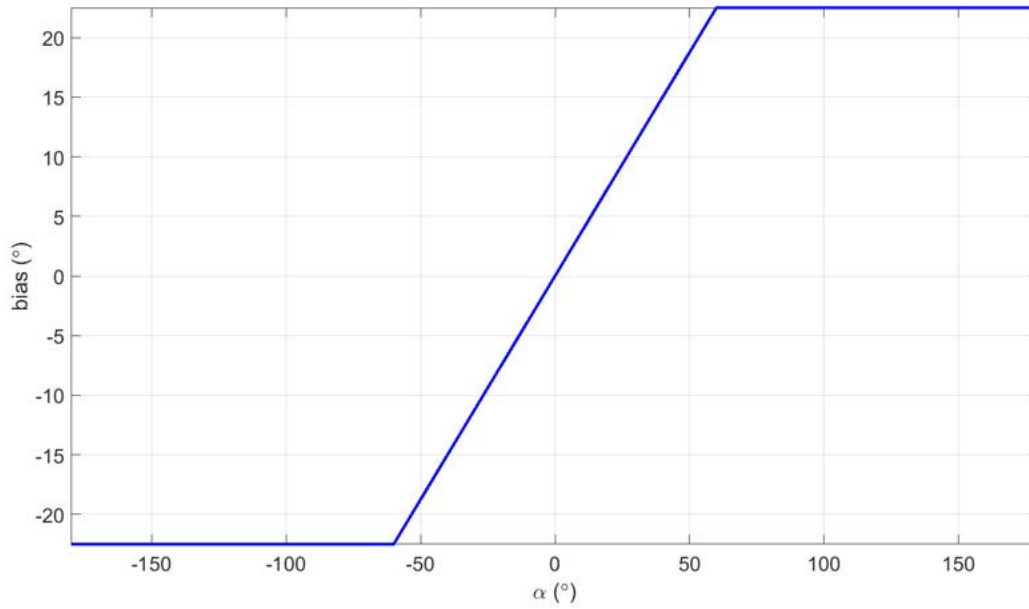


**Figure 2.10: Tail bias vs. angle difference  $\alpha$ .**

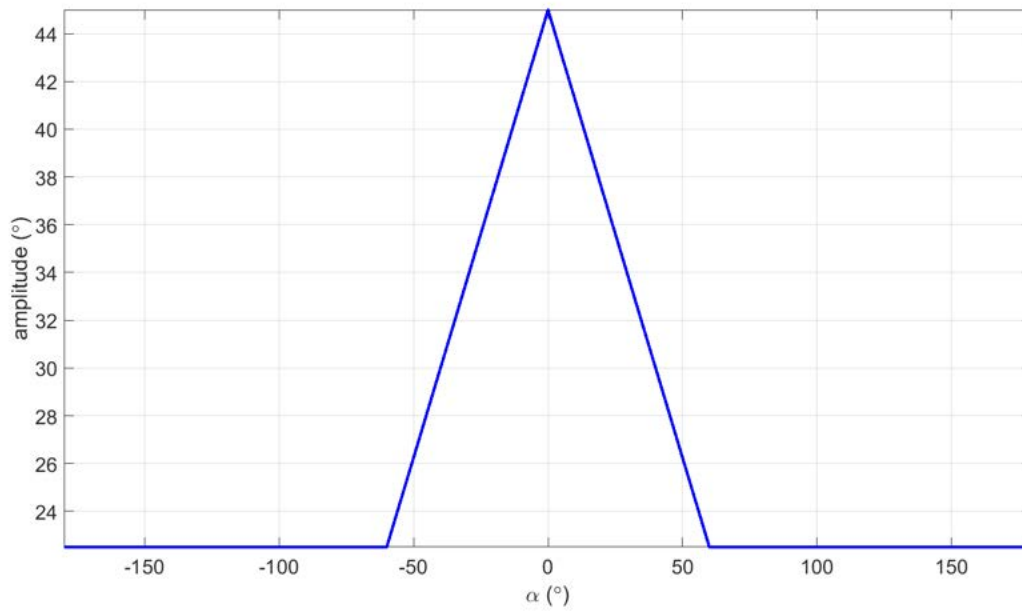


**Figure 2.11: Flapping amplitude vs. angle difference  $\alpha$ .**

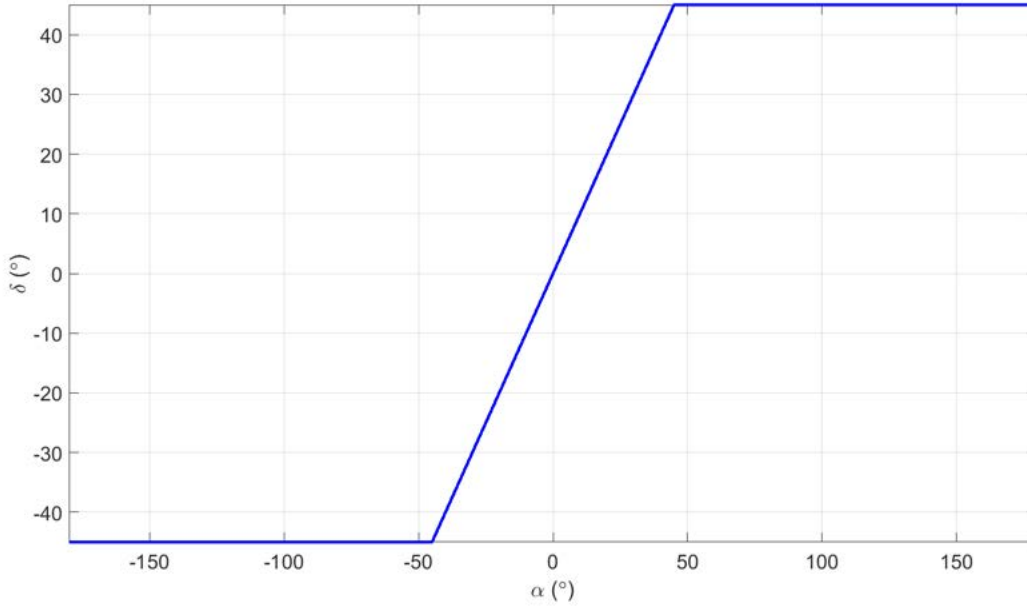


**Figure 2.12: Tail deflection  $\delta$  vs. angle difference  $\alpha$ .**

For that reason, it is desirable to use the gliding mode to navigate from one point to another. Gliding-based navigation begins by acquiring a valid GPS fix and calculating the bearing angle to the target location. Once this process is completed, the robot begins diving by typical adjustment of the mass position and net buoyancy. While diving, the tail fin is deflected at an angle  $\delta$  that is proportional to the difference  $\alpha$ . To prevent damage to the servo motor, the tail deflection angle is saturated to  $\pm 45^\circ$ . Fig. 2.12 shows the relationship between the tail deflection angle and the heading difference  $\alpha$  during a dive.

When the robot completes a dive, it waits on the surface for another GPS fix before repeating the process. During that time, the robot applies the swimming-based navigation using the latest computed heading angle  $\gamma$  to move towards the target GPS location.

## 2.4 Summary & Future Work

We discussed the design improvements implemented onto the gliding robotic fish originally presented in [1]. The modified version significantly improved the serviceability, computational power, payload-carrying capacity, and battery capacity of the robot. A new power design was

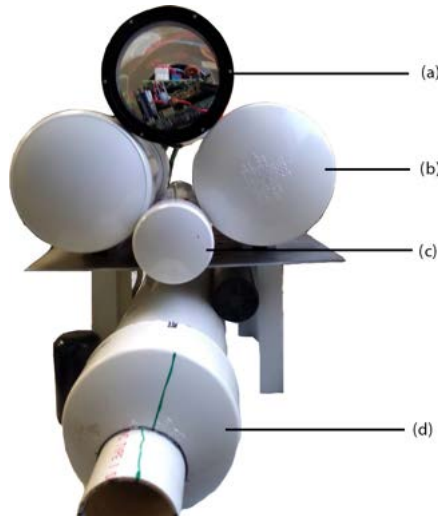


**Figure 2.13: Front view for components for next-generation design depicting individually sealed for (a) electronics, (b) battery packs, (c) movable mass, and (d) buoyancy control tank.**

introduced to efficiently power the various electronics and environmental sensors. Furthermore, a new system architecture was implemented that included a Raspberry Pi computer which worked alongside the embedded MCUs. The new RPi design helped separate high-level tasks (such as communication, data storage, and task-specific algorithms) from low-level tasks such as control of the robot's actuators and communication with the various sensors. This, in turn, facilitated testing out new ideas at a quicker rate, while also offering the convenience of a Linux-like environment and all its available tools (e.g., ROS implementation).

The current robot design did, however, suffer from some issues that future work should address. The main drawback that this design faced was the time and resources needed for fabrication and manufacturing. Since this was a novel design, almost all mechanical components of the robot needed to be custom-built (and at times hand-crafted) for this project. While the effect of such an issue is expected to diminish if these designs are mass-produced, they still presented a bottleneck for prototyping and rapid testing. As an alternative, future work should focus on reducing the cost and time needed for fabrication. Currently, a design that utilizes individually sealed components is being investigated. These components are to be built from readily available material, and are expected to greatly speed up fabrication (see Fig. 2.13). Moreover, these individually-sealed components are expected to improve the modularity of the robot, as future designs can use different

combinations of these pre-built components depending on the tasks at hand.

The electrical system architecture of the next-generation robots will still use much of the design elements developed here (e.g., power design and RPi architecture). However, there are still additional features that need to be implemented in future designs. Specifically, next-generation robots should focus on implementing underwater acoustic communication, satellite communication, and solar charging for these robots. Moreover, new electrical systems should also mimic the modularity of the mechanical components, such that these components offer “plug-and-play” functionality.

The proposed advancements to the system design will allow for the implementation of more interesting behaviors by next-generation robots. In particular, strategies for trajectory tracking and depth maintenance are being investigated [33]. Moreover, the new set of electronics is expected to facilitate fault detection, such as detecting hitting the bottom of a water body, which are useful strategies for practical implementation of these robots.

## **CHAPTER 3**

### **CHARACTERIZATION OF ACOUSTIC DETECTION USING A GLIDING ROBOTIC FISH AS A MOBILE RECEIVER PLATFORM**

In this chapter, we present the applicability of Grace 2 to acoustic telemetry. Generally speaking, TDOA algorithms rely on a target emitting a signal periodically, which is detected by special receivers deployed either at fixed locations or on mobile robots. If multiple receivers detect the same signal, it is possible to infer the target's location using the differences between the detection times at these receivers, which is explored in detail later in Chapter 4.

As the demand for AUVs to study ecology of fish and other aquatic animals increases, there remains a growing need to understand how design elements, operational characteristics, and environmental conditions influence detection performance of telemetry-equipped AUVs. In this chapter, we describe detection performance of an acoustic telemetry receiver mounted on Grace 2 during a series of field trials in a freshwater lake (Figs. 3.2– 3.4). Although the primary purpose of field trials was to field-test hardware and software changes during development, detection performance (efficiency) of the glider-mounted acoustic receiver was also evaluated during each field test. Specific objectives were to (1) compare the detection performance (efficiency vs range) of the AUV-mounted receiver to that of stationary receivers and (2) determine if the detection range performance was related to the direction of travel (i.e., toward vs. away from a remote transmitter), the robot depth, and the pitch during gliding. Environmental variables (wind, water temperature, and acoustic noise) were also explored but data limitations prevented incorporating those data into formal analyses. Results and lessons learned are expected to inform further development of gliding robotic fish and improve the design of AUV-based telemetry performance assessments.



**Figure 3.1: Grace 2 carrying a forward-facing acoustic receiver.**

## **3.1 Methods**

### **3.1.1 Mobile Receiver**

The ability of Grace 2 in carrying larger payloads has allowed us to mount a forward-facing acoustic receiver on the robot (Fig. 3.1), and compare its performance to that of stationary receivers.

The GPS sensor (Garmin GPS 18x LVC) was used for obtaining UTC time and establish the robot's position when it is on the surface, while the pressure sensor was used to measure robot depth underwater. The XBee wireless serial interface was used for communication with a laptop on a boat close to the robot. This channel was used to send commands to the robot or query data from the robot when it was on the surface.

As was discussed in Chapter 2, the hardware and software capabilities of the robot evolved over the duration of this study. In the 2016 trial, all robot operations (i.e., control, communication, and data processing) were implemented on the embedded MCU, and the robot sent its GPS position along with a UTC time-stamp over the XBee channel every 5 seconds whenever it was on the surface. When the robot performed a dive, it temporarily stored depth data that was time-stamped and sent through the XBee channel upon surfacing. In 2017, the robot also temporarily stored



**Figure 3.2: Grace 2 at Higgins Lake, Michigan, 3 November 2017.**



**Figure 3.3: A gliding robotic fish prototype during field experiments in Higgins Lake.**



**Figure 3.4: A gliding robotic fish prototype during field experiments in Higgins Lake.**

orientation (yaw, pitch, and roll angles) information whenever it was underwater. In 2018, we incorporated a Raspberry Pi Zero W that performed high-level tasks such as communication and data storage. This allowed us to complement the original broadcasted messages by storing all available data onto an on-board SD card every 5 seconds. This data consisted of GPS coordinates and UTC time, environmental sensor readings, orientation of the robot (yaw, pitch, and roll angles), positions of each actuator, and battery level.

### **3.1.2 Field Tests**

A self-contained acoustic receiver (VEMCO model VR2Tx; 69 kHz) was attached to the robot as a payload, and field trials were conducted in Higgins lake, Michigan, USA, during 2016 - 2018. The receiver was mounted at the bottom of the robot, facing forward (Fig. 3.1). The receiver measured temperature (internal), tilt (degrees from vertical), and environmental acoustic noise

every 10 minutes. Detection performance was investigated as a function of distance between a test transmitter or ‘tag’ and the receiver, robot direction (toward or away from tag), robot depth, and robot pitch. Wind (from a regional model; see below) and environmental acoustic noise (from the receiver) were also considered as possible explanatory variables but were not included in analyses. Tests (‘runs’) were conducted on 11 November 2016, 3 November 2017, and 14-15 June 2018 in Higgins Lake, Michigan, where water depths ranged between 10-20 m (Fig. 3.5; Table 3.1). These sites were selected to facilitate field testing of navigation and actuation systems on a given day and not necessarily with detection range tests in mind. During each trial, an acoustic transmitter (VEMCO model V8-4H; source power level 147 dB re 1  $\mu$ Pa @ 1 m) was deployed on a stationary mooring (depth ranged 1.5–7.0 m among runs) and emitted a uniquely encoded signal every 24 seconds. The specific model tag was used because it provided a detection range amenable to the field evaluation of the robot in the study system. Specific tag programming (24 s transmit interval) was selected to ensure that testing would provide sufficient sample size for regression models and to capture relatively fine-scale changes in variables of interest (e.g., depth, pitch).

For every test, a target GPS waypoint was sent to the robot from a laptop on a boat over the wireless communication channel, and the robot was tasked with navigating to that location through a series of dives. A depth of 4.5 m was deemed as the “safe” (maximum) diving depth for the robot as the depth rating had not been established for the robot hull. Each dive was completed in approximately 3 minutes on average. Robot heading was controlled by changes in tail position such that the tail acted as a rudder during gliding to maintain course toward the target location. Between dives, the robot remained on the surface for 20 seconds to ensure that a GPS lock was established, and a new GPS position was obtained to calculate the desired heading angle.

### **3.1.3 Mobile Detection Range Tests**

The main objectives for the 2016 trials were to (1) field-test hardware and software and identify any necessary changes, and (2) establish the range of detection for the mobile receiver and compare its detection performance with that of stationary receivers deployed at various distances from the

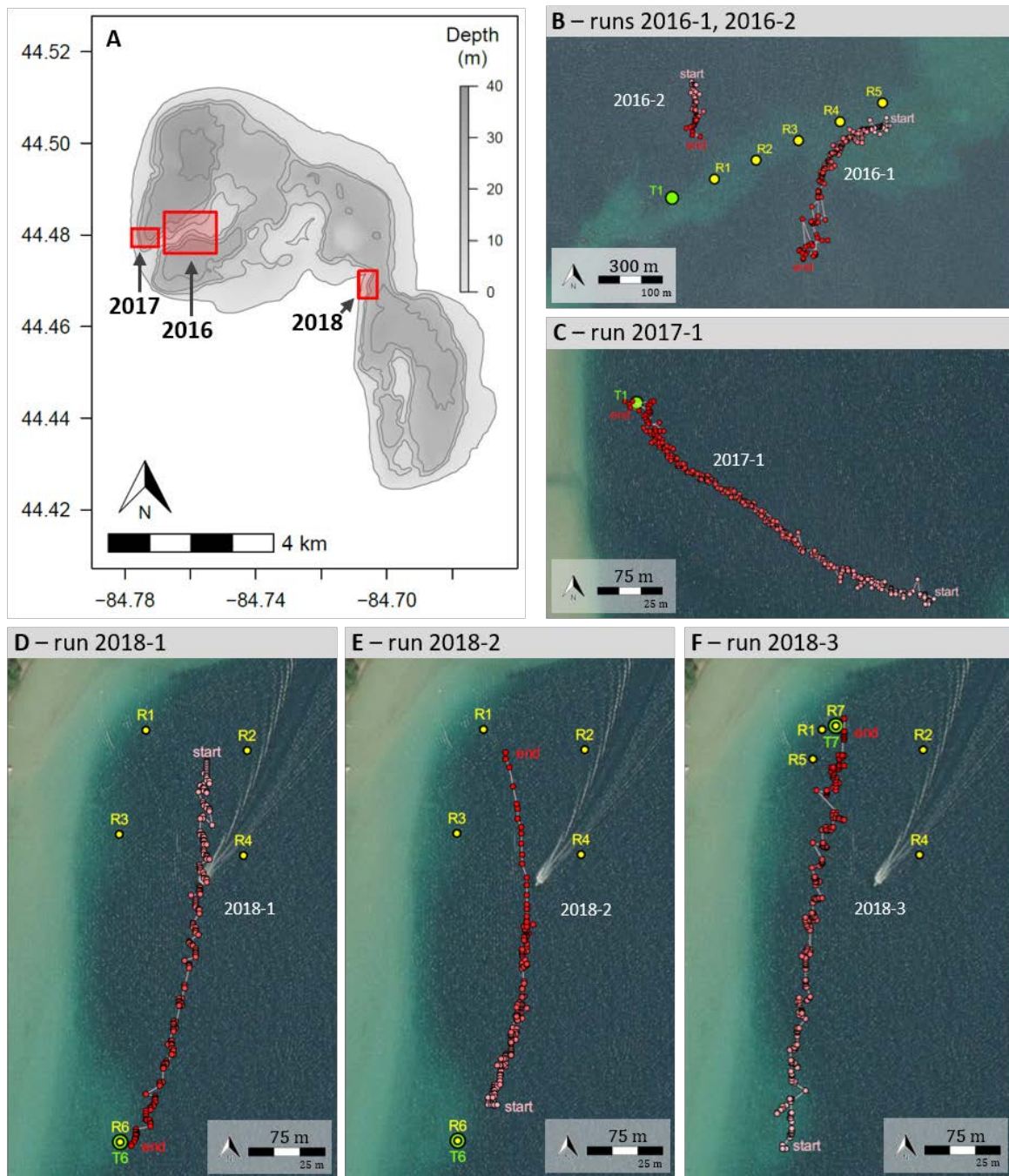


**Figure 3.5: Lake tests (Panel A) Map of Higgins Lake, Michigan showing regions (red rectangles) where gliding robotic fish GRACE was tested 11 Nov 2016 (panel B), 03 Nov 2017 (panel C), and 14-15 June 2018 (panels D-F) with stationary transmitter locations (green circles), stationary receiver locations (yellow circles), and GPS locations (pink/red circles) recorded by the gliding robotic fish during each run. GPS points are shaded along a gradient from start (pink) to end (red) of each run.**

tag. Five acoustic telemetry receivers (VEMCO model VR2Tx 69 kHz) were deployed vertically (hydrophone up) on stationary moorings, suspended 1.5 m below the surface in 7.3–10.0 m water depth. Stationary receivers were arranged in a line with the transmitter such that the receivers were spaced 200, 400, 600, 800, and 1000 m from the transmitter, which was suspended 1.5 m below the surface in 11.0 m water depth. During the first trial (run 2016-1), the robot began navigating 996 m from the transmitter, in a direction roughly parallel to the line of stationary receivers and toward the transmitter. As the trial progressed, winds (approximately 4.9–5.8 m/s, based on a regional model) moved the robot off course while it attempted to obtain a GPS fix. Magnetic disturbance, resulting from the internal electronics and actuators, which affected the stability of the measured heading angle using the on-board Inertial Measurement Unit (IMU), also contributed to the robot veering off-course. Consequently, the robot was removed from water about 563 m from the transmitter, and then returned to the water for a second trial (run 2016-2). During the second trial, the robot started 411 m away from the tag, and was removed from the water 288 m from the transmitter.

Prior to the next field test, robot navigation problems observed in 2016 were addressed. First, the IMU was calibrated to reject larger magnetic disturbances, which improved the stability of the measured heading angle. Additionally, to combat high winds, the robot was tasked with “swimming” (by continuously flapping its tail) on the surface while waiting for a GPS fix.

After these corrections, a second field trial was carried out in 2017. During this trial (run 2017-1), the gliding robotic fish navigated from 389 m to less than 1 m from the tag, in a direction roughly northwest. The tag was suspended 3.0 m below the surface in 19.8 m water depth. Stationary receivers were not deployed during the test in 2017 due to logistical constraints. While the windspeeds during this trial were close to those in 2016 (approximately 4.2 m/s, based on a regional model), the provisions we took with surface swimming allowed the robot to complete its task. During navigation, the tag transmitted 323 times and the robot repeatedly ascended and descended between the surface and 4.5 m depth.

A third set of field trials were conducted in 2018 to investigate the effect of the robot’s direction of travel, depth, and pitch on detection efficiency. In addition, four stationary receivers (R1–R4;

Fig. 3.5) were deployed in roughly a square-shaped pattern to explore the utility of obtaining fine-scale robot tracks using time-difference-of-arrival-based positioning (not evaluated in this work). Stationary receivers were suspended vertically (hydrophone up) 4.7–19.8 m below the surface in 9.3–24.0 m water depth. A fifth stationary receiver was collocated with the stationary tag; both were suspended vertically (hydrophone up) 4.6 m below the water surface in 9.1 m water depth. The robot was tasked with navigating toward the tag during two runs (runs 2018-1, 2018-3) and away from the tag during one run (run 2018-2). Similar to the trials in 2017, the robot was tasked with swimming while awaiting a GPS fix on the surface to counteract surface waves that could push the robot away from its desired course.

Water current and wind data (e.g., velocity and direction) were not measured at the site during testing, but regional wind data were obtained from NCEP’s Global Forecast System [34] using the R package RWind. Model-based estimates of mean wind speed and direction during 3-h intervals (e.g., 00:00–02:59 UTC, 03:00–05:59 UTC, etc.) at 10 m above land surface were obtained for two locations about 24 km west ( $85.0^{\circ}\text{W}$ ,  $44.5^{\circ}\text{N}$ ) and 17 km east ( $84.5^{\circ}\text{W}$ ,  $44.5^{\circ}\text{N}$ ) of the study site. Mean speed and direction between the two locations were used to represent conditions at the study site during the 3-h interval that contained each run.

### **3.1.4 Data Analysis**

Transmitter detection efficiency curves were estimated for stationary and mobile receivers using generalized additive models (GAMs) with binomial error structure<sup>1</sup>. GAMs were used because they relax distributional assumptions and allow greater flexibility in modelling non-linear responses than generalized linear models [35]. For example, a GAM allowed comparisons of the shape of detection range curves among runs and between stationary and mobile receivers. First, the time of each missed detection (i.e., transmitted but not detected) was estimated by sequencing every 24-s through each detection data set to identify time stamps that were not in the detection file

---

<sup>1</sup>Analysis of the acoustic detection data and the GAM models presented in this section were prepared by Dr. Chris Holbrook from the US Geological Survey.

**Table 3.1: Summary of mobile range detection trials with GRACE at Higgins Lake in 2016, 2017, and 2018. Mean heading reflects the bearing from the first GPS measurement toward the last GPS measurement in each run. Wind speed and direction (heading; note that this is the direction the wind vectors are following, not “blowing from” as is customary) are coarse-scale regional estimates based on the NCEP’s Global Forecast System, as described in methods.**

<i>Run ID</i>	<i>Date Time (UTC - 4)</i>		<i>Tag Location</i>	<i>Distance to tag (m)</i>		<i>Mean Heading (°)</i>	<i>Wind Speed (m/s)</i>	<i>Wind Heading (°)</i>
	<i>Start</i>	<i>End</i>		<i>Start</i>	<i>End</i>			
2016-1	11/11/16 10:47	11/11/16 12:38	T1	996	563	219 (SSW)	5.8	187 (S)
2016-2	11/11/16 12:52	11/11/16 13:30	T1	411	288	214 (SSW)	4.9	182 (S)
2017-1	11/3/17 12:45	11/3/17 14:54	T1	389	8	303 (WNW)	4.2	148 (SE)
2018-1	6/14/18 18:06	6/14/18 19:00	T6	360	11	191 (S)	4.1	163 (SSE)
2018-2	6/14/18 19:20	6/14/18 21:13	T6	44	361	3 (N)	1.7	157 (SE)
2018-3	6/15/18 10:06	6/15/18 11:09	T7	408	10	8 (N)	1.9	324 (NW)

for the receiver. A binary indicator variable was used to represent detection (1) or non-detection (0). All data types recorded by the robot (i.e., latitude, longitude, depth, pitch, water temperature) were estimated at time of each detection or non-detection using time-based linear interpolation over measurements recorded by the robot (Fig. 3.6–3.7). Detection efficiency curves were first described separately for each run and for stationary and mobile receivers during each run, by fitting a GAM to data from each run separately, except that runs 2016-1 and 2016-2 were combined. These GAMs simply estimated the probability of detection (binomial response) as a function of distance between tag and receiver (Fig. 3.8).

A GAM was fit to the data from runs 2017-1, 2018-1, 2018-2, and 2018-3 to estimate the detection efficiency as a function of distance between receiver and transmitter, direction of robot relative to transmitter (toward, away), robot depth (meters below water surface), and robot pitch (degrees from horizontal). Runs 2016-1 and 2016-2 were not included in the model because (1) there was little overlap in distances covered between those runs and others (Fig. 3.8); (2) they lacked

pitch data; and (3) depth data were incomplete during those runs. Specifically, the model estimated the log odds (logit) of the probability of detecting each transmitted tag signal as a function of the predictors

$$\text{logit}(p) = b_0 + \text{dir} + s_{rt\_dist:dir} + s_{rt\_dist:run} + s_{depth:dir} + s_{pitch:dir} + \varepsilon$$

where  $b_0$  is the intercept;  $dir$  is the fixed effect of direction;  $s_{rt\_dist:dir}$  and  $s_{rt\_dist:run}$  are smoothed functions of distance for each direction and run;  $s_{depth:dir}$  and  $s_{pitch:dir}$  are smoothed functions of depth and pitch for each direction; and  $\varepsilon$  is error assumed from an independent draw from a normal distribution with zero mean and variance  $\sigma^2$ . Direction-specific smoothers were included to estimate the partial effects of each level of each continuous predictor on the response (detection efficiency). The run-specific smoother for distance was included to account for run-specific variability in detection efficiency not explained by other predictors. To eliminate confounding between run and direction, effects of direction were limited to contrast between runs 2018-1 and 2018-2, which occurred on the same day. This was accomplished by treating runs 18-1 and 18-2 as a single run (“18-1 & 18-2”) in the model. Thus, we assumed that differences between runs 2018-1 and 2018-2 were attributed to change in direction relative to tag and not other variables or conditions. This assumption is supported by similar detection ranges of stationary receivers during those runs (Fig. 3.8C, 3.8D)

An added advantage of a run-specific smoother is that it allows exploration of the unique shape of each curve that might inform future hypotheses about factors influencing the shape of the curve during each run. While it is possible that some across-run variation could be explained by wind, ambient noise, or water temperatures, our observational data set did not have replicate runs (wind, water temperature) or sufficient within-predictor contrast (ambient noise) and thus we did not include those variables in the model. Rather, we use those observations to generate hypotheses from our descriptive analyses.

The model was fit to the data using the *gam* function in the *mgcv* library (v. 1.8.31) [36] in R (v. 3.6.2)[37]. The basis for all smoothing functions was a cubic regression spline with shrinkage ( $bs = “cs”$  in *mgcv*) and 10 knots. Shrinkage smoothers are useful for identifying non-significant

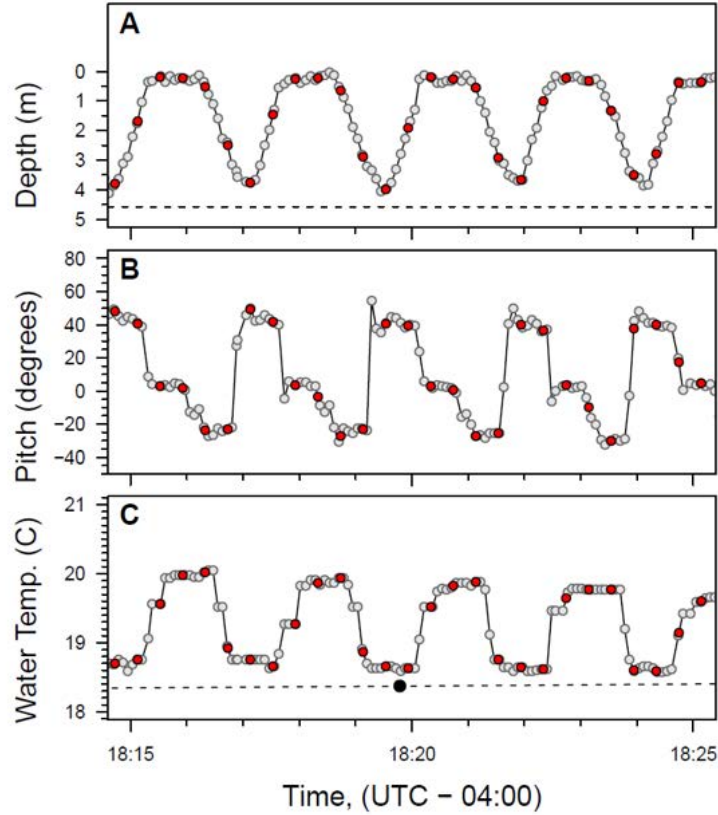


**Figure 3.6: Depth, pitch, and temperature profiles of gliding robotic fish Grace 2 during a 10-minute segment of run 2018-1 in Higgins Lake, with depths recorded by the on-board sensors (open symbols) and estimated depths at the time of test tag signal transmissions (red symbols). Horizontal broken lines show depth (panel A) and temperature (panel C) of stationary transmitter at site T6.**

smoothers by reducing the effective degrees of freedom to a value as small as zero [35]. All smoothers were estimated using restricted maximum likelihood. Prior to model fitting, data were checked for evidence of collinearity (correlations among predictors). Model fit was evaluated by checking for concurvity (non-independence) among smoothers and evidence of non-normality among residuals. Significance of each smoothing term was determined based on estimated degrees of freedom and approximate p-value for the null hypothesis that the smoothing term was zero (see Table 3.2). The significance level for all tests was 0.05. Partial effects plots (see Fig. 3.9) were used to assess the influence of each smoother on the log odds of detection efficiency at each level of the predictor. Plots of fitted values were used to assess the influence of each predictor on detection efficiency during each run on the probability scale.

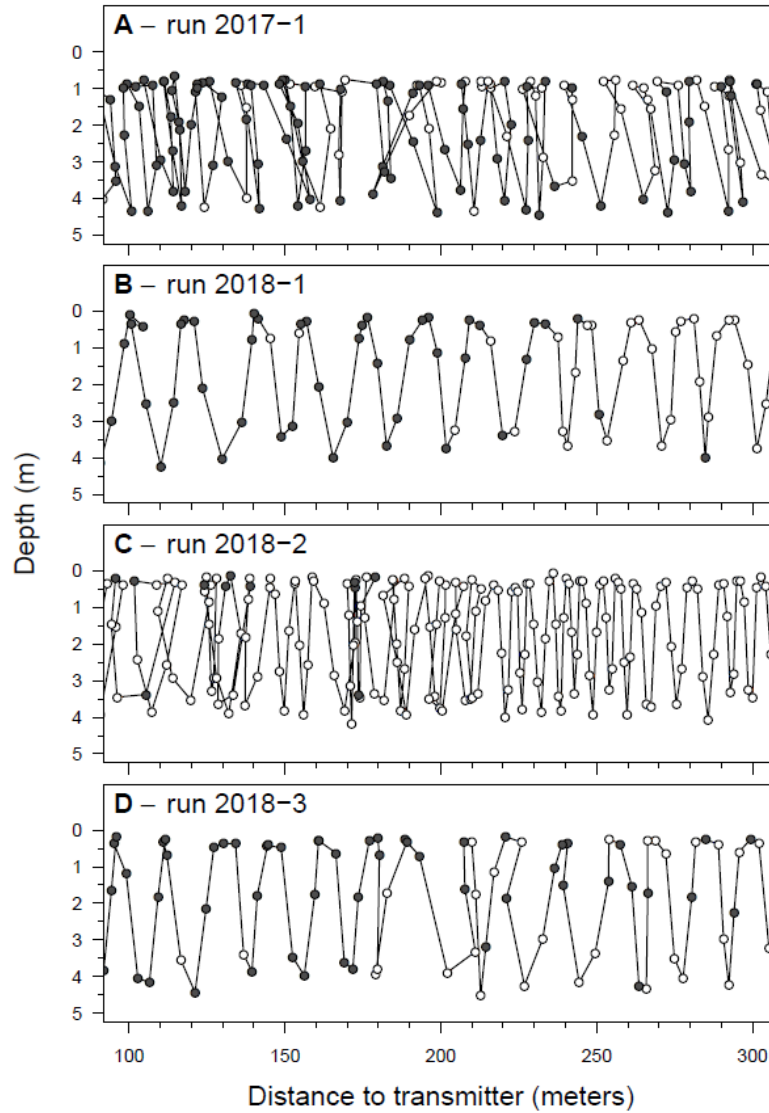


**Figure 3.7:** Depth profiles of gliding robotic fish Grace 2 during a selected 100– to 300–m segment of each run (panels A-D) in Higgins Lake, with locations of test tag transmissions that were detected (closed symbols) or not detected (open symbols) by the on-board receiver.

**Table 3.2: Summary of parametric coefficients (linear terms) and smoothing terms from GAM used to determine if detection range was related to distance from transmitter (Tag Distance, in meters), direction of robot travel relative to transmitter (toward or away), robot depth (Depth, in meters from water surface), or robot pitch (Pitch, in degrees from horizontal). Included for each parametric coefficient is the estimate, standard error (SE), test statistic (Z), and p-value for the null hypothesis that the corresponding parameter is zero. Included for each smoothing term is the estimated degrees of freedom (EDF), test statistic ( $\chi^2$ ), and approximate p-value for the null hypothesis that the smoothing term is zero. Bold faced p-values are significant at significance level of 0.05.**

<i>Linear Terms</i>	<i>Estimate</i>	<i>SE</i>	<i>Z</i>	<i>p-value</i>
(Intercept)	-4.194	0.562	-7.466	<b>8.24E-14</b>
<i>dir = toward</i>	5.19	0.573	9.071	<b>1.18E-19</b>
<i>Smoothing terms</i>	<i>EDF</i>		$\chi^2$	<i>p-value</i>
<i>s(rt_distance) : dir = away</i>	6.33E-04		4.03E-04	0.318
<i>s(rt_distance) : dir = toward</i>	1.432		3.313	<b>1.55E-03</b>
<i>s(rt_distance) : run = 2017 – 1</i>	2.085		6.316	<b>3.62E-04</b>
<i>s(rt_distance) : run = 2018 – 1, 2018 – 2</i>	2.480		46.726	<b>1.25E-13</b>
<i>s(rt_distance) : run = 2018 – 3</i>	1.223		3.417	<b>2.09E-03</b>
<i>s(pitch) : dir = away</i>	0.105		0.112	0.293
<i>s(pitch) : dir = toward</i>	1.103		5.804	<b>8.15E-03</b>
<i>s(depth) : dir = away</i>	1.256		11.658	<b>3.06E-04</b>
<i>s(depth) : dir = toward</i>	0.649		1.326	0.120

**Table 3.3: Speed of the robot relative to ground from the field trials.**

<i>Component</i>	<i>Description</i>
Swimming speed	25 cm/s on average (20 to 30 cm/s)
Glide speed	13 cm/s on average (as low as 5 cm/s against current and a high of 35 cm/s with current)

## 3.2 Results

A rough estimate of the robot's glide speed and swimming speed relative to ground was obtained from the logged data and is shown in Table 3.3.

Estimated detection efficiency of the robot-mounted receiver was lower than concurrently-operated stationary receivers during all three runs where stationary receivers covered the full range of mobile runs(Fig. 3.8A, 3.8C, 3.8D). Scale and shape of detection curves from both stationary and mobile receivers varied among runs. During 2016, when detection range for both stationary

and mobile receivers was larger than during any other run, detection efficiencies for the mobile receiver were only slightly lower than the stationary receivers up to 600 m from the transmitter, but substantially lower at 800 m and 1000 m. The shape of the stationary range curve was unexpected (e.g., higher efficiency at 800 m than 600 m), suggesting that stationary receivers were affected by processes that were not observed. During 2018-1, estimated range was similar between stationary and mobile receivers at distances up to 200 m but differed at larger distances due to mobile detection range declining much faster than stationary detection range. The greatest difference between stationary and mobile detection range was observed during 2018-2 when the robot was moving away from the transmitter. During that run, mobile detection range was markedly lower, even at 50 m—the closest distance between receiver and transmitter during that run.

The GAM model explained 50% of the null deviance. Detection efficiency differed by direction of travel (Table 3.2) with more than a 5-fold increase in the log-odds of detection when moving toward the transmitter than away from the transmitter. Significance of distance-based smoothers suggested that variation in the shape of range curves was attributed to direction of movement and other run-specific variables not included in the model. Pitch was significant when the robot was moving toward the transmitter, but not when the robot was moving away from the transmitter (Fig. 3.9A, 3.9C). Depth was significant when the robot was moving away from the transmitter but not when the robot was moving toward the transmitter (Fig. 3.9B, 3.9D). Over the ranges of depth and pitch observed, the effect of depth on detection efficiency moving away from the transmitter was greater than the affect of pitch moving toward the transmitter (Fig. 3.10).

### **3.3 Discussion**

Understanding detection performance of telemetry receivers can be critical for designing and conducting a successful animal tracking project [5]. Although it is sometimes possible to derive an animal location from detection time differences among multiple hydrophones [22], the location of a receiver at the time of detection is often used to represent the location of a tagged animal at time of detection for “presence-absence”-type data. Detection range data is useful for interpreting spatial

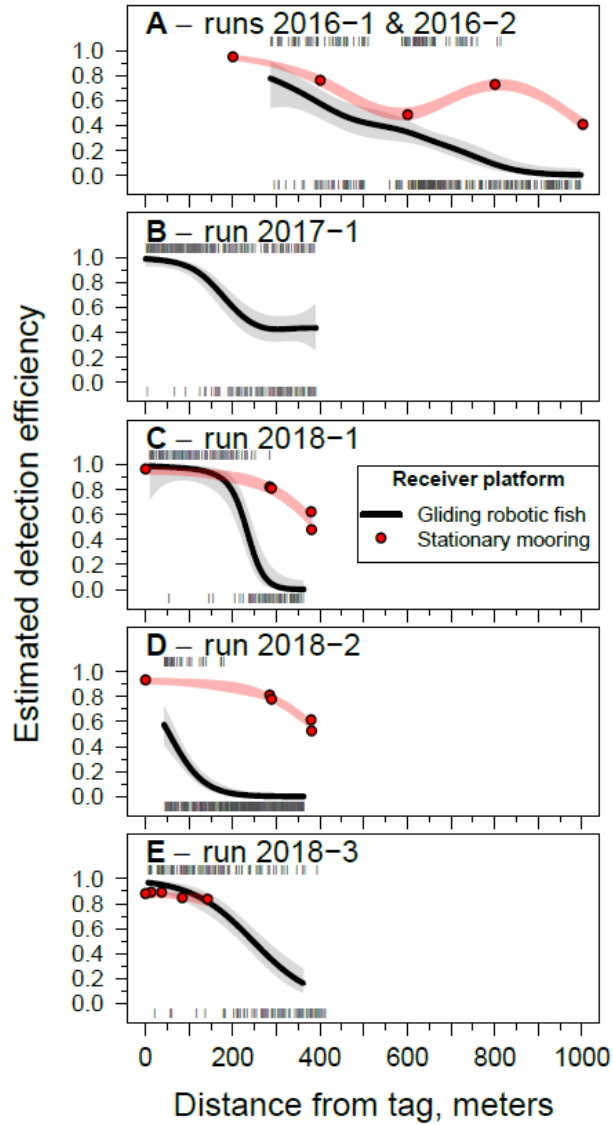


**Figure 3.8:** Estimated efficiencies (proportion of coded signals detected) of detecting an acoustic transmitter on acoustic receivers affixed to stationary moorings (red symbols; red shaded regions are GAM-based 95% confidence regions) and gliding robotic fish Grace 2 (black line; grey shaded regions are GAM-based 95% confidence regions) in Higgins Lake, Michigan during field tests in 2016 (panel A), 2017 (panel B), and 2018 (panels C-E). Vertical grey bars show distances between robot and the transmitter when each coded signal was detected (1) or not detected (0).

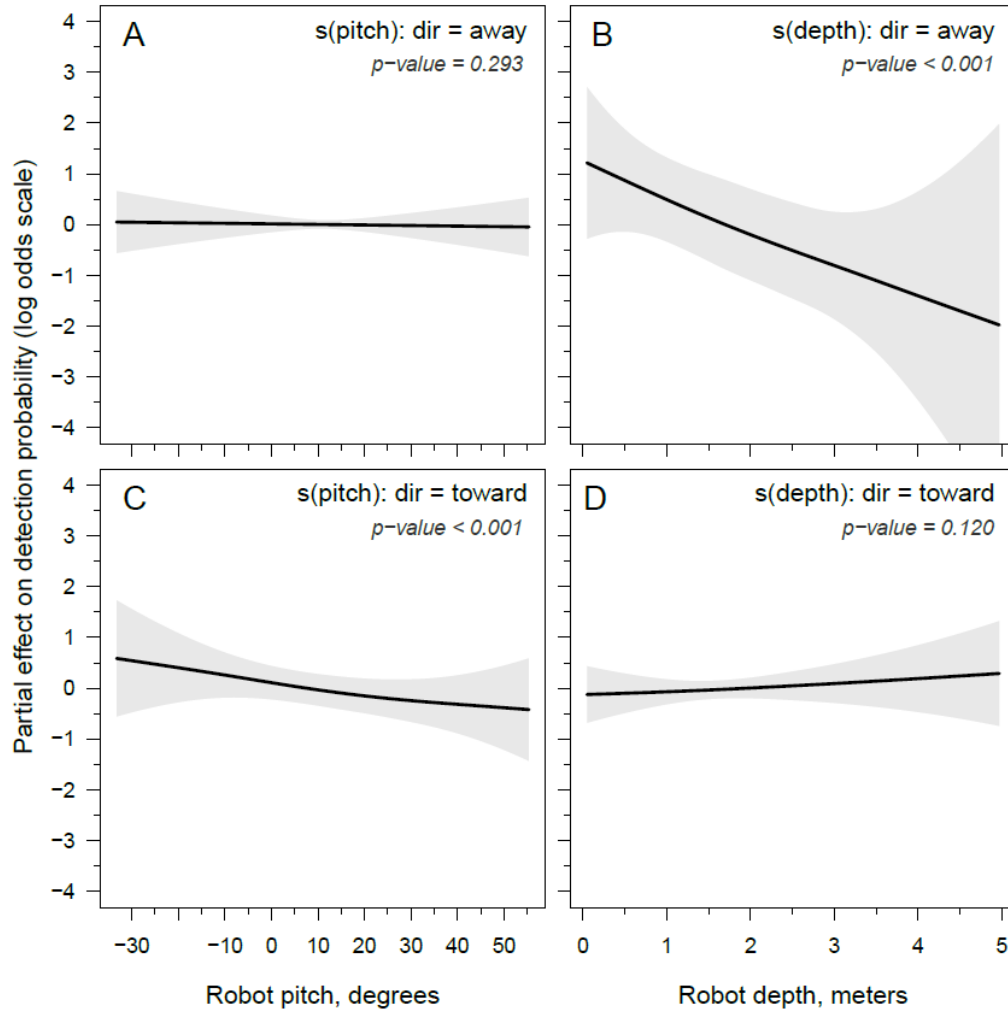


**Figure 3.9: Partial effects of robot depth and pitch on detection probability.** Estimated partial effects of robot depth and pitch on the log odds of detection probability when the robot is moving away from (panels A, B) or toward (panels C, D) a stationary transmitter in Higgins Lake, Michigan.

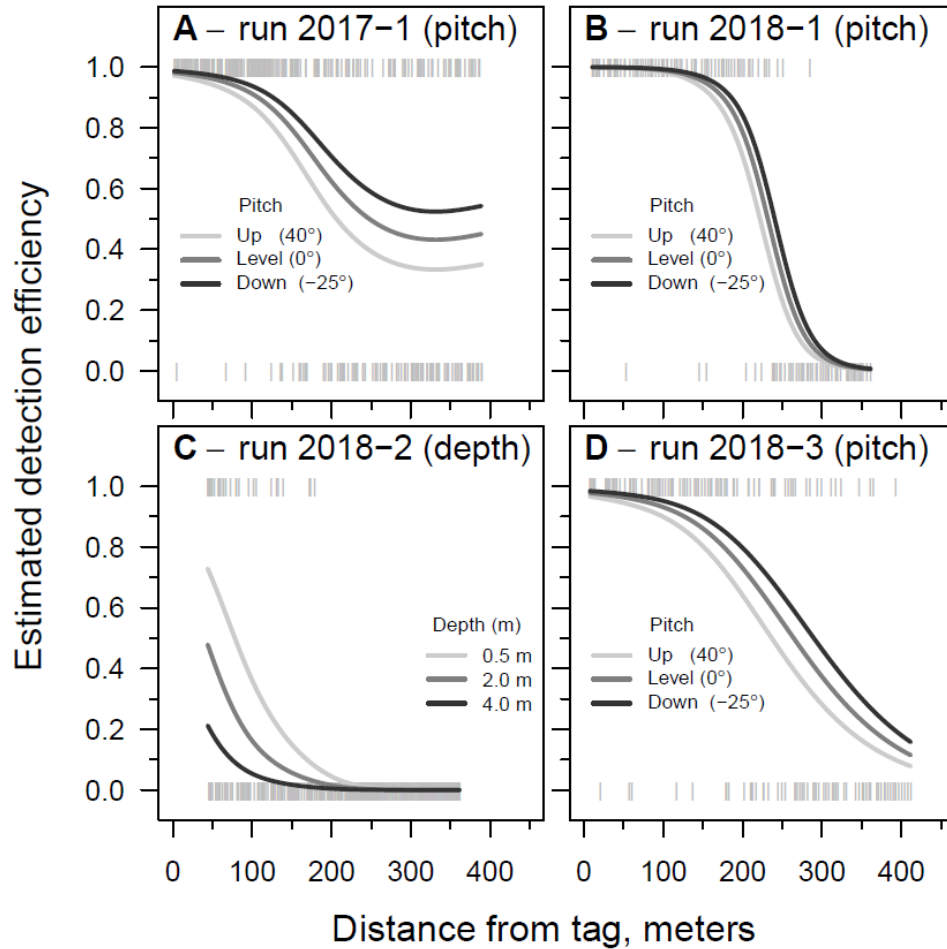


**Figure 3.10:** Estimated efficiencies (proportion of coded bursts detected) of detecting an acoustic transmitter on acoustic receivers affixed to gliding robotic fish Grace 2 in Higgins Lake, Michigan, during field tests in which evidence (GAM model results) suggested that detection range was influenced most by depth when the robot was moving away from the transmitter (panel C) and pitch when the robot was moving toward the transmitter (panel A, B, D).

ambiguity or uncertainty around detection locations but is not commonly collected [38]. Moreover, receivers are often assumed omnidirectional, though several processes contributing to directional or non-uniform detection areas have been described [39]. In our study, decreased detection efficiency when the robot was moving away from the transmitter was not unexpected due to potential shielding of the signal based on position and orientation of the receiver on the robot (attached to the bottom with the hydrophone facing forward) and the importance of line-of-site to acoustic detection. The magnitude of the effect, however, has important implications for the ability of an AUV in this configuration to detect tagged fish and for inferences of fish locations based on detection data.

Depth and pitch are critical control parameters of AUVs that are carefully programmed to ensure mission success in the face of environmental and energetic constraints. When the objective is to detect acoustic-tagged fish, operational adjustments may be needed to achieve favorable balance among detection efficiency and other operational processes (e.g., navigation, communication). Our results suggest that both depth and pitch can influence detection efficiency, even under a narrow scope of environmental conditions. Vertical gradients of environmental variables known to affect acoustic signals in water (e.g., salinity, temperature, suspended particulates, entrained air) exist in most aquatic systems but we were not aware of any such gradients during this study. Although lack of environmental heterogeneity may limit application of these results to other systems, it may have improved our ability to detect relatively small effects by minimizing background variability during our study. Moreover, the potential silver lining of observed variability that is not environmentally-driven is that it may be related to variables that can be controlled or modified.

We hypothesize that decreasing detection efficiency from the surface to 4 m depth when moving away from the transmitter was driven by shielding of the signal by the body of the robot at depth. As described above, this seems reasonable based on position and orientation of the receiver on the robot. If true, then the depth variable used in our analysis may be a proxy for the difference in depth between the hydrophone and the transmitter. Although the range in depth difference between receiver and transmitter in our tests (receiver ranged 0 to 4 m above the tag) may be representative of some shallow environments, potential clearly exists for much greater vertical separation in many

aquatic systems. For an AUV with bottom-mounted receiver, shielding effects are expected to be largest when the vehicle is deeper than a tagged fish and smallest when the vehicle is shallower than the tagged fish. Thus, effects of shielding may be minimized by operational parameters (e.g., depth range) based on knowledge of the ecology of the target organisms (i.e., remaining near the surface for pelagic fish) or structural changes to the vehicle (i.e., positioning the receiver on top of the AUV for surface-oriented fish).

Although the mobile receiver on the gliding robotic fish did not perform as well as stationary receivers throughout the entire range tested, detection performance over shorter distances (300 m or less) are likely still adequate for many active tracking needs. In practice, acoustic transmitter detection ranges vary considerably by hardware and software differences and environmental conditions. Future work may seek to determine if differences between the robot-mounted receiver and stationary receivers are due to characteristics of the robot (e.g., electrical or mechanical noise) or interaction of the robot with the environment (e.g., turbulence of flow over the hydrophone). Regardless of future improvements, however, knowledge of the robot-mounted detection ranges will be useful for planning future missions, including active tracking with a network of AUVs.

Although these results add to our knowledge of AUV performance, much variation in detection efficiency remained unexplained in our analysis. Unfortunately, we were not able to account for the influence of the environmental variables (e.g. wind, water temperature, ambient noise) on the results because availability of those data were limited. However, we are still able to use those observations to generate hypotheses from our descriptive analyses. Our observational data set did not have sufficient replication (multiple runs) over environmental variables (e.g., wind, ambient noise, thermal stratification). Future work should seek to obtain a balanced study design with replicate runs over a range of environment variables, so that one can attribute variation in the detection range to those variables. Obtaining environmental measurements at appropriate resolution and scale is also important, and these measurements likely need to be recorded locally and frequently to be relevant to tag transmissions that occur every minute or less.

### 3.4 Summary and Future Work

AUVs are becoming important tools for understanding the relationships between aquatic organisms and their environment. We present results on the applicability of Grace 2 to acoustic telemetry of tagged fish in fresh and shallow water.

A forward-facing acoustic receiver (VR2Tx) was attached to Grace 2 in order to compare its detection efficiency of acoustic tags (VEMCO model V8-4H) to stationary receivers. Initial tests indicate that the detection efficiency for the mobile and fixed receivers are close up to 600 m, with good detection efficiency at a distance of 300 m (78% for stationary receivers compared to 76% for the mobile receiver). However, the detection efficiency for the mobile receiver drops faster than that of the stationary receivers at greater distances. Lowest detection efficiency is observed when the mobile receiver is facing away from the tag, indicating that alignment between the tag and the receiver's detection cone is important. This can help guide the development of tag tracking controllers and future robot prototypes to minimize shielding of the mobile receiver. As an example, tag-tracking controllers should consider the directionality of the receiver, as well as the relative position of the tag with respect to the receiver. Other options to mitigate this effect include the use of vertically mounted receivers, pointing upwards or downwards [14, 10], using two receivers mounted back to back, or mounting the receiver on an active bracket that can rotate freely to better align the receiver towards the transmitters.

On the other hand, there are some questions that need to be addressed to further characterize the robot's applicability to active tracking of acoustic signals, and acoustic telemetry in general, such as capability of overcoming currents, battery life, and maximum depth rating. Understanding these parameters is important to comparing such prototypes to commercially available tools, and future work will compare using these robots to that of other vehicles. Future work should also focus on conducting more replicate runs over a range of environmental variables (e.g., wind, noise, stratification), and testing real-time control algorithm for active tracking of acoustic tags.

## CHAPTER 4

### TIME-DIFFERENCE-OF-ARRIVAL (TDOA)-BASED DISTRIBUTED TARGET LOCALIZATION BY A ROBOTIC NETWORK

Motivated by the application of tracking tagged fish by a network of gliding robotic fish, we present theoretical treatment for the localization and tracking of a moving target. Much of the work on TDOA-based localization in the literature adopts a centralized approach, in which a reference node is chosen and the times of arrival (TOA) of the emitted signal for all other nodes in the network are subtracted from the reference node's TOA, generating TDOA measurements at fusion hub. If the propagation speed of the signal is known, the TDOA measurements can be converted to range-difference measurements, which are then used to estimate the location of the target [40, 41]. This centralized approach has a long history and is widely used in aerospace systems [42]. Geometric treatment of the problem for a stationary target was considered in [43] and [44], where the target location is inferred from the geometric relations imposed by the TDOA measurements. When the target's location changes with time, dynamic approaches are generally used for localization, in which a filter is used to estimate the target's location. Examples of these methods include utilizing an Extended Kalman Filter (EKF) in [45], or an Unscented Kalman Filter and Particle Filters in [46].

Due to power and bandwidth constraints in robotic networks, centralized information processing is often infeasible, particularly for a large-scale and unreliable networks. Moreover, some sensors cannot transmit their measurements to the reference node due to their limited communication ranges. These drawbacks motivated the investigation of distributed strategies for TDOA-based localization. In [47], decentralized source localization in multihop networks was considered, where a connected dominating set of nodes work as the network backbone to collect the measurements, and a leader node of that set is selected to estimate the target's location, essentially acting as a centralized estimator of the target's position. The need for a common reference node is alleviated in [48], where a network of paired sensors is utilized while requiring all such pairs to be able communicate

with one another. As we discuss later in Section 4.2, this decentralized approach can be improved upon by exchanging estimate information between nodes, allowing for successful estimation without requiring all agents in the network to be connected.

In Appendix A, we show the boundedness of the estimation error using the stochastic stability lemma [49, 50]. However, the conditions developed there are difficult to verify. Namely, finding positive definite matrices which satisfy Lemma A.2.1 are difficult to compute. Moreover, it is not clear how such matrices relate to the underlying communication graph among agents for exchanging information. For those reasons, structural observability is used in this chapter to investigate the network topology conditions for distributed localization of a moving target. It is shown that source localization is not possible (centrally, and therefore distributively) when the total number of TDOA measurement is insufficient. Then, we demonstrate that the target's position can be successfully estimated in a distributed manner if and only if every agent is part of a connected network that collectively has a sufficient number of TDOA measurements, even if each agent has an insufficient number of measurements.

Structural analysis deals with system properties that do not depend on the numerical values of the parameters, but only on the underlying structure (zeros and non-zeros) of the system matrices [51, 52, 53]. It turns out that if a structural property holds for one possible choice of non-zero elements as free parameters, it is true for almost all choices of non-zero elements and, therefore, is called a *generic property* of the system. Furthermore, it can be shown that those particular (non-admissible) choices for which the generic property does not hold, lie on some algebraic variety with zero Lebesgue measure [54]. While this work is similar to [52] and [55] in that it employs structural analysis on the system matrices, there is a significant difference. In particular, the results reported in [52] and [55] treat all non-zero elements as free parameters, which in turn disguises the importance of the *number* of TDOA measurements used in this localization scheme. In Section 4.2, we explicitly consider the role played by using more TDOA measurements, and prove that the system can be rendered generically observable when a sufficient number of TDOA measurements are used.

The work presented here introduces a fully distributed solution to target localization under fixed and time-varying undirected communication topologies. This approach does not require a common reference node or data fusion center, nor does it require each agent to be heavily connected to estimate the target's location on its own. Instead, we show that every agent in the network can successfully localize the target if it is part of a network that has a minimum of 4 connected, non-coplanar agents. As the target moves away from the convex hull formed by the agents, estimation performance begins to degrade and it becomes paramount to track the target as it moves through space. Rather than continuously tracking the target, we further propose an adaptive movement strategy, where the robotic network moves only when the norm of the estimation covariance matrix exceeds a certain limit, to balance the trade-off between estimation performance and distance traveled by the entire mobile network.

## 4.1 Problem Setup

We consider a moving target in the 3D space with  $p(t) = \begin{bmatrix} p^x(t) & p^y(t) & p^z(t) \end{bmatrix}'$  denoting its coordinates at time  $t$ . The target moves randomly in space according to

$$\begin{bmatrix} \dot{p}(t) \\ \ddot{p}(t) \end{bmatrix} = \begin{bmatrix} 0 & I_3 \\ 0 & 0 \end{bmatrix} \begin{bmatrix} p(t) \\ \dot{p}(t) \end{bmatrix} + \begin{bmatrix} 0 \\ I_3 \end{bmatrix} w(t), \quad (4.1)$$

where  $I_3$  is the  $3 \times 3$  identity matrix and  $w(t) \in \mathbb{R}^3$  is the process noise, which is assumed to be zero-mean, white Gaussian noise with covariance matrix  $Q$ .

The target emits a signal periodically that gets detected by a group of  $N$  robotic agents, or nodes, at different times depending on each agent's relative distance to the target. At each detection, agent  $i$  records the signal's TOA and acquires the TOAs of all other agents that can communicate their information to agent  $i$ . These agents form the set of *neighbors* of agent  $i$ , which is denoted as  $\mathcal{N}_i$ . Each agent then subtracts the TOAs of its neighbors from its own TOA, generating a list of time-difference-of-arrival (TDOA) measurements. Assuming that the propagation speed of the signal is known, the measurements available for each agent are given by

$$y_i(kT) = h_i(kT) + v_i(kT), \quad (4.2)$$

where

$$h_i(t) = \begin{bmatrix} h_{i,1}(t) \\ \vdots \\ h_{i,|\mathcal{N}_i|}(t) \end{bmatrix}, \quad (4.3)$$

with

$$h_{i,j}(t) = \|p(t) - p_i(t)\| - \|p(t) - p_{i,j}(t)\|. \quad (4.4)$$

Here,  $T$  is the period at which the signal is emitted,  $v_i(t) \in \mathbb{R}^{|\mathcal{N}_i|}$  is the measurement noise, assumed to be zero-mean, white Gaussian noise with covariance matrix  $R_i$ ,  $p_i(t)$  is the position of agent  $i$ , and  $p_{i,j}(t)$  is the position of the  $j$ -th neighbor of agent  $i$ .

Denoting the target's state as  $x(t) = \begin{bmatrix} p'(t) & \dot{p}'(t) \end{bmatrix}'$ , and discretizing the model in (4.1) with sampling time  $T$ , with slight abuse of notation, we can write the discrete-time model of the target as

$$x(k+1) = Ax(k) + Bw(k), \quad (4.5)$$

where

$$A = \begin{bmatrix} 1 & 0 & 0 & T & 0 & 0 \\ 0 & 1 & 0 & 0 & T & 0 \\ 0 & 0 & 1 & 0 & 0 & T \\ 0 & 0 & 0 & 1 & 0 & 0 \\ 0 & 0 & 0 & 0 & 1 & 0 \\ 0 & 0 & 0 & 0 & 0 & 1 \end{bmatrix}, \quad B = \begin{bmatrix} \frac{T^2}{2} & 0 & 0 \\ 0 & \frac{T^2}{2} & 0 \\ 0 & 0 & \frac{T^2}{2} \\ T & 0 & 0 \\ 0 & T & 0 \\ 0 & 0 & T \end{bmatrix}. \quad (4.6)$$

The time-varying measurement matrix  $H_i(k)$  can be obtained from (4.2), where

$$H_i(k) = \begin{bmatrix} \frac{\partial h_{i,1}(k)}{\partial p^x(k)} & \frac{\partial h_{i,1}(k)}{\partial p^y(k)} & \frac{\partial h_{i,1}(k)}{\partial p^z(k)} & 0 & 0 & 0 \\ \vdots & \vdots & \vdots & \vdots & \vdots & \vdots \\ \frac{\partial h_{i,|\mathcal{N}_i|}(k)}{\partial p^x(k)} & \frac{\partial h_{i,|\mathcal{N}_i|}(k)}{\partial p^y(k)} & \frac{\partial h_{i,|\mathcal{N}_i|}(k)}{\partial p^z(k)} & 0 & 0 & 0 \end{bmatrix}, \quad (4.7)$$

and

$$\frac{\partial h_{i,j}(k)}{\partial p^x(k)} = \frac{p^x(k) - p_i^x(k)}{\|p(k) - p_i(k)\|} - \frac{p^x(k) - p_{i,j}^x(k)}{\|p(k) - p_{i,j}(k)\|}, \quad (4.8)$$

$$\frac{\partial h_{i,j}(k)}{\partial p^y(k)} = \frac{p^y(k) - p_i^y(k)}{\|p(k) - p_i(k)\|} - \frac{p^y(k) - p_{i,j}^y(k)}{\|p(k) - p_{i,j}(k)\|}, \quad (4.9)$$

$$\frac{\partial h_{i,j}(k)}{\partial p^z(k)} = \frac{p^z(k) - p_i^z(k)}{\|p(k) - p_i(k)\|} - \frac{p^z(k) - p_{i,j}^z(k)}{\|p(k) - p_{i,j}(k)\|}. \quad (4.10)$$

## 4.2 Distributed Estimation

In this section, we look into the problem of distributed localization of a moving target using TDOA measurements. The goal is for every agent to estimate the target's position without requiring a central node to collect all measurements and propagate an estimate to all agents in the network. To that end, we first discuss a decentralized estimation scheme, where structural observability analysis is conducted to derive the minimum number of TDOA measurements required for an agent to estimate the target state on its own. We will then discuss the distributed estimation scheme where agents exchange estimate information, and present the necessary and sufficient condition in terms of network topology for achieving stable estimates.

### 4.2.1 Decentralized Estimation

In this approach, each agent runs its own filter using its own TDOA measurements. Here, agents exchange only their locations and TOA values to generate TDOA measurements without exchanging any other pieces of information. Each node implements an extended Kalman filter (EKF) to estimate the target's state

$$\hat{x}_i(k|k-1) = A\hat{x}_i(k-1|k-1), \quad (4.11)$$

$$\begin{aligned} \hat{x}_i(k|k) = & \hat{x}_i(k|k-1) \\ & + K_i(k)[y_i(k) - h_i(\hat{x}_i(k|k-1))], \end{aligned} \quad (4.12)$$

where  $\hat{x}_i(k|j)$  is the  $i$ -th node's estimate of the state at time  $k$  after the  $j$ -th measurement has been processed, and  $K_i(k)$  is its filtering gain, which is computed according to

$$K_i(k) = P_i(k|k-1)H_i(k)' \times [H_i(k)P_i(k|k-1)H_i(k)' + R_i]^{-1}, \quad (4.13)$$

and

$$P_i(k|k-1) = AP_i(k-1|k-1)A' + BQB', \quad (4.14)$$

$$P_i(k|k) = [I - K_i(k)H_i(k)]P_i(k|k-1)[I - K_i(k)H_i(k)]' + K_i(k)R_iK_i(k)', \quad (4.15)$$

where  $P_i(k|j)$  is the  $i$ -th agent's error covariance matrix at time  $k$  after the  $j$ -th measurement has been processed.

It is well-known (see [56] and [57]) that the estimation error for agent  $i$  under this scheme, which propagates as follows,

$$\tilde{x}_i(k+1) = A(I - K_i(k)H_i(k))\tilde{x}_i(k) + \eta_i(k), \quad (4.16)$$

is stable if and only if the pair  $(A, H_i(k))$  is observable, where  $\tilde{x}_i(k) \triangleq x(k) - \hat{x}_i(k|k)$  is the estimation error for agent  $i$  and the vector  $\eta_i(k)$  collects the terms independent of  $\tilde{x}_i(k)$ . In the following, we will show that the pair  $(A, H_i(k))$  is unobservable when agent  $i$  has less than 3 TDOA measurements. To avoid clutter, we will consider only agent 1 of the network, and drop the  $i$  subscript from the following analysis.

As discussed earlier, if a structural property is true for one *admissible* choice of non-zero elements, it is true for *almost all* choices of non-zero elements. Additionally, it can be shown that the choices of parameters for which the generic property does not hold, lie on a hypersurface (see Definition 4.2.1) in the free parameter space with zero Lebesgue measure [54]. Due to the fixed structure of our system matrix  $A$  in (4.6) and the time-varying measurement matrix  $H(k)$  in (4.7), it is beneficial to utilize structural analysis when examining the observability of our system. In the following, we employ a structural approach to establish the minimum number of TDOA measurements needed to render the process generically observable.



**Figure 4.1:** Network of 3 agents monitoring the target with agent 1 as the reference node.

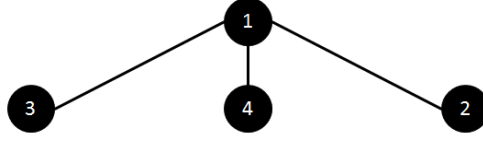


**Figure 4.2:** Network of 4 agents monitoring the target with agent 1 as the reference node.

**Definition 4.2.1** Let  $f = f(x_1, \dots, x_n)$  be a polynomial in the  $n$  variables  $x_1, \dots, x_n$  with coefficients in  $\mathbb{R}$ . Then the point  $\bar{x} = (\bar{x}_1, \dots, \bar{x}_n)$  in  $\mathbb{R}^n$  is called a zero of  $f$  if  $f(\bar{x}_1, \dots, \bar{x}_n) = 0$ . The set of zeros of  $f$  is called the locus of  $f$ . A subset  $V$  of  $\mathbb{R}^n$  is called a hypersurface in  $\mathbb{R}^n$  if it is the locus of a nonconstant polynomial.

First, we consider the case where agent 1 only has two neighbors and, therefore, only two TDOA measurements as shown in Figure 4.1. The measurement matrix  $H(k)$ , in this case, admits the following structure

$$H_\lambda = \begin{bmatrix} \lambda_1 & \lambda_2 & \lambda_3 & 0 & 0 & 0 \\ \lambda_4 & \lambda_5 & \lambda_6 & 0 & 0 & 0 \end{bmatrix}. \quad (4.17)$$

The system is said to be generically observable if the pair  $(A, H_\lambda)$  is observable for almost all values of  $T, \lambda_1, \dots, \lambda_6$ . In other words, the system is generically observable if and only if the observability matrix  $O$  is full rank for almost all values of  $T, \lambda_1, \dots, \lambda_6$ , where

$$O = \begin{bmatrix} H'_\lambda & (H_\lambda A)' & (H_\lambda A^2)' & \dots & (H_\lambda A^5)' \end{bmatrix}'. \quad (4.18)$$

It is well known that  $\text{rank}(O) < 6$  if and only if all  $6 \times 6$  minors of  $O$  are zero [54]. We can easily verify that all  $6 \times 6$  minors of  $O$  in (4.18) are zero, regardless of the values of  $T, \lambda_1, \dots, \lambda_6$ . This implies that the process in (4.5) with measurement matrix (4.7) is unobservable when the node has two or less TDOA measurements<sup>1</sup>.

---

<sup>1</sup>If the node has only one TDOA measurement, and therefore only one neighbor, then there is only one  $6 \times 6$  minor of  $O$  and it is  $\det(O)$ .

Now we consider the case where agent 1 has three neighbors and, therefore, three TDOA measurements as shown in Figure 4.2. The measurement matrix  $H(k)$ , in this case, admits the following structure

$$H_\lambda = \begin{bmatrix} \lambda_1 & \lambda_2 & \lambda_3 & 0 & 0 & 0 \\ \lambda_4 & \lambda_5 & \lambda_6 & 0 & 0 & 0 \\ \lambda_7 & \lambda_8 & \lambda_9 & 0 & 0 & 0 \end{bmatrix}. \quad (4.19)$$

Checking all  $6 \times 6$  minors of  $O$ , we observe that some minors of  $O$  are not identically zero and are all of the form

$$\begin{aligned} \alpha T^3 (\lambda_3 (\lambda_5 \lambda_7 - \lambda_4 \lambda_8) + \lambda_2 (\lambda_4 \lambda_9 - \lambda_6 \lambda_7) \\ + \lambda_1 (\lambda_6 \lambda_8 - \lambda_5 \lambda_9))^2, \end{aligned} \quad (4.20)$$

for some  $\alpha \in \mathbb{R}$ . Therefore, we conclude that  $\text{rank}(O) = 6$  for almost all values of  $T$  and  $\lambda_1, \dots, \lambda_9$ , and that the pair  $(A, H(k))$  is generically observable if the agent has a minimum of 3 TDOA measurements<sup>2</sup>. Furthermore, the set of values that render the pair unobservable is a hypersurface in the free parameter space where the expression in (4.20) is zero. Interestingly, this means that the process is generically observable except when:

- The sampling time used for discretization of the system in (4.5) is 0, or
- All of the points that satisfy

$$\det \begin{pmatrix} \lambda_1 & \lambda_2 & \lambda_3 \\ \lambda_4 & \lambda_5 & \lambda_6 \\ \lambda_7 & \lambda_8 & \lambda_9 \end{pmatrix} = 0,$$

i.e., when the 3 TDOA measurements are linearly dependent, and the 4 agents are coplanar.

For all agents in the network to be able to estimate the target's position under this decentralized scheme, we would require that all such pairs  $(A, H_1(k)), (A, H_2(k)), \dots, (A, H_N(k))$  to be observable, i.e., we would require the pair  $(I_N \otimes A, D_H)$  to be observable, where  $\otimes$  denotes the Kronecker

---

<sup>2</sup>If the node has more than 3 TDOA measurements, it can be verified that  $\text{rank}(O) = 6$  if  $\text{rank}(H_\lambda) \geq 3$ .

product, and

$$D_H(k) \triangleq \begin{bmatrix} H_1(k) & & 0 \\ & \ddots & \\ 0 & & H_N(k) \end{bmatrix}. \quad (4.21)$$

Let  $\hat{\underline{x}}(k|k) = [\hat{x}_1(k|k)' \ \dots \ \hat{x}_N(k|k)']'$  denote the network-wide estimate of the network-wide state  $\underline{x}(k) = [x(k)' \ \dots \ x(k)']' = 1_N \otimes x(k)$ , where  $1_N \in \mathbb{R}^N$  is the column vector whose entries are all 1. The dynamics of this network-wide state can be derived as follows

$$\begin{aligned} \underline{x}(k+1) &= 1_N \otimes (Ax(k) + Bw(k)) \\ &= (I_N \otimes A) (1_N \otimes x(k)) \\ &\quad + (I_N \otimes B)(1_N \otimes w(k)) \\ &= (I_N \otimes A) \underline{x}(k) + (I_N \otimes B) \underline{w}(k), \end{aligned} \quad (4.22)$$

with  $\underline{w}(k) \triangleq 1_N \otimes w(k)$  representing the network-wide process noise. Denoting the  $i$ -th agent's estimation error by  $\tilde{x}_i(k) \triangleq x(k) - \hat{x}_i(k|k)$ , and the network-wide estimation error  $\underline{\tilde{x}}(k) \triangleq [\tilde{x}_1(k)' \ \dots \ \tilde{x}_N(k)']'$ , the dynamics of  $\underline{\tilde{x}}(k)$  are given by

$$\begin{aligned} \underline{\tilde{x}}(k+1) &= (I_N \otimes A) (I_{6N} - K(k)D_H(k)) \underline{\tilde{x}}(k) \\ &\quad + \underline{\eta}(k), \end{aligned} \quad (4.23)$$

where  $K(k)$  is a block-diagonal matrix of the filter gains  $K_1(k) \dots K_N(k)$ , and the vector  $\underline{\eta}(k)$  collects the terms independent of  $\underline{\tilde{x}}(k)$ . This network-wide estimation error can be stabilized if the pair  $(I_N \otimes A, D_H(k))$  is generically observable, where each agent needs to have a sufficient number of neighbors to estimate the process using only its own TDOA measurements.

Under this formulation, each agent can estimate the target's location when it has a minimum of 3 TDOA measurements, corresponding to each agent having a minimum of 3 neighbors. This decentralized approach requires each agent to be heavily connected such that the target system is observable using each agent's own measurements. Next, we discuss how the number of required communication links can be reduced, and argue that it is possible to estimate the target's location without the need for heavily connecting the agents.

### 4.2.2 Distributed Estimation

Consider the dynamical system in (4.22), and noting that for a stochastic matrix  $W \in \mathbb{R}^{N \times N}$ ,  $W1_N = 1_N$ , we can rewrite (4.22) as

$$\begin{aligned}\underline{x}(k+1) &= 1_N \otimes (Ax(k) + Bw(k)) \\ &= W1_N \otimes Ax(k) + 1_N \otimes Bw(k) \\ &= (W \otimes A)\underline{x}(k) + (I_N \otimes B)\underline{w}(k).\end{aligned}\tag{4.24}$$

For this modified dynamical system in (4.24), a centralized filter can be designed with estimation error dynamics that can be expressed as

$$\begin{aligned}\tilde{\underline{x}}(k+1) &= (W \otimes A)(I_{6N} - K_c(k)D_H(k))\tilde{\underline{x}}(k) \\ &\quad + \underline{\eta}(k),\end{aligned}\tag{4.25}$$

where  $K_c(k)$  is the filter gain, which can stabilize the error dynamics if the pair  $(W \otimes A, D_H(k))$  is generically observable. In the following, we will show that it is possible to obtain a network-wide estimation error with dynamics similar to (4.25) by averaging the estimates among neighboring agents.

Let  $W \in \mathbb{R}^{N \times N}$  be a stochastic matrix with entries  $w_{ij} > 0$  if  $i = j$  or if agents  $i$  and  $j$  can exchange information; otherwise  $w_{ij} = 0$ . We assume here that every agent has access to its own information (i.e.,  $w_{ii} > 0$ ), and that the communication links are bidirectional, namely, if agent  $j$  can send its information to agent  $i$ , then the reverse is also true,  $w_{ij}, w_{ji} > 0$ . Every agent in the network implements a filtering scheme similar to the decentralized case, but followed by updating its estimate by averaging the estimates from neighbors and itself. The filter implemented by each agent in the network is then given by

$$\hat{x}_i(k|k-1) = A\bar{x}_i(k-1), \quad (4.26)$$

$$\begin{aligned} \hat{x}_i(k|k) &= \hat{x}_i(k|k-1) \\ &\quad + K_i(k) [y_i(k) - h_i(\hat{x}_i(k|k-1))], \end{aligned} \quad (4.27)$$

$$\bar{x}_i(k) = \sum_{j=1}^N w_{ij} \hat{x}_j(k|k). \quad (4.28)$$

Denoting  $\hat{x}_i(k|k-1)$  by  $\hat{x}_i(k)$ , and substituting (4.27) and (4.28) into (4.26), we can express a one-step formulation of agent  $i$ 's estimate can as

$$\begin{aligned} \hat{x}_i(k+1) &= \sum_{j=1}^N w_{ij} \left[ A\hat{x}_j(k) + \right. \\ &\quad \left. AK_j(k) (y_j(k) - h_j(\hat{x}_j(k))) \right]. \end{aligned} \quad (4.29)$$

The  $i$ -th agent's estimation error is then given by

$$\begin{aligned} \tilde{x}_i(k+1) &= \sum_{j=1}^N w_{ij} \left[ A(I - K_j(k)H_j(k))\tilde{x}_j(k) \right. \\ &\quad \left. + \eta_j(k) \right]. \end{aligned} \quad (4.30)$$

Denoting the network-wide estimation error by  $\underline{\tilde{x}}(k) \triangleq [\tilde{x}_1(k)' \ \dots \ \tilde{x}_N(k)']'$ , then

$$\begin{aligned} \underline{\tilde{x}}(k+1) &= (W \otimes A) (I_{6N} - K(k)D_H(k)) \underline{\tilde{x}}(k) \\ &\quad + \underline{\eta}(k), \end{aligned} \quad (4.31)$$

which is similar to (4.25), except that here the gain matrix  $K(k)$  is restricted to be block-diagonal. As explained in [52], computing such a constrained gain is possible via an iterative cone-complementary optimization algorithm; see [58] and [59] for details. In [60], the authors derived a suboptimal filtering gain inspired by the Markovian jump linear system filtering problem, where

$$\begin{aligned} K_i(k) &= P_i(k|k-1)H_i(k)' \\ &\quad \times [H_i(k)P_i(k|k-1)H_i(k)' + R_i]^{-1}, \end{aligned} \quad (4.32)$$

and

$$P_i(k|k-1) = A\bar{P}_i(k-1)A' + BQB', \quad (4.33)$$

$$\begin{aligned} P_i(k|k) &= [I_6 - K_i(k)H_i(k)]P_i(k|k-1) \\ &\quad \times [I_6 - K_i(k)H_i(k)]' \\ &\quad + K_i(k)R_iK_i(k)', \end{aligned} \quad (4.34)$$

$$\bar{P}_i(k) = \sum_{j=1}^N w_{ij}P_j(k|k). \quad (4.35)$$

Therefore, to ensure the convergence of the networked filter, one has to ensure that the networked system is observable [52]. To that end, we investigate the conditions on the matrix  $W$  and, therefore, the topology of the undirected communication graph among agents, that would render the pair  $(W \otimes A, D_H)$  observable, and therefore ensure the convergence of the networked filter. We first note the following property regarding the powers of the matrix  $W$  from [61].

**Lemma 4.2.2** *Let  $[W^l]_{ij}$  denote the  $(i, j)$  element of the matrix  $W^l$ , where  $W$  is the stochastic matrix representing the communication topology with  $w_{ii} > 0$ . Then,  $[W^l]_{ij} > 0$  if there is a path between agents  $i$  and  $j$  of length less than or equal to  $l$ ; otherwise  $[W^l]_{ij} = 0$ .*

The pair  $(W \otimes A, D_H)$  is observable if and only if  $\text{rank}(O) = 6N$ . Here,

$$O = \begin{bmatrix} D_H(k) \\ D_H(k)(W \otimes A) \\ D_H(k)(W \otimes A)^2 \\ \vdots \\ D_H(k)(W \otimes A)^p \end{bmatrix} = \begin{bmatrix} D_H(k) \\ D_H(k)(W \otimes A) \\ D_H(k)(W^2 \otimes A^2) \\ \vdots \\ D_H(k)(W^p \otimes A^p) \end{bmatrix} \quad (4.36)$$

where  $p = 6N - 1$ . Equivalently, denoting  $O_i$  as the block column representing agent  $i$ 's subsystem, we can write  $O = \begin{bmatrix} O_1 & \dots & O_N \end{bmatrix}$ . From the structure of  $D_H$ , it is easy to see that  $\text{rank}(O) = \sum_{i=1}^N \text{rank}(O_i)$ .

We are now ready to present the main results in this chapter.

**Theorem 4.2.3** *For a network of agents with time-invariant and undirected topology, the system under the proposed distributed TDOA-based localization is observable if and only if every agent is part of a (sub)network that has at least 4 connected, non-coplanar agents.*

**Proof:** *Sufficiency:* We consider the case where agent  $i$  is part of a network that has only 4 connected agents, and note that the following results can be easily extended to the cases where the network has more agents. Since it is always possible to renumber the agents, we will only consider the subsystem corresponding to agent 1, and write

$$O_1 = \begin{bmatrix} H_1(k) \\ \vdots \\ [W^{23}]_{41} H_4(k) A^{23} \end{bmatrix}. \quad (4.37)$$

This agent can be connected to the network in 4 possible ways that are shown in Fig. 4.3<sup>3</sup>. For the ease of presentation, in the following, we examine *Case (d)*, where the agent has only one neighbor, and show that  $\text{rank}(O_1) = 6$ . The other three cases are discussed in Appendix B.1.

#### Case (d)

The structure of  $H_i(k)$  for  $i = 1, \dots, 4$  is as

$$\begin{aligned} H_1(\lambda) &= \begin{bmatrix} \lambda_1 & \lambda_2 & \lambda_3 & 0 & 0 & 0 \end{bmatrix}, \\ H_2(\lambda) &= \begin{bmatrix} -\lambda_1 & -\lambda_2 & -\lambda_3 & 0 & 0 & 0 \\ \lambda_4 & \lambda_5 & \lambda_6 & 0 & 0 & 0 \end{bmatrix}, \\ H_3(\lambda) &= \begin{bmatrix} -\lambda_4 & -\lambda_5 & -\lambda_6 & 0 & 0 & 0 \\ \lambda_7 & \lambda_8 & \lambda_9 & 0 & 0 & 0 \end{bmatrix}, \\ H_4(\lambda) &= \begin{bmatrix} -\lambda_7 & -\lambda_8 & -\lambda_9 & 0 & 0 & 0 \end{bmatrix}. \end{aligned}$$

---

<sup>3</sup>The graphs shown in Fig. 4.3 represent the minimum number of links required for each graph to be connected. It is possible to add more edges among agents in these graphs and adding more links will only help in terms of observability.

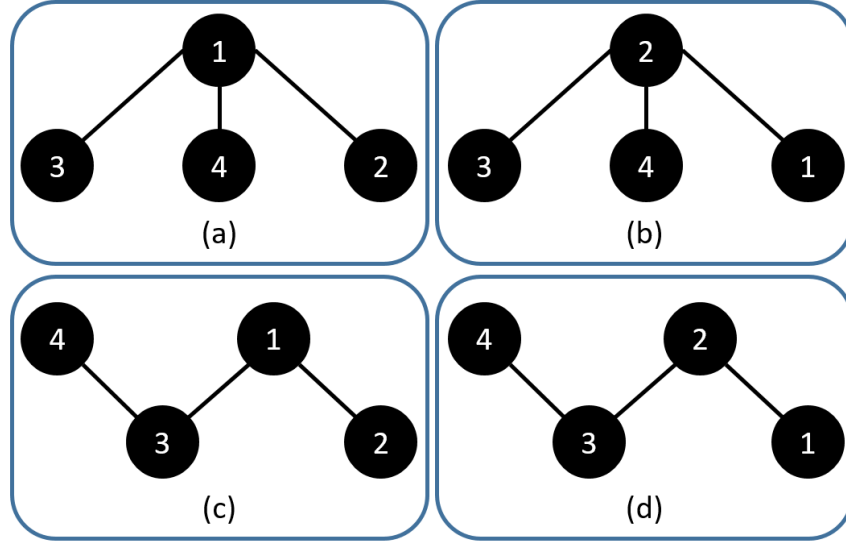


**Figure 4.3:** The 4 possible configurations for node 1 to be connected to the network using the minimum number of edges.

Recalling that

$$\text{rank} \begin{pmatrix} C \\ \vdots \\ CA^{n-1} \end{pmatrix} = \text{rank} \begin{pmatrix} CA^k \\ \vdots \\ CA^{k+n-1} \end{pmatrix},$$

it can be shown that the pair

$$\left( A, \begin{bmatrix} H_1(\lambda) \\ H_3(\lambda) \\ H_4(\lambda) \end{bmatrix} \right)$$

is generically observable, implying that

$$\text{rank} \begin{pmatrix} H_1(\lambda) \\ H_3(\lambda) \\ H_4(\lambda) \\ \vdots \\ H_1(\lambda)A^6 \\ H_3(\lambda)A^6 \\ H_4(\lambda)A^6 \end{pmatrix} = 6.$$

for almost all values of  $T$  and  $\lambda$ . Additionally,  $\text{rank}(O_1) = 6$  for almost all values of  $T$  and  $\lambda$ . Specifically, this generic property holds for all values of  $T$  and  $\lambda$ , except for when the 4 agents are coplanar. Since it is always possible to renumber the agents, then if every agent is connected to the network that has a minimum of 4 connected, non-coplanar agents, then the pair  $(W \otimes A, D_H(k))$  is generically observable. The proof for the other cases follows a similar approach, and is presented in Appendix B.1.

*Necessity:* If an agent is disconnected, or is part of a network that has less than 4 agents, then there are not enough pieces of information to estimate the target's position centrally, let alone distributively, and the error dynamics in (4.25) – and therefore (4.31) – cannot be stabilized. ■

For a time-varying, undirected communication graph, Theorem 4.2.3 can be extended to offer a scalable approach that is somewhat robust to communication link dropout.

**Corollary 4.2.4** *For a time-varying undirected network, if every agent remains part of a network that has a minimum of 4 connected, non-coplanar agents then the networked system under the proposed distributed estimation scheme is observable.*

**Proof:** As the network connectivity changes, if every agent remains part of a network that has a minimum of 4 connected, non-coplanar agents, then it can be shown that  $\text{rank}(O_i) = 6$  for every agent in the network. This, in turn, ensures that the networked system is observable by Theorem 4.2.3. ■

## 4.3 Target Tracking with Coordinated Robotic Network Movement

In this section we look into the second part of the problem. We begin the discussion by investigating the agent formation needed for optimum localization of the target.

### 4.3.1 Optimal Formation

For a network of  $N$  agents, there is a total number of  $N(N - 1)/2$  possible agent pairs. Let  $\mathcal{I}_0 = \{(i, j) | 1 \leq j < i \leq N\}$  denote the set of all agent pairs and  $\mathcal{I} = \{(i, j) | j < i, w_{ij} > 0\}$ , a

subset of  $\mathcal{I}_0$ , represent the set of agent pairs used for estimation. From the definition of  $w_{ij}$ , it is clear that  $\mathcal{I}$  depends on the communication topology among agents.

The Cramer-Rao bound (CRB) is a lower bound for the covariance matrix of unbiased estimators and is given by the inverse of the Fisher information matrix [62]. With  $y \triangleq [y'_1 \ \dots \ y'_N]$ , the Fisher information matrix is given by

$$J = E \left[ \left( \frac{\partial}{\partial p} \ln f(y|p) \right) \left( \frac{\partial}{\partial p} \ln f(y|p) \right)' \right], \quad (4.38)$$

where  $f(y|p)$  is the probability density function (PDF) of  $y$  given  $p$  and  $E[\cdot]$  denotes the expectation on  $y$ . Note that the measurement noise  $v_i$  is assumed to be Gaussian with zero mean. Assuming that  $R_i = \sigma_v^2 I_{|\mathcal{N}_i|}$ , one arrives at a  $3 \times 3$  Fisher information matrix by Chan and Ho<sup>4</sup> [63]

$$J = \frac{1}{\sigma_v^2} G G', \quad (4.39)$$

where

$$G = \left[ g_{ij} \ \dots \right]_{(i,j) \in \mathcal{I}}, \quad (4.40)$$

$$g_{ij} = g_i - g_j, \quad (4.41)$$

$$g_i = \frac{p - p_i}{\|p - p_i\|}. \quad (4.42)$$

Clearly,  $g_i$  is a unit-length vector pointing from agent  $i$  to the target, and the matrix  $G$  depends on the target position, agents' positions, and the set  $\mathcal{I}$  of agent pairs used for localization.

Since the CRB is a square matrix, we seek a formation of agents that minimizes of the trace of the CRB,

$$\text{tr}(J^{-1}) = \sigma_v^2 \text{tr}([G G']^{-1}), \quad (4.43)$$

which is a lower bound for the sum of variances of unbiased estimators for all elements of the target's position  $p$ . In order to obtain the lowest possible CRB, and therefore a better performance by the estimator, all agent pairs in the network need to be considered, and  $\mathcal{I} = \mathcal{I}_0$ , requiring a fully-connected network. The necessary and sufficient conditions to achieve a minimum CRB are

---

<sup>4</sup>Here, the propagation speed of the transmitted signal is normalized to one.

presented in [62]. It is known that the optimum 2D formation is that of a *uniform angular array* where all agents are equally distributed around a circle of radius  $R$ , for some arbitrary  $R > 0$ , centered around the target [62]. Similarly, in the 3D case, the optimal configurations for a complete network are the 3D equivalent of uniform angular arrays, known as the Platonic solids.

**Remark 4.3.1** *The biggest drawback in achieving optimal estimation is that it requires the complete connectivity of the corresponding agent network. This requirement can be relaxed if one is interested in sub-optimal performance. We note that since the performance depends on the shape of the formation, one can search the shape space of the agent formation space to arrive at topology-specific shapes that minimize (at least locally), the associated CRB. In this work, we specify the formation to be that of a Platonic solid, even when the network is not completely connected.*

The goal of tracking the moving target by the network is to ensure adequate localization using the distributed estimator. However, it is not necessary to continuously move the robots with the target. In order to balance the trade-off between the cumulative distance traveled and the estimation performance, each agent can utilize the norm of the error covariance matrix,  $\|P_i\|$ , and only apply the tracking control if the  $\|P_i\| > \underline{b}$  for some constant  $\underline{b} > 0$ . Note that  $\underline{b}$  is a design parameter a user can set depending on the specific problem. In particular, this parameter allows the user to mediate between two extreme cases, 1) minimizing energy and remaining stationary ( $\underline{b} = \infty$ ), and (2) maximizing estimation performance by continuously tracking the moving target ( $\underline{b} = 0$ ). While this switching control strategy is not guaranteed to drive each agent to its corresponding desired location, it can greatly reduce the total distance traveled by all agents, as is illustrated in the following section.

In order to guarantee that all agents move together, or keep still at the same time, we exploit the average-based consensus scheme in (4.28) and (4.35) between TDOA measurements. Namely, every  $\tau \ll T$  seconds, each robotic agent  $i$  in the network communicates and averages its estimate and covariance matrix with its neighbors  $\mathcal{N}_i$ . This ensures that all agents agree on their covariance

matrices and coordinate their movements<sup>5</sup>.

## 4.4 Simulation Results

In this work, we use each robot's estimate of the target's state to arrive at the desired position of each robot. To facilitate the simulation, we consider a simplified model of a propelled underwater vehicle with steering control in yaw and pitch. The model used for each agent in the network is given by:

$$\begin{bmatrix} \dot{p}_i^x \\ \dot{p}_i^y \\ \dot{p}_i^z \\ \dot{v}_i \\ \dot{\phi}_i \\ \dot{\gamma}_i \\ \dot{\omega}_{i,\phi} \\ \dot{\omega}_{i,\gamma} \end{bmatrix} = \begin{bmatrix} v_i \cos(\phi_i) \cos(\gamma_i) \\ v_i \sin(\phi_i) \cos(\gamma_i) \\ v_i \sin(\gamma_i) \\ a_i \\ \omega_{i,\phi} \\ \omega_{i,\gamma} \\ u_{i,2} \\ u_{i,3} \end{bmatrix} \quad (4.44)$$

where  $p_i = \begin{bmatrix} p_i^x & p_i^y & p_i^z \end{bmatrix}$  denotes the position of agent  $i$  in the inertial frame,  $v_i$  represents the agent's linear velocity along its body-fixed  $x$  axis, which stretches from the robot center to the front of the robot. The angle  $\gamma_i$  is the angle between the inertial  $z$  axis and agent  $i$ 's body-fixed  $x$  axis, while  $\phi_i$  is the robot's yaw angle measured as the angle between the inertial  $x$  axis and the projection of the body-fixed  $x$ -axis onto the inertial  $x - y$  plane. The terms  $\omega_{i,\phi}$  and  $\omega_{i,\gamma}$  are the rates of change of the angles  $\phi_i$  and  $\gamma_i$ , while  $a_i, u_{i,2}$ , and  $u_{i,3}$  represent the control inputs for the robot. Figure 4.4 illustrates the the robot position and relevant angle in the sagittal ( $x - z$ ) plane.

The estimated position of the moving target is fed into a feedback linearization control strategy to drive each agent to its desired position (see Appendix B.2 for details). The desired state for agent

---

<sup>5</sup>Exchanging information on a much quicker time scale is only needed to ensure that the agents coordinate their movement, and is not a requirement for the distributed estimator.

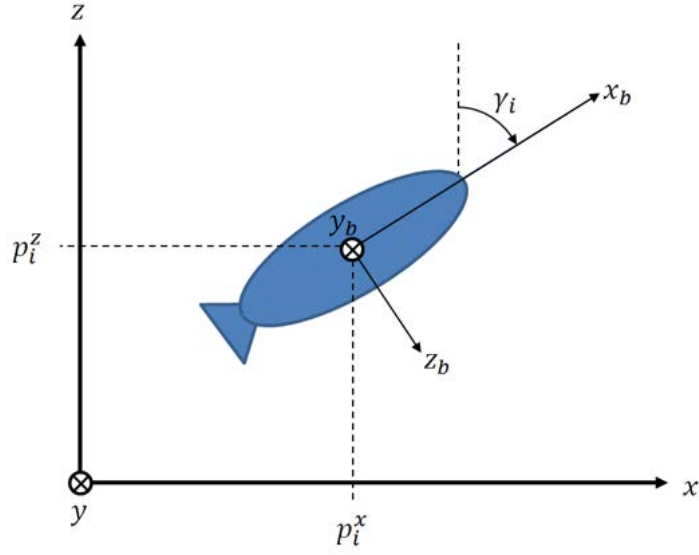


**Figure 4.4: Illustration of the simplified model of a propelled underwater robot with steering control, with a view on the sagittal plane. The robot has similar yaw control in the horizontal plane.**

$i$  can be obtained from its estimate of target's state:

$$p_i^\star = \hat{p}_i + d_i \quad (4.45)$$

$$v_i^\star = \|\hat{p}_i\| \quad (4.46)$$

$$\phi_i^\star = \tan^{-1} \left( \frac{\hat{p}_i^y}{\hat{p}_i^x} \right) \quad (4.47)$$

$$\gamma_i^\star = \sin^{-1} \left( \frac{\hat{p}_i^z}{\|\hat{p}_i\|} \right) \quad (4.48)$$

$$(4.49)$$

where  $d_i$  is a constant vector that defines the position of agent  $i$  relative to the target.

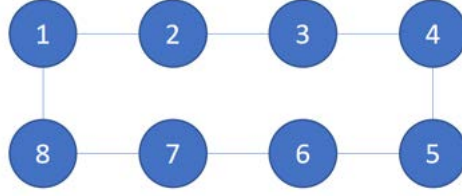


**Figure 4.5:** The fixed communication topology among a network of 8 agents. It is clear that no agent in the network has a sufficient number of neighbors (and therefore TDOA measurements) to estimate the process on its own.

The proposed approach was simulated for a network of  $N = 8$  agents with initial positions:

$$\begin{aligned}
 p_1 &= [-7 \quad 3 \quad 5]' \\
 p_2 &= [1 \quad -2 \quad -5]' \\
 p_3 &= [5 \quad -1 \quad 4]' \\
 p_4 &= [7 \quad 4 \quad -2]' \\
 p_5 &= [-5 \quad 2 \quad -2]' \\
 p_6 &= [0 \quad -6 \quad 7]' \\
 p_7 &= [7 \quad -5 \quad 1]' \\
 p_8 &= [-1 \quad 2 \quad -1]'
 \end{aligned}$$

as shown in Figure 4.6. The measurement noise covariance matrix for each agent was set to  $R_i = I_{|\mathcal{N}_i|}$ . Estimators of each agent were initialized with  $\hat{x}_i = [0 \quad 0 \quad 0 \quad 0 \quad 0 \quad 0]'$  and  $P_i = 100I_6$ . The initial position of the moving target was set to  $[17 \quad -5 \quad -15]'$ , with a process noise covariance matrix  $Q = 0.01I_3$ . The emitted signal from the source was assumed to have a period of  $T = 1$  s, while the average-based consensus was carried every  $\tau = 0.1$  s. The desired formation for all agents was set to that of a cube, i.e. a Platonic solid with 8 vertices, with a the radius of the underlying sphere set to 10.

First we utilized the fixed communication topology shown in Fig. 4.5. Figs. 4.7a and 4.7b show the final network configuration for the two extreme cases  $\underline{b} = 0$  and  $\underline{b} = \infty$ , respectively.

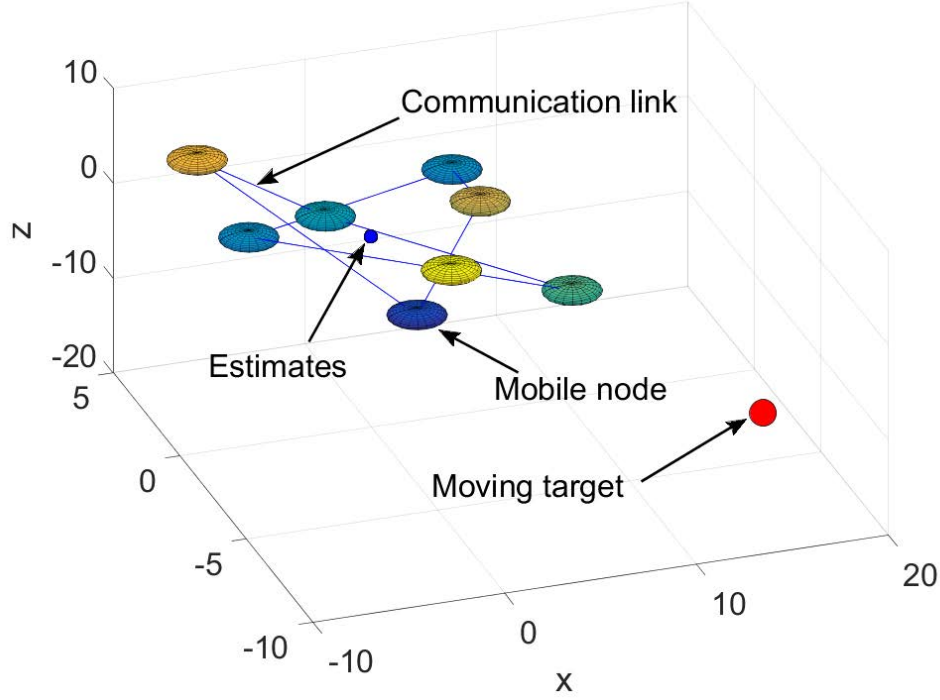


**Figure 4.6: Initial setup for simulation environment with a fixed communication topology. The big circle represents the moving target, while the small circles (overlapping one another at the origin) represent the initial estimates of the target's location for each robot. The ellipsoids represent the mobile robots, while the thin lines connecting them represent the communication links.**

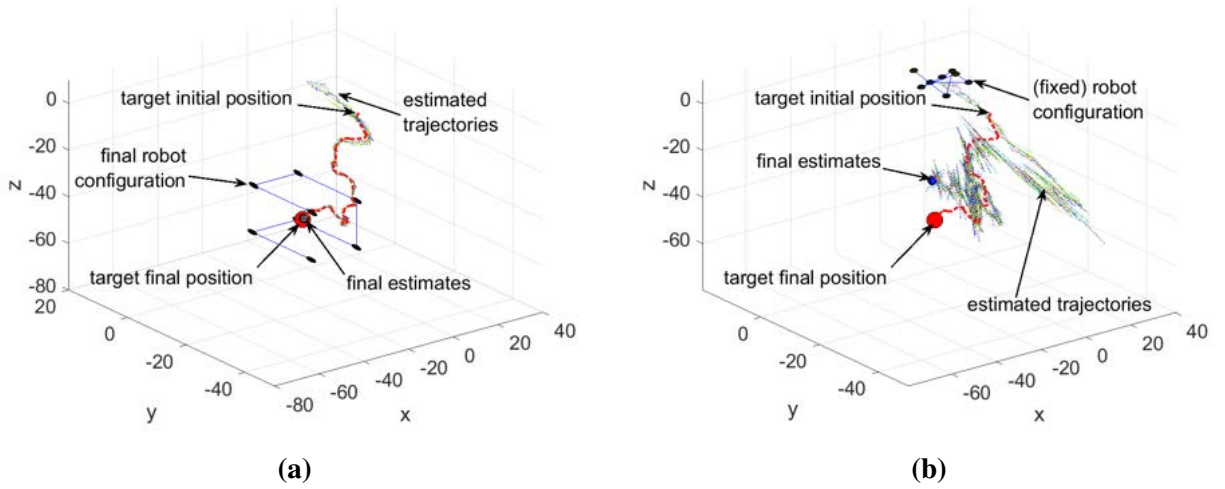


**Figure 4.7: Simulation results of the robots for the two extreme values of  $\underline{b}$  under a fixed communication topology where (a) the robots are constantly moving with target ( $\underline{b} = 0$ ), and (b) the robots are staying put ( $\underline{b} = \infty$ ).**

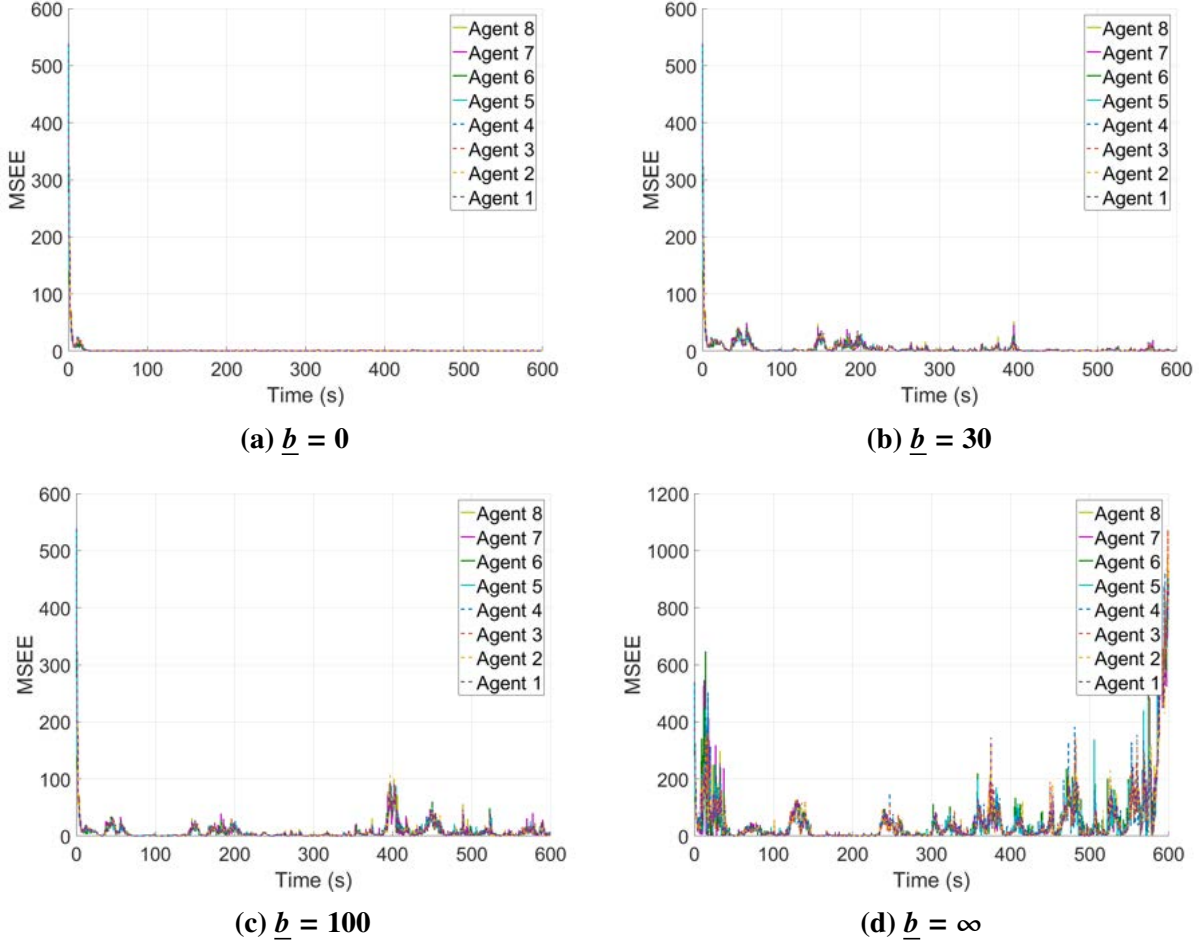


**Figure 4.8: Comparison of the Mean Squared Estimation Error (MSEE) of for each agent in the network for different values of  $\underline{b}$  under a fixed communication topology.**

When  $\underline{b} = 0$ , the network prioritizes minimizing the covariance norms over the total traveled distance, causing the network to continuously track the moving target with its desired formation. On the other hand, when  $\underline{b} = \infty$ , the robots attempt to hold their positions to minimize the overall traveled distance without any consideration to the covariance norms. Figs. 4.8 and 4.9 show the estimation performance (estimation error and covariance in (4.31) and (4.35), respectively) for different values of  $\underline{b}$ , while Fig. 4.10 depicts the corresponding cumulative distance traveled by all agents in the network. From these figures, it can be seen that as  $\underline{b}$  increases, the overall traveled distance decreases while the covariance norms increase, causing the network to remain stationary more often in exchange for less reliable estimation, as is also captured in Fig. 4.9.

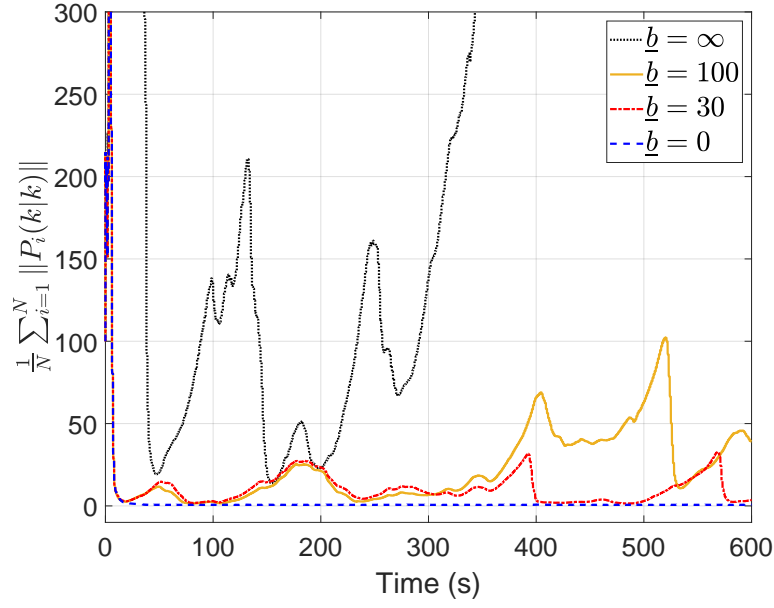


**Figure 4.9: Comparison of average covariance norms for different  $\underline{b}$  values under a fixed communication topology.**

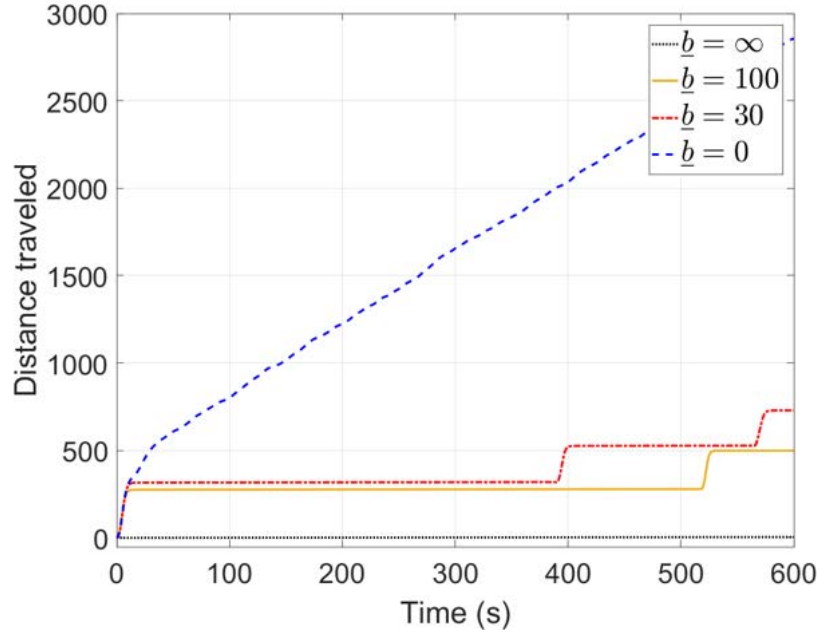


**Figure 4.10: Comparison of the collective distance traveled by the entire network for different  $\underline{b}$  values under a fixed communication topology.**

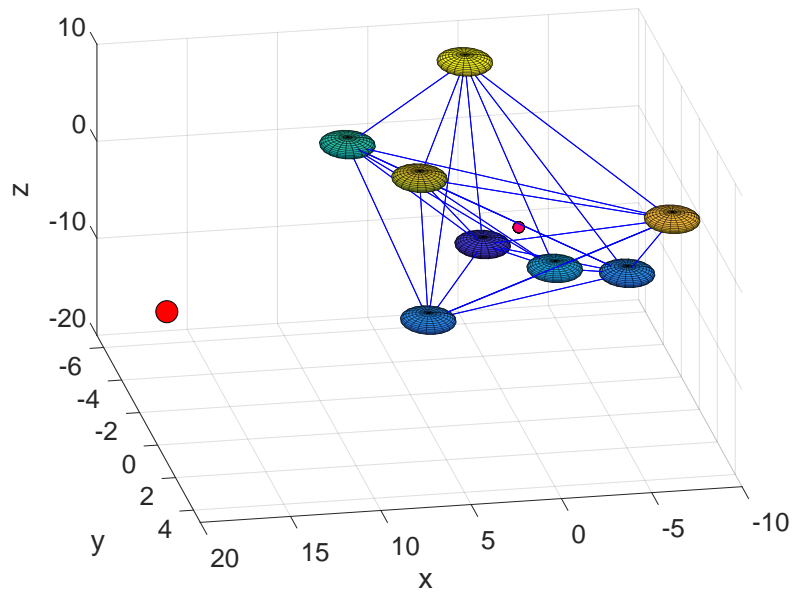


**Figure 4.11: Initial setup for distance-based communication links.**

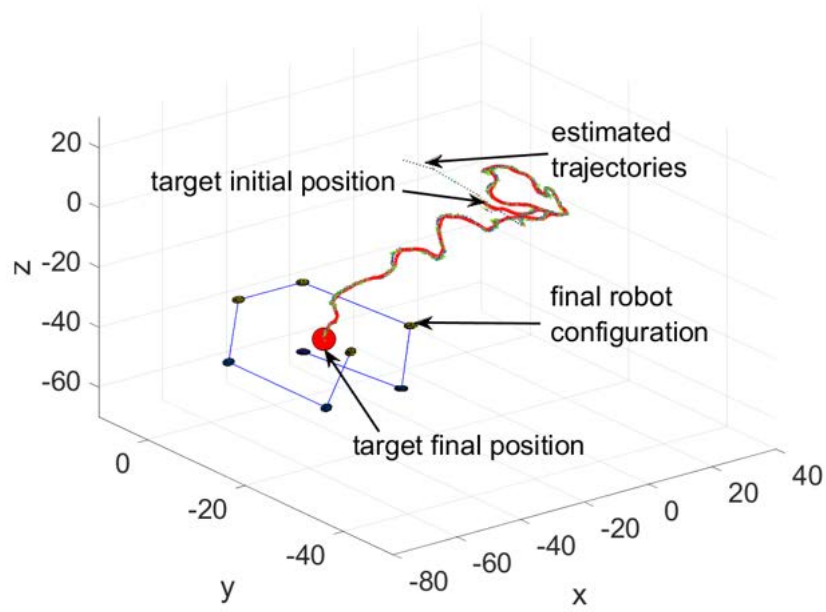


**Figure 4.12: Final setup for distance-based communication links.**

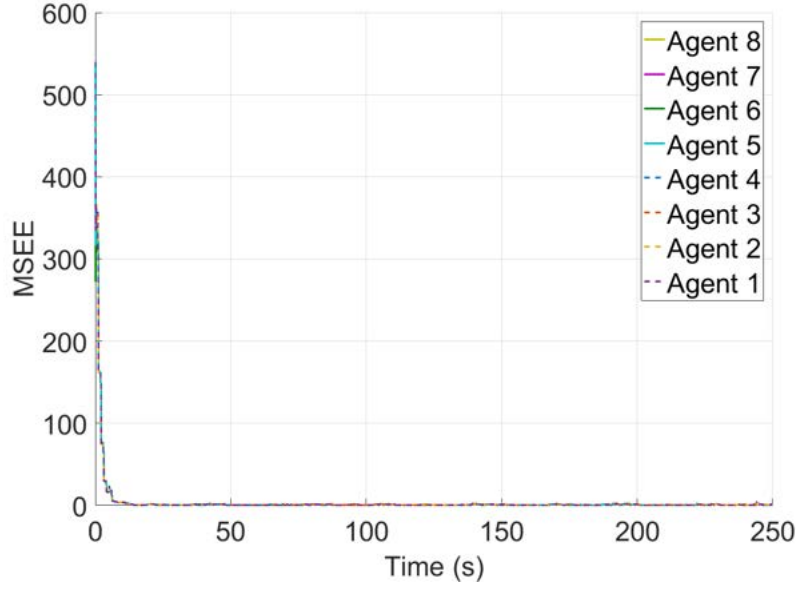


**Figure 4.13: Mean Squared Estimation Error (MSEE) under a time-varying communication graph with continuous tracking ( $\underline{b} = 0$ ) .**

For the case of a time-varying communication network, we implemented a *distance* rule where a communication link exists between any two agents if the distance between them is strictly less than 21. To ensure that no agent has a sufficient number of measurements to estimate the process on its own, we deformed the desired tracking formation so that the distance between some agents would be large enough. Figs. 4.11–4.12 show the initial and final setup, respectively, as the agents constantly track the target position (i.e.,  $\underline{b} = 0$ ). Initially the communication graph is fully connected as all agents are close enough. As the distance between the robots increases, some of the communication links are lost. Finally, it is clear from Fig. 4.13 that successful estimation is achieved even as the communication graph changes and some of the communication links are dropped.

## 4.5 Summary and Future Work

We investigated the problem of distributed localization of a moving target by a network of agents using TDOA measurements from first observability principles. Structural observability principles were utilized to highlight the importance of having enough measurements to accurately localize the moving target. We showed that a decentralized approach without exchanging estimates

requires every agent in the network to be heavily connected to localize the target on its own. On the other hand, under the distributed approach, we showed that when the agents exchange information and fuse their estimates, then it is indeed possible for every agent in the network to estimate the target's position without needing to be heavily connected. Specifically, we showed that if every agent is connected to a network with a minimum of 4 connected, non-coplanar agents, then the process is rendered generically observable and each agent can accurately localize the target. This work can be extended to time-varying communication topologies that are commonly encountered when the communication links depend on the distances between the robots as they move. The distributed filtering approach offers a degree of robustness to communication link dropouts, and has been shown to perform well if the minimum connectivity condition holds. Furthermore, we proposed a movement control strategy that aims to balance the trade-off between estimation performance and total distance traveled by the network. A single parameter,  $\underline{b}$ , is specified to tune the network performance between the two extreme cases of continuously tracking the target (best estimation performance and high energy consumption), or remaining stationary (maximum energy conservation at the expense of accurate localization). Through simulation, we notice a graceful degradation in estimation performance for larger values of  $\underline{b}$  in order to reduce energy expenditure.

This work can be expanded in several ways, including the analysis of directed communication graphs. Additionally, different distributed control strategies can be introduced for formation control and tracking of the target with obstacle and collision avoidance. Other interesting problems include online-tuning of the parameter  $\underline{b}$  to change the network objective and react to changes in the environment (e.g., to reduce energy expenditure further when the robots are low on battery). Future work should ultimately seek experimental validation of the proposed approach using mobile acoustic receivers using Grace 2, similar to the setup presented in Chapter 3. Finally, future work can consider stochastic models for the moving target, such as the correlated random walk model [67], along with different filtering methodologies, such as the particle filtering [68].

## CHAPTER 5

### NECESSARY CONDITIONS FOR THE CONVERGENCE OF THE DISTRIBUTED KALMAN FILTER AND ITS COUPLED RICCATI EQUATIONS

The problem of distributed localization of a moving target in Chapter 4 motivated the study of a more general application of sensor networks: the distributed estimation problem. In many applications involving large-scale complex systems, the state of the system is monitored by a group of sensors spatially distributed over large networks where the communication between sensors is limited. To model such a scenario, consider the discrete-time linear time-invariant (LTI) dynamical system

$$x(k+1) = Ax(k) + \omega(k) \quad (5.1)$$

where  $k$  is the discrete-time index,  $A \in \mathbb{B}(\mathbb{R}^n)$ <sup>1</sup> is the system matrix,  $x(k) \in \mathbb{R}^n$  is the state vector, and  $\omega(k) \in \mathbb{R}^n$  is a driving noise assumed to be Gaussian with zero mean and positive definite covariance  $Q$ . The state of the system is monitored by a network of  $N$  agents indexed by  $i$ , each of which is equipped with a sensor that receives a partial measurement of the state that is modeled by

$$y_i(k) = C_i x(k) + v_i(k), \quad i = 1, \dots, N, \quad (5.2)$$

where  $y_i(k) \in \mathbb{R}^{p_i}$  is the measurement made by sensor  $i$  with  $C_i \in \mathbb{B}(\mathbb{R}^n, \mathbb{R}^{p_i})$ , and  $v_i \in \mathbb{R}^{p_i}$  is the measurement noise assumed to be Gaussian with zero mean and positive definite covariance  $R_i$ . An important problem in such networks is to develop distributed algorithms for state estimation of the process in (5.1), where the goal is for each agent to estimate the entire system state using its respective local measurements and the information obtained from neighbors. While this model does not directly capture the time-varying nature of the distributed localization problem, it allows us to consider a wider range of system dynamics (stable, unstable, and marginally stable systems),

---

<sup>1</sup>For Banach spaces  $\mathbb{X}$  and  $\mathbb{Y}$ , we set  $\mathbb{B}(\mathbb{X}, \mathbb{Y})$  as the Banach spaces of all bounded linear operators of  $\mathbb{X}$  into  $\mathbb{Y}$ , and use  $\mathbb{B}(\mathbb{X}) \triangleq \mathbb{B}(\mathbb{X}, \mathbb{X})$ . We denote by  $\mathbb{R}^n$  the  $n$ -dimensional real Euclidean spaces and  $\mathbb{B}(\mathbb{R}^n, \mathbb{R}^m)$  the normed bounded linear space of  $m \times n$  real matrices, with the uniform induced-norm represented by  $\|\cdot\|$ , and use  $\mathbb{B}(\mathbb{R}^n) \triangleq \mathbb{B}(\mathbb{R}^n, \mathbb{R}^n)$ .

as well as a more general view into the relationship between system dynamics, agent measurement models, and network requirements.

This distributed filtering problem has received significant attention over the past years, with early studies considering two-time-scale algorithms with multiple data fusion iterations between two consecutive time steps of the plant dynamics [24, 25]. Bandwidth and energy limitations motivated the study of single-time-scale algorithms where the data fusion occurs once per time step of plant dynamics. In [26, 27], the authors used state augmentation to cast the distributed estimation problem as a problem for designing a decentralized stabilizing controller for an LTI plant and provided conditions for successful estimation under their proposed approaches. In [28], the authors alleviated the need for state augmentation and proposed a distributed filter where each sensor performs consensus only on the portion of the state it cannot estimate on its own. In the most general case, this would require the partitioning of the system dynamics into observable and unobservable components and enforcing consensus on the unobservable modes at each sensor site. In [29], the authors introduced the idea of consensus-based distributed linear filters (CBDLF), where each sensor updates its estimate in two steps: a local update step using its own observations followed by a consensus step with its neighbors. The authors went on to provide sub-optimal filtering gains to minimize an upper bound on a quadratic filtering cost, and provided some sufficient conditions for the convergence of their scheme in terms of the feasibility of a set of linear matrix inequalities (LMIs).

The gains obtained in [29] are similar, in some sense, to the ones obtained from applying a centralized Kalman filter, and the convergence results are tied to the convergence properties of a set of coupled Riccati equations. However, the work in [29] does not, in general, shed light on the network conditions required to satisfy such LMIs. In this work, we utilize some of the results developed in the Markovian jump linear systems (MJLS) literature to connect the convergence properties of these coupled Riccati equations to certain conditions on the network topology and consensus weights.

## 5.1 Problem Setup

For ease of exposition, in this section we consider a CBDLF where consensus is performed before local filtering, and discuss in Appendix C.3 how these results hold when the order is reversed to consider the CBDLF in [29].

Here, in the first step, each agent produces an intermediate estimate of the state by performing a convex combination of its own estimate,  $\hat{x}_i(k)$ , and the state estimates by all other agents within its communication range, i.e.,

$$\xi_i(k) = \sum_{j=1}^N w_{ij} \hat{x}_j(k), \quad i = 1, \dots, N, \quad (5.3)$$

where  $w_{ij}$  are nonnegative scalars summing up to one ( $\sum_{j=1}^N w_{ij} = 1$ ) with  $w_{ij} > 0$  if  $i = j$  or if agent  $i$  can obtain information from agent  $j$ ; otherwise,  $w_{ij} = 0$ . After all agents complete the consensus step, each agent then updates its estimate by performing a local filtering step based on the intermediate estimate  $\xi(k)$ , i.e.,

$$\hat{x}_i(k+1) = A\xi_i(k) + L_i \left( y_i(k) - C_i \xi_i(k) \right). \quad (5.4)$$

where  $L_i$  is the filter gain.

Let  $\epsilon_i(k) = x(k) - \hat{x}_i(k)$  denote the estimation error for agent  $i$  at time  $k$ . Combining (5.3) and (5.4), we have<sup>2</sup>

$$\epsilon_i(k+1) = (A - L_i C_i) \sum_{j=1}^N w_{ij} \epsilon_j(k) + \omega(k) - L_i v_i(k). \quad (5.5)$$

In Appendix C.2, we show that it is possible to derive filtering gains that minimize an upper bound of the following finite horizon quadratic filtering cost function

$$J(k) = \sum_{t=0}^k \sum_{i=1}^N E \{ \|\epsilon_i(t)\|^2 \}, \quad (5.6)$$

with  $E\{\cdot\}$  denoting the expected value. These sub-optimal filtering gains can be computed in two steps under the same communication topology and consensus weights used in (5.3)–(5.4). The

---

<sup>2</sup>We assume that the initial state  $x(0)$ , and the noises  $v_i(k)$  and  $\omega(k)$  are independent for all  $k \geq 0$ .

filtering gains require each agent to store a matrix  $P_i(k)$  that represents, as we discuss in Section 5.2, an upper bound of the error covariance for agent  $i$ .

During the consensus step, the agents compute an intermediate covariance by performing a convex combination of their own  $P_i(k)$  and that of their neighbors, i.e.,

$$\Pi_i(k) = \sum_{j=1}^N w_{ij} P_j(k). \quad (5.7)$$

Then, during the filtering step, each agent computes the local filtering gain to be used in (5.4) using the intermediate covariance

$$L_i(k) = A\Pi_i(k)C_i'(R_i + C_i\Pi_i(k)C_i')^{-1}, \quad (5.8)$$

where  $'$  represents the matrix transpose, and updates its covariance upper bound according to

$$P_i(k+1) = A\Pi_i(k)A' + Q - A\Pi_i(k)C_i' \times \\ (C_i\Pi_i(k)C_i' + R_i)^{-1} C_i\Pi_i(k)A'. \quad (5.9)$$

Substituting  $\Pi_i(k)$  from (5.7) into (5.9) yields a set of *coupled Riccati equations*. The CBDLF in (5.3)–(5.4) and (5.7)–(5.9) is referred to as the *distributed Kalman filter* – due to its similarity to the centralized Kalman filter – and provides an attractive solution to the distributed filtering problem. However, the numerical tools used to analyze the convergence of this filter and its associated coupled Riccati equations do not offer much insight into the required network connectivity and consensus weights.

## 5.2 Necessary Conditions

For a centralized estimation problem, the detectability of the pair  $(A, C)$  plays an important role in the convergence of the Riccati equation that governs the centralized Kalman filter. Therefore, it is natural for us to seek a similar notion for the distributed problem. In what follows, we consider the noise-free dynamics of the estimation errors in (5.5), namely

$$\epsilon_i(k+1) = (A - L_i C_i) \sum_{j=1}^N w_{ij} \epsilon_j(k). \quad (5.10)$$

Denoting the network-wide estimation error by  $\epsilon(k) = [\epsilon_1(k)' \cdots \epsilon_N(k)']'$ , one can show that the noise-free dynamics for this network-wide error are given by

$$\epsilon(k+1) = \mathcal{B}\epsilon(k), \quad (5.11)$$

where  $\mathcal{B} \triangleq \text{diag}[A - L_i C_i](W \otimes I_n) \in \mathbb{B}(\mathbb{R}^{Nn})^3$ , with  $\otimes$  denoting the Kronecker product and  $W \in \mathbb{B}(\mathbb{R}^N)$  is the consensus weights matrix whose  $(i, j)$  entry is  $w_{ij}$ . Clearly, the system in (5.11) is asymptotically stable if  $r_\sigma(\mathcal{B}) < 1$ , where  $r_\sigma(\cdot)$  denotes the spectral radius of a linear operator.

**Definition 5.2.1 (Detectability)** *Let  $C = \{C_1, \dots, C_N\}$  be the set of measurement matrices of all sensors. For the system in (5.1)–(5.2) and the consensus weights  $W$ , we say  $(A, C, W)$  is detectable if there exists a set of gain matrices  $L_i$ ,  $i = 1, \dots, N$ , such that  $r_\sigma(\mathcal{B}) < 1$ .*

As we discuss later in this section, detectability in the sense of Definition 5.2.1 is not sufficient to ensure the convergence of the coupled Riccati equations in (5.7) and (5.9), even though it would ensure exponential convergence of  $\epsilon(k)$  to zero in (5.11).

To facilitate the analysis and discussion of these coupled Riccati equations, we make use of the following notation. Let  $\mathbb{H}^{n,m}$  denote the linear space made up of all  $N$ -sequences of matrices  $V = (V_1, \dots, V_N)$  with  $V_i \in \mathbb{B}(\mathbb{R}^n, \mathbb{R}^m)$ . For  $V \in \mathbb{H}^{n,m}$  we write  $V' = (V'_1, \dots, V'_N) \in \mathbb{H}^{m,n}$  and say that  $V \in \mathbb{H}^n \triangleq \mathbb{H}^{n,n}$  is symmetric if  $V = V'$ . For a symmetric  $V \in \mathbb{H}^n$ , we use the notation  $V \in \mathbb{H}^{n0}$  (respectively,  $V \in \mathbb{H}^{n+}$ ) when all of the matrices  $V_i$  are positive semidefinite (respectively, positive definite)<sup>4</sup>. For any  $V \in \mathbb{H}^n$ , define the operators  $\mathcal{E}(V) = (\mathcal{E}_1(V), \dots, \mathcal{E}_N(V)) \in \mathbb{B}(\mathbb{H}^n)$ , and  $\mathcal{L}(V) = (\mathcal{L}_1(V), \dots, \mathcal{L}_N(V)) \in \mathbb{B}(\mathbb{H}^n)$ , where

$$\mathcal{E}_i(V) \triangleq \sum_{j=1}^N w_{ij} V_j \in \mathbb{B}(\mathbb{R}^n), \quad (5.12)$$

$$\mathcal{L}_i(V) \triangleq \Gamma_i \mathcal{E}_i(V) \Gamma_i' \in \mathbb{B}(\mathbb{R}^n), \quad (5.13)$$

---

<sup>3</sup>For a set of  $N$  matrices,  $M_i \in \mathbb{B}(\mathbb{R}^n)$ , we denote by  $\text{diag}[M_i]$  the  $Nn \times Nn$  block-diagonal matrix with  $M_i$  in the diagonal.

<sup>4</sup>For  $V, S \in \mathbb{H}^n$ , we write  $V \geq S$  if  $V - S = (V_1 - S_1, \dots, V_N - S_N) \in \mathbb{H}^{n0}$ , and that  $V > S$  if  $V - S \in \mathbb{H}^{n+}$ .

for some  $\Gamma_i \in \mathbb{B}(\mathbb{R}^n)$ , for  $i = 1, \dots, N$ . It can be verified that the spaces  $\mathbb{H}^n$  and  $\mathbb{R}^{Nn^2}$  are uniformly homeomorphic, and that any operator  $\mathcal{Z}$  in  $\mathbb{B}(\mathbb{H}^n)$  can be represented in  $\mathbb{B}(\mathbb{R}^{Nn^2})$  [30]. The following result is important in the analysis of the coupled Riccati equations.

**Lemma 5.2.2 (Proof in [30])** *Consider the operator  $\mathcal{L}(\cdot)$  defined above. We have that*

$$r_\sigma(\mathcal{L}) = r_\sigma(\mathcal{A}),$$

where  $\mathcal{A} = \text{diag}[\Gamma_i \otimes \Gamma_i](W \otimes I_{n^2}) \in \mathbb{B}(\mathbb{R}^{Nn^2})$ . Furthermore,  $r_\sigma(\mathcal{A}) < 1$  iff there exists some  $P \in \mathbb{H}^{n+}$  such that  $P - \mathcal{L}(P) > 0$ .

With the above notation, we present the following lemma regarding the upper bounds for the error covariances along with a stronger definition for detectability.

**Lemma 5.2.3** *Define  $\Xi(k) \in \mathbb{H}^{n0}$ , where  $\Xi_i(k)$  denotes the noise-free covariance of the estimation error in (5.10) for agent  $i$  at time  $k$ . Let  $P(k) \in \mathbb{H}^{n0}$  be defined recursively as*

$$P(k+1) = \mathcal{L}(P(k)), \quad P(0) = \Xi(0), \quad (5.14)$$

with  $\Gamma_i = (A - L_i C_i)$ . Then,

$$\Xi(k) \leq P(k), \quad \forall k \geq 0.$$

Furthermore, define  $\Sigma(k) \in \mathbb{H}^{n+}$  and  $P(k) \in \mathbb{H}^{n+}$ , where  $\Sigma_i(k)$  denotes the covariance of agent  $i$ 's estimation error with noise in (5.5), and  $P_i(k)$  is defined recursively as

$$P_i(k+1) = \mathcal{L}_i(P(k)) + Q + L_i R_i L_i', \quad P(0) = \Sigma(0), \quad (5.15)$$

with  $\Gamma_i = (A - L_i C_i)$ . Then,

$$\Sigma(k) \leq P(k), \quad \forall k \geq 0.$$

**Proof:** See Appendix C.1. ■

**Definition 5.2.4 (S-detectability)** *For the system in (5.1)–(5.2) and the consensus weights  $W$ , we say  $(A, C, W)$  is square detectable (S-detectable) if there exists a set of gain matrices  $L_i$ ,  $i = 1, \dots, N$ , such that  $r_\sigma(\mathcal{L}) < 1$  with  $\Gamma_i = A - L_i C_i$ .*

Note that S-detectability implies that there exists a set of gain matrices such that upper bounds for the noise-free covariances in (5.14) are asymptotically stable. Using Lemma 5.2.3, it is easy to check that if  $(A, C, W)$  is S-detectable, then it is detectable in the sense of Definition 5.2.1, since

$$\|\epsilon(k)\|^2 = \sum_{i=1}^N \|\epsilon_i(k)\|^2 = \sum_{i=1}^N \text{tr}(\Xi_i(k)) \leq \sum_{i=1}^N \text{tr}(P_i(k)),$$

and thus, if  $r_\sigma(\mathcal{L}) < 1$  then  $r_\sigma(\mathcal{B}) < 1$ . However, detectability in the sense of Definition 5.2.1 does not imply S-detectability. Indeed, consider the case with  $n = 1$ ,  $N = 2$ ,  $A = C_1 = C_2 = 1$ ,  $L_1 = 0.3$ , and  $L_2 = -0.25$ , then  $r_\sigma(\mathcal{B}) = 0.975$  while  $r_\sigma(\mathcal{L}) = 1.026$ .

This notion of S-detectability is similar in some way to the notion of mean square detectability in MJLS. This allows us to leverage some of the results there in analyzing the conditions on the consensus weights and network connectivity needed for the stability of the coupled Riccati equations. Specifically, it has been shown in [30] that these coupled Riccati equations converge to a stabilizing solution<sup>5</sup> only if there exists a set of gains  $L_i$  such that  $r_\sigma(\mathcal{L}) < 1$  with  $\Gamma_i = A - L_i C_i$ . That is, the coupled Riccati equations converge to a stabilizing solution only if their noise-free counterparts are stable. This is precisely the definition of S-detectability in this distributed estimation context.

The remainder of this section is aimed at providing the necessary conditions for S-detectability of  $(A, C, W)$  in terms of network topology and communication weights.. Before presenting the main result, however, we review some of the relevant results from MJLS. Specifically, we make use of the notion of weak detectability (W-detectability), which has been shown to play an important role in the LQR control problem of MJLS [64, 65].

For some  $X \in \mathbb{H}^{n0}$ , consider the system

$$X(k+1) = \mathcal{L}(X(k)), \tag{5.16}$$

---

<sup>5</sup> $P \in \mathbb{H}^{n+}$  is called a stabilizing solution if  $P_i = A\mathcal{E}_i(P)A' + Q - A\mathcal{E}_i(P)C_i'(C_i\mathcal{E}_i(P)C_i' + R_i)^{-1}C_i\mathcal{E}_i(P)A'$  for all  $i = 1, \dots, N$ , and the gains  $L_i$  defined in (5.8) with  $\Pi_i = \mathcal{E}_i(P)$  stabilize (5.14).

with  $\Gamma_i = A_i$ , and introduce the functional

$$U(k) = \sum_{i=1}^N \text{tr}(X_i(0)' F_i(k)) \quad (5.17)$$

where the matrices  $F(k) \in \mathbb{H}^{n0}$  are defined recursively by

$$F_i(k+1) = C_i' C_i + A_i' \mathcal{E}_i(F(k)) A_i, \quad F_i(0) = 0. \quad (5.18)$$

**Definition 5.2.5 (W-detectability)** Consider the system (5.16). We say that  $(A, C, W)$  is *W-detectable* if there exist integers  $N_d, k_d \geq 0$  and scalars  $0 \leq \delta < 1, \gamma > 0$  such that  $U(N_d) \geq \gamma \|X(0)\|$  whenever  $\|X(k_d)\| \geq \delta \|X(0)\|$ , where the norm is defined as  $\|X\|^2 = \sum_i \text{tr}(X_i' X_i)$ .

Associated with the matrices  $F(k)$  in (5.18), are the set of observability matrices  $O = \{O_1, \dots, O_N\}$ , where

$$O_i = \begin{bmatrix} O_i(0) & \dots & O_i(n^2 N - 1) \end{bmatrix}' \quad (5.19)$$

for each  $i \in \{1, \dots, N\}$ , where  $F_i(k) = \sum_{t=0}^{k-1} O_i(t)$ , and the matrices  $O(k)$  are defined recursively as

$$O_i(k+1) = A_i' \mathcal{E}_i(O(k)) A_i, \quad O_i(0) = C_i' C_i. \quad (5.20)$$

With the above definition of W-detectability, the following results (Lemmas 5.2.6 and 5.2.7) are adapted from [64] and [65].

**Lemma 5.2.6** If  $(A, C, W)$  is *S-detectable*, then  $(A, C, W)$  is *W-detectable*.

**Lemma 5.2.7**  $(A, C, W)$  is *W-detectable* iff for some  $x(0) \in \text{null}(O_i)$ , for any  $i \in \{1, \dots, N\}$ , we have that  $\lim_{k \rightarrow \infty} \|x(k)\|^2 = 0$ .

In our distributed estimation problem, we have  $A_i = A$  for all  $i$ , and the condition in Lemma 5.2.7 is equivalent to the detectability of the pairs  $(A, O_i)$  for all  $i$ , allowing us to employ these results in deriving necessary conditions on the network for the distributed estimation problem.

For a weight matrix  $W$ , define recursively,

$$w_{ij}^{(l)} = \sum_{k=1}^N w_{ik}^{(l-1)} w_{kj}, \quad w_{ij}^{(0)} = \delta_{ij}, \quad (5.21)$$

where  $\delta_{ij}$  is the Kronecker delta, and recall the definition of a source component [28] in the network.

**Definition 5.2.8 (Source component)** A set of agents  $\mathbb{S} = \{s_1, \dots, s_p\}$ ,  $\mathbb{S} \subseteq \{1, \dots, N\}$ , is a source component of the network if there exists  $l > 0$ , such that  $w_{ij}^{(l)} > 0$  for any  $i, j \in \mathbb{S}$ , and for any  $i \in \mathbb{S}$  and  $j \notin \mathbb{S}$ ,  $w_{ij}^{(l)} = 0$  for all  $l > 0$ .

**Definition 5.2.9 (Detectable source component)** A source component  $\mathbb{S} = \{s_1, \dots, s_p\}$  is detectable if the pair  $(A, C_{\mathbb{S}})$  is detectable, where  $C_{\mathbb{S}} = \begin{bmatrix} C'_{s_1} & \dots & C'_{s_p} \end{bmatrix}'$ .

We can present our main result.

**Theorem 5.2.10**  $(A, C, W)$  is S-detectable only if:

1. Every source component in the network is detectable.
2.  $w_{ii} < (1/r_{\sigma}(A_i^u))^2$  for each  $i = 1, \dots, N$ , where  $A_i^u$  is the unobservable partition of  $A$  using  $C_i$ .

**Proof:** First, we show that the first statement holds. To that end, if  $(A, C, W)$  is S-detectable, then it is necessarily W-detectable, and from Lemma 5.2.7 we have that  $(A, O_i)$  is detectable for each  $i$ . It is easy to check that  $O_i(k)$  in (5.20) can be written as

$$O_i(k) = \sum_{j=1}^N w_{ij}^{(k)} A'^k C'_j C_j A^k.$$

Let  $\mathbb{S}$  be a source component, and denote by  $O_{\mathbb{S}}$  the observability matrix corresponding to the pair  $(A, C_{\mathbb{S}})$ . It is known that each agent  $i \in \{1, \dots, N\}$  is either part of a source component, or there exists a directed path to  $i$  from some agent  $j$  in a source component.

On the one hand, for some agent  $i \in \mathbb{S}$ , it follows from Definition 5.2.8 that there exists an  $l > 0$  such that  $w_{ij}^{(l)} > 0$  for every  $j \in \mathbb{S}$ . It can then be checked that for any  $i \in \mathbb{S}$ ,  $\text{null}(O_i) = \text{null}(O_{\mathbb{S}})$ , and  $\mathbb{S}$  is a detectable source component since for any  $x(0) \in \text{null}(O_{\mathbb{S}})$ ,  $\lim_{k \rightarrow \infty} \|x(k)\|^2 = 0$ .

On the other hand, if  $i \notin \mathbb{S}$ , then there is no directed path from  $i$  to  $j \in \mathbb{S}$ , and  $\text{null}(O_i) \subseteq \text{null}(O_{\mathbb{S}})$ . However, since  $(A, O_i)$  and  $(A, O_j)$  are detectable, with  $\text{null}(O_j) = \text{null}(O_{\mathbb{S}})$ , then  $\mathbb{S}$  is a detectable source component.

Now we show that the second statement holds. Indeed, if  $(A, C, W)$  is S-detectable, then there exist gain matrices  $L_i, i = 1, \dots, N$ , such that  $r_\sigma(\mathcal{L}) < 1$ . From Lemma 5.2.2, this implies that  $P - \mathcal{L}(P) > 0$  for some positive definite matrices  $P \in \mathbb{H}^{n+}$ . Following the same approach as in [66], we have that

$$\begin{aligned} P_i - (A - L_i C_i)' \sum_{j=1}^N w_{ij} P_j (A - L_i C_i) &> 0, \\ \Rightarrow P_i - (\sqrt{w_{ii}})(A - L_i C_i)' P_i (\sqrt{w_{ii}})(A - L_i C_i) &> 0, \end{aligned}$$

for  $i = 1, \dots, N$ , and therefore  $(\sqrt{w_{ii}}A, C_i)$  is detectable. We can then find a similarity transformation to transform the pair  $(\sqrt{w_{ii}}A, C_i)$  into

$$\begin{aligned} \bar{A}_i &= T_i (\sqrt{w_{ii}}A) T_i' = \sqrt{w_{ii}} \begin{bmatrix} A_i^o & 0 \\ A_i^c & A_i^u \end{bmatrix}, \\ \bar{C}_i &= C_i T_i' = \begin{bmatrix} C_i^o & 0 \end{bmatrix}, \end{aligned}$$

where  $\sqrt{w_{ii}}A_i^u$  represents the unobservable modes. Clearly, if  $(\sqrt{w_{ii}}A, C_i)$  is detectable then  $\sqrt{w_{ii}}A_i^u$  must be stable, and  $w_{ii} < (1/r_\sigma(A_i^u))^2$ . ■

These necessary conditions allow us to consider the weakest communication topologies that will ensure S-detectability, as well as the maximum values for the *self-weights* used in consensus.

## 5.3 Numerical Examples

### 5.3.1 Example 1

We consider an unstable system with  $n = 2$ , monitored by  $N = 3$  sensors, where

$$A = \begin{bmatrix} 2 & 0 \\ 0 & 2 \end{bmatrix}, \quad C_1 = \begin{bmatrix} 1 & 0 \end{bmatrix}, \quad C_3 = \begin{bmatrix} 1 & 0 \\ 0 & 1 \end{bmatrix},$$

Clearly, we have that  $(A, C_1)$  and  $(A, C_2)$  are not detectable, implying that agents 1 and 2 cannot estimate the process on their own. On the other hand, it is easy to check that the pairs

$$(A, C_3), \left( A, \begin{bmatrix} C_1 \\ C_2 \end{bmatrix} \right), \left( A, \begin{bmatrix} C_1 \\ C_3 \end{bmatrix} \right), \left( A, \begin{bmatrix} C_2 \\ C_3 \end{bmatrix} \right)$$

are all detectable. Therefore, to satisfy the condition that  $(A, O_1)$  is detectable, the minimal connectivity requirement we need is  $w_{12} > 0$  or  $w_{13} > 0$ . Similarly for  $(A, O_2)$  to be detectable, we need  $w_{21} > 0$  or  $w_{23} > 0$ . Finally,  $(A, O_3)$  is detectable without needing a path from any other agent. Figure 5.1 represents the communication networks with minimum links that satisfy these conditions. It is easy to check in Figure 5.1 that every source component in those graphs is detectable, and adding more communication links between the nodes will not affect the detectability of  $(A, O_i)$ .

Note that the spectral radius of the unobservable partitions for agents 1 and 2 is  $r_\sigma(A_1^u) = r_\sigma(A_2^u) = 2$ , and therefore we require  $w_{11} < 0.25$  and  $w_{22} < 0.25$ . To show the importance of the values of self weights  $w_{ii}$ , we simulate the response of a distributed Kalman filter using (5.7)–(5.9) with the filtering gains shown in (5.8) for the case when agent 3 is disconnected from agents 1 and 2. Figure 5.2 shows the norms of the covariance matrices under different values for  $w_{11}$  and  $w_{22}$ ,

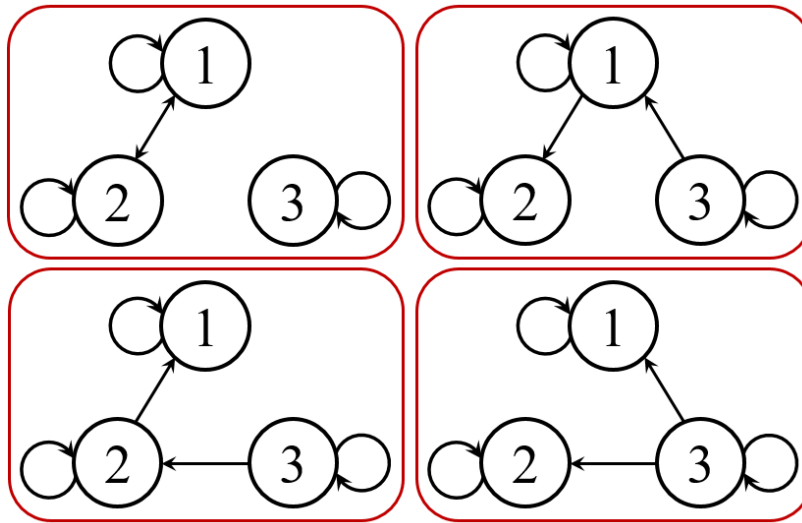


**Figure 5.1:** The minimal communication links required to satisfy the detectability requirement of all  $(A, O_i)$  pairs for Example 1.

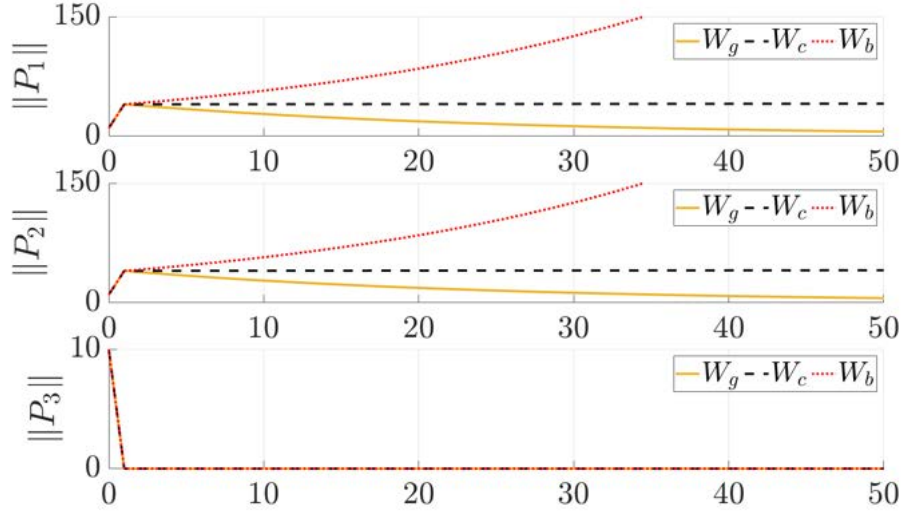


**Figure 5.2: Comparison of the norms of the covariance matrices under the consensus-then-filter distributed Kalman filter for Example 1.  $W_g$  represents the network that satisfies  $(1/r_\sigma(A_i^u))^2$ .**

where we used the following weights

$$W_g = \begin{bmatrix} 0.24 & 0.76 & 0 \\ 0.76 & 0.24 & 0 \\ 0 & 0 & 1 \end{bmatrix},$$

for the case that satisfies the condition  $w_{11}, w_{22} < 0.25$ , and

$$W_c = \begin{bmatrix} 0.25 & 0.75 & 0 \\ 0.75 & 0.25 & 0 \\ 0 & 0 & 1 \end{bmatrix}, \quad W_b = \begin{bmatrix} 0.26 & 0.74 & 0 \\ 0.74 & 0.26 & 0 \\ 0 & 0 & 1 \end{bmatrix}$$

for the cases that violate this condition, and the simulations were initialized with  $x(0) = [-15 \ 15]'$ ,  $\hat{x}_i(0) = [0 \ 0]'$ ,  $P_i(0) = 10I$ ,  $Q = 0.1I$ , and  $R_i = 0.1I$ .

Figure 5.2 shows that  $P_3(k)$  converges very quickly to its steady state value without agent 3 needing additional information from its neighbors, since it can estimate the process on its own. An interesting behavior is observed for the coupled dynamics for  $P_1(k)$  and  $P_2(k)$  as  $w_{ii}$  approaches  $(1/r_\sigma(A_i^u))^2$ . We see that covariance matrices for agents 1 and 2 converge to steady values when

$w_{ii} < 0.25$  and grow unbounded for  $w_{ii} > 0.25$ , highlighting the importance of the consensus weights when performing distributed estimation.

### 5.3.2 Example 2

We consider an unstable system with  $n = 3$ , monitored by  $N = 3$  sensors, where

$$A = \begin{bmatrix} 0.8147 & 0.8147 & 0.2785 \\ 0.9058 & 0.9058 & 0.5469 \\ 0 & 0 & 0.9575 \end{bmatrix}, \quad \begin{aligned} C_1 &= \begin{bmatrix} 1 & 0 & 0 \end{bmatrix}, \\ C_2 &= \begin{bmatrix} 0 & 1 & 0 \end{bmatrix}, \\ C_3 &= \begin{bmatrix} 0 & 0 & 1 \end{bmatrix}. \end{aligned}$$

It can be checked that  $(A, C_1)$  and  $(A, C_2)$  are observable, implying that agents 1 and 2 can estimate the process on their own. On the other hand,  $(A, C_3)$  is not detectable, and agent 3 requires information from agents 1 or 2 to successfully estimate the process. Therefore, to satisfy the condition that  $(A, O_3)$  is detectable, the minimal connectivity requirement we need is  $w_{31} > 0$  or  $w_{32} > 0$ .

Note that the spectral radius of the unobservable partitions for agent 3 is  $r_\sigma(A_3^u) = 1.7205$ , and therefore we require  $w_{33} < 0.3378$ . We simulate the response of a distributed Kalman filter using (5.7)–(5.9) with the filtering gains shown in (5.8) for the case when agent 3 obtains information from both agents 1 and 2. Figure 5.3 shows the norms of the covariance matrices under different values for  $w_{33}$  where we used the following weights

$$W_g = \begin{bmatrix} 1 & 0 & 0 \\ 0 & 1 & 0 \\ 0.34 & 0.34 & 0.32 \end{bmatrix},$$

for the case that satisfies the condition  $w_{33} < 0.3378$ , and

$$W_b = \begin{bmatrix} 1 & 0 & 0 \\ 0 & 1 & 0 \\ 0.33 & 0.33 & 0.34 \end{bmatrix},$$

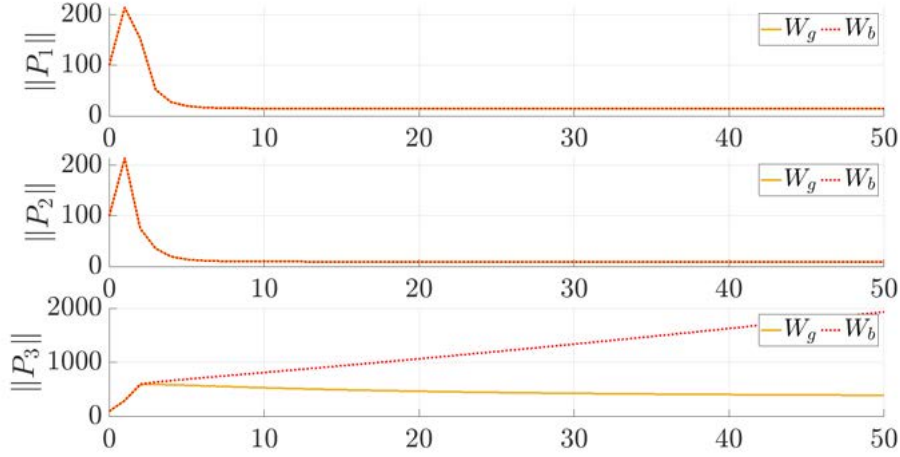


**Figure 5.3: Comparison of the norms of the covariance matrices under the consensus-then-filter distributed Kalman filter for Example 2.**  $W_g$  represents the network that satisfies  $(1/r_\sigma(A_i^u))^2$ .

for the case which violates that condition, and the simulations were initialized with  $x(0) = [-2.2691 \quad -2.0143 \quad 1.6173]'$ ,  $\hat{x}_i(0) = [0 \quad 0 \quad 0]'$ ,  $P_i(0) = 100I$ ,  $Q = I$ , and  $R_i = I$ .

Figure 5.3 shows that  $P_1(k)$  and  $P_2(k)$  converge to their respective steady state values without agent needing additional information from its neighbors, since they can estimate the process on their own. An interesting behavior is observed for the coupled dynamics for  $P_3(k)$  as  $w_{33}$  approaches  $(1/r_\sigma(A_3^u))^2$ , further highlighting the importance of the consensus weights.

## 5.4 Summary and Future Work

We consider the problem of distributed estimation of an LTI system by a network of sensors using consensus-based distributed linear filters, where the agents update their estimates by performing consensus followed by local filtering. We present a distributed version of the centralized Kalman filter, in which the filtering gains minimize an upper bound of a quadratic filtering cost. These filtering gains are computed using a set of coupled Riccati equations that, in turn, can be updated in a distributed manner under the same network. We then provide the notion of S-detectability that is necessary for the convergence of these coupled Riccati equations, and build on that to provide necessary conditions in terms of the minimum network connectivity and a limit on the self-weights

used during the consensus step. Future work will first focus on the other half of this problem, in which we consider the sufficient conditions for S-detectability and their implication on the network in order to ensure successful estimation and asymptotic convergence of the distributed Kalman filters. Future work will also seek to extend these results to distributed estimation of time-varying systems, and investigate the conditions for convergence of the coupled Riccati equations with time-varying matrices.

## CHAPTER 6

### SUMMARY AND FUTURE WORK

#### 6.1 Summary

In this dissertation, we discussed the role gliding robotic fish play in environmental monitoring, and focus on their application to acoustic telemetry of fish movement. We presented the improvements of mechanical and electrical designs of the gliding robotic fish to enhance their serviceability, operational time, and computational power.. These improvements were facilitated by the introduction of a water-tight interface that allowed for opening and closing the robot for regular maintenance and inspection. The new serviceable nature of these robots allowed us to rapidly test new electrical systems. The final design of the robot featured a Raspberry Pi computer, which operates on a Linux-like environment that facilitated the development of high-level tasks, such as navigation and data storage.

The new design allowed for a larger sensor payload to be integrated into the robot, as well as for carrying an acoustic receiver for detecting acoustic signals. Gliding robotic fish prototypes were tested in Higgins Lake to investigate the applicability of these robots to tracking tagged animals in fresh and shallow water. The field tests were also helpful in evaluating gliding- and swimming-based navigation strategies that drive the robot to a specified GPS location. The lake experiments showed that the robot can indeed carry an acoustic receiver and detect acoustic signals reliably at a distance of approximately 300 m. Furthermore, these tests shed the light onto the importance of aligning the acoustic receiver towards the tag to maximize detection, as the detection performance of the mobile receiver degraded when the receiver was facing away from the target. The depth and pitch of the robot also affected the detection performance of the mobile receiver. However, the effect of these variables was less prominent than facing the receiver away from the transmitter.

Motivated by the problem of tracking fish movement, we then investigated the problem of localization and tracking of a moving target by a network of robots. A distributed EKF was

presented to estimate the target's position based on the TDOA measurements model, without the need for centralized processing of these measurements. Under the proposed scheme, we showed that any given agent in the network can accurately estimate the target's position when it is part of a connected network with 4 non-coplanar agents. We then presented a movement strategy for the network to actively track the target, ensuring adequate localization of the target as it moves in space. A tuning parameter was introduced to achieve a balance between estimation performance and energy consumption.

The distributed localization problem motivated the study of the more general distributed estimation problem, in which a network of sensors are used to monitor and estimate the state of an LTI system. Under this general setup, it is assumed that interactions between agents are dictated by a directed and weighted communication graph. We then presented a suboptimal distributed filtering strategy in which each agent updates its estimates in two steps: a consensus step followed by a filtering step. We showed that the suboptimal filtering gains are related to the convergence of a set of coupled Riccati equations. We then went on to discuss the necessary conditions in terms of graph topology and consensus weights needed for the convergence of these coupled Riccati equations.

## **6.2 Future Work**

The work presented here can be further improved in future studies. The main drawback that the current robot design faces involves the time and resources needed for fabrication and manufacturing. Future designs will focus on reducing the cost and time needed for fabrication. As for the electrical side, future designs will incorporate underwater acoustic communication, satellite communication, and solar charging for these robots. Furthermore, additional work will be done to fully characterize the operational specifications of these robots, such as their capability of overcoming currents, battery life, and maximum depth rating.

Additional field trials will also be carried out to further characterize the performance of gliding robotic fish as a mobile receiver platform. In particular, future work will focus on conducting more replicate runs over a range of environmental variables (e.g., wind, noise, stratification), and

examine different methods to mitigate shielding the acoustic signals from the receivers. As an example, future work can compare the detection performance of vertically mounted receivers, as well as investigating navigation controllers that take into account the relative positions between the tag and receiver. Ultimately, future work will seek experimental validation of TDOA-based localization and tracking of an acoustic tag using a network of gliding robotic fish operating as mobile receivers. Future work can also consider stochastic models for the moving target, such as the correlated random walk model [67], along with different filtering methodologies, such as the particle filtering [68].

Finally, future work will focus on the other half of the distributed estimation problem. Specifically, sufficient conditions for the convergence of the coupled Riccati equations in terms of network topology and consensus weights will be investigated. It will also be of interest to extend the results obtained here to time-varying systems, and consider the necessary and sufficient conditions for the convergence of the coupled Riccati equations with time-varying matrices.

## **APPENDICES**

## APPENDIX A

### STOCHASTIC STABILITY FOR DISTRIBUTED TDOA-BASED LOCALIZATION OF A MOVING TARGET

Analyzing the stability of the extended Kalman filter has been investigated in [56] and [69]. A similar framework to the one presented in [56] can be utilized for analyzing the stochastic stability of the EKF under the weighted averaging scheme in (4.26)–(4.28), and (4.32)–(4.35) when implemented by each agent in the network.

Throughout this appendix,  $\|\cdot\|$  denotes the Euclidian norm of real vectors or the spectral norm of real matrices,  $E\{x\}$  is the expectation value of  $x$ , and  $E\{x|y\}$ , the expectation value of  $x$  conditioned on  $y$ . Moreover,  $\mathbb{R}^q$  denotes the real  $q$ -dimensional vector space,  $I_n$  denotes the  $n \times n$  identity matrix, and  $A \otimes B$  denotes the Kronecker product of matrices  $A$  and  $B$ .

Let  $d$  denote the dimension of in which the target is moving in space ( $d = 2$  for 2D, and  $d = 3$  for 3D), and let  $n = 2d$  denote the dimension of the target's state. For ease of writing, let  $x_k = x(k)$ , and similarly let  $\hat{x}_k^i = \hat{x}_i(k)$ ,  $\tilde{x}_k^i = \tilde{x}_i(k)$ ,  $K_k^i = K_i(k)$ , and  $H_k^i = H_i(k)$ . Furthermore, let  $z_k^i$  denote agent  $i$ 's measurement at time instant  $k$  (rather than  $y_i(k)$  in (4.2), for consistency with discrete-time literature), and for notational consistency, let  $h^i(\cdot)$  denote the measurement model  $h_i(\cdot)$  in (4.3). Finally, let  $v_k^i$  denote the measurement noise for agent  $i$  with covariance matrix  $R^i$ . The one step formulation of the each agent's estimation in (4.29) can be written as

$$\hat{x}_{k+1}^i = \sum_{j=1}^N w_{ij} \left[ A\hat{x}_k^j + AK_k^j \left( z_k^j - h^j(\hat{x}_k^j) \right) \right] \quad (\text{A.1})$$

Similarly, a one step formulation of the  $i$ -th agent's error covariance matrix in (4.33)–(4.35) can be derived by substituting (4.35) and (4.34) into (4.33), and denoting  $P_i(k|k-1)$  by  $P_k^i$

$$P_{k+1}^i = \sum_{j=1}^N w_{ij} \left[ A(I_n - K_k^j H_k^j) P_k^j (I_n - K_k^j H_k^j)^T A^T \right] + \sum_{j=1}^N w_{ij} \left[ AK_k^j R^j K_k^{jT} A^T \right] + BQB^T \quad (\text{A.2})$$

For notation consistency, we redefine  $K_k^i$  as

$$K_k^i = P_k^i H_k^{iT} \left( H_k^i P_k^i H_k^{iT} + R^i \right)^{-1} \quad (\text{A.3})$$

In the averaged EKF formulation, we note the use of the linearized measurement function,  $H_k^i$ . It is possible to expand the measurement function  $h_k^i$  via

$$h^i(x_k) - h^i(\hat{x}_k^i) = H_k^i(x_k - \hat{x}_k^i) + \chi^i(x_k, \hat{x}_k^i) \quad (\text{A.4})$$

The  $i$ -th agent's estimation error is defined as

$$\tilde{x}_k^i = x_k - \hat{x}_k^i \quad (\text{A.5})$$

which can be obtained by subtracting (A.1) from (4.5), yielding

$$\tilde{x}_{k+1}^i = \sum_{j=1}^N w_{ij} \left[ A(I - K_k^j H_k^j) \tilde{x}_k^j + \rho_k^j + \psi_k^j \right] \quad (\text{A.6})$$

where

$$\rho_k^i = -AK_k^i \chi^i(x_k, \hat{x}_k^i) \quad (\text{A.7})$$

$$\psi_k^i = Bw_k - AK_k^i v_k^i \quad (\text{A.8})$$

which follows the form in (4.30), with  $\eta_j(k) = \rho_k^j + \psi_k^j$ .

## A.1 Error Bounds for the Averaged EKF

The basis of the convergence analysis is the stochastic stability lemma [49, 50], which is given as follows:

**Lemma A.1.1** *If there exist real numbers  $\bar{v}, \underline{v}, \mu > 0$  and  $0 < \alpha \leq 1$ , and there is a stochastic process  $V_k(\zeta_k)$  with the following properties:*

$$\underline{v} \|\zeta_k\|^2 \leq V_k(\zeta_k) \leq \bar{v} \|\zeta_k\|^2 \quad (\text{A.9})$$

$$E\{V_{k+1}(\zeta_{k+1}) | \zeta_k\} - V_k(\zeta_k) \leq \mu - \alpha V_k(\zeta_k) \quad (\text{A.10})$$

*then the random process  $\zeta_k$  is exponentially bounded in mean square with probability one, as in*

$$E\{\|\zeta_k\|^2\} \leq \frac{\bar{v}}{\underline{v}} E\{\|\zeta_0\|^2\} (1 - \alpha)^k + \frac{\mu}{\underline{v}} \sum_{l=1}^{k-1} (1 - \alpha)^l \quad (\text{A.11})$$

*for every  $k \geq 0$ . Moreover, the stochastic process is bounded with probability one.*

**Proof:** The proof of this lemma is provided in [50] and [56]. ■

Let  $\tilde{\mathbf{x}}_k = \begin{bmatrix} \tilde{x}_k^1 & \dots & \tilde{x}_k^N \end{bmatrix}^T$  denote the network-wide estimation error of all agents in the network. Using (A.6), we can obtain the dynamics for the network-wide estimation error

$$\tilde{\mathbf{x}}_k = (W \otimes A)(I_{2dN} - K_k H_k) \tilde{\mathbf{x}}_k + (W \otimes I_{2d}) \boldsymbol{\rho}_k + (W \otimes I_{2d}) \boldsymbol{\psi}_k \quad (\text{A.12})$$

Here,  $K_k = \text{blkdiag} \begin{bmatrix} K_k^1 & \dots & K_k^N \end{bmatrix}$  and  $H_k = \text{blkdiag} \begin{bmatrix} H_k^1 & \dots & H_k^N \end{bmatrix}$  are block diagonal matrices for the filtering gain and linearized measurement matrices, respectively, while  $W$  is a stochastic matrix representing the averaging weights,  $[W]_{ij} = w_{ij}$ . The terms  $\boldsymbol{\rho}_k$  and  $\boldsymbol{\psi}_k$  are the concatenations of the terms  $\rho_k^i$  and  $\psi_k^i$ , respectively. From (A.7) and (A.8), we can write

$$\boldsymbol{\rho}_k = -(I_N \otimes A) K_k \boldsymbol{\chi}(\mathbf{x}_k, \hat{\mathbf{x}}_k) \quad (\text{A.13})$$

$$\boldsymbol{\psi}_k = (I_N \otimes B) \mathbf{w}_k - (I_N \otimes A) K_k \mathbf{v}_k \quad (\text{A.14})$$

where

$$\mathbf{w}_k = \mathbf{1}_N \otimes w_k,$$

$$\mathbf{x}_k = \mathbf{1}_N \otimes x_k,$$

$$\mathbf{v}_k = \begin{bmatrix} v_k^1 & \dots & v_k^N \end{bmatrix}^T,$$

and

$$\boldsymbol{\chi}(\mathbf{x}_k, \hat{\mathbf{x}}_k) = \begin{bmatrix} \chi^1(x_k, \hat{x}_k^1) & \dots & \chi^N(x_k, \hat{x}_k^N) \end{bmatrix}^T.$$

Similarly, we define the network-wide error covariance,  $P_k = \text{blkdiag} \begin{bmatrix} P_k^1 & \dots & P_k^N \end{bmatrix}$ . Using the matrix inversion lemma, it can be noted that (A.2) is equivalent to

$$P_{k+1}^i = \sum_{j=1}^N w_{ij} \left[ A P_k^j A^T - A P_k^j H_k^{jT} K_k^{jT} A^T \right] + B Q B \quad (\text{A.15})$$

we get

$$P_{k+1} = (\sqrt{W} \otimes A) P_k (\sqrt{W} \otimes A)^T - (\sqrt{W} \otimes A) P_k H_k^T K_k^T (\sqrt{W} \otimes A)^T + (\sqrt{W} \sqrt{W}^T \otimes B Q B) \quad (\text{A.16})$$

Furthermore, we restrict  $P_k$  to have a block diagonal structure in order to capture the distributed nature of this problem. The network-wide gain matrix  $K_k$  can then be expressed as

$$K_k = P_k H_k^T (H_k P_k H_k^T + R)^{-1} \quad (\text{A.17})$$

where the matrix  $R = \text{blkdiag} \begin{bmatrix} R^1 & \dots & R^N \end{bmatrix}$  is the network-wide measurement noise covariance matrix.

Before stating the main result of this section, we present the following lemmas that will aid in analyzing the averaged EKF.

**Lemma A.1.2** *Consider the system given by (4.5), (4.2) and the averaged EKF in (A.1)–(A.3). Let  $\mathcal{N} \triangleq \sum_{i=1}^N \mathcal{N}_i$ , and assume that there exist positive real numbers  $\bar{a}, \bar{h}, \bar{p}, \underline{p}, \delta, \sigma_w, \sigma_v > 0$  such that the following inequalities hold for all  $k \geq 0$ :*

$$\|A\| \leq \bar{a} \quad (\text{A.18})$$

$$BB^T \leq \delta I \quad (\text{A.19})$$

$$\|H_k\| \leq \bar{h} \quad (\text{A.20})$$

$$\underline{p}I \leq P_k \leq \bar{p}I \quad (\text{A.21})$$

$$Q \geq \sigma_w^2 I_{2d} \quad (\text{A.22})$$

$$R \geq \sigma_v^2 I_{|\mathcal{N}|} \quad (\text{A.23})$$

then there exists a real number  $0 < \alpha < 1$  such that the inequality

$$(I_{2dN} - K_k H_k)^T (W \otimes A)^T P_{k+1}^{-1} \times (W \otimes A) (I_{2dN} - K_k H_k) \leq (1 - \alpha) P_k^{-1} \quad (\text{A.24})$$

with  $K_k$  given by (A.17), holds for  $k \geq 0$ .

**Proof:** Rearranging the terms in (A.16)

$$\begin{aligned} P_{k+1} = & (\sqrt{W} \otimes A) \left[ (I_{2dN} - K_k H_k) P_k (I_{2dN} - K_k H_k)^T \right. \\ & + K_k H_k P_k (I_{2dN} - K_k H_k)^T \\ & \left. + (I_N \otimes B Q B^T) \right] (\sqrt{W} \otimes A)^T \end{aligned} \quad (\text{A.25})$$

Now, we consider the term  $K_k H_k P_k (I_{2dN} - K_k H_k)^T$ . With (A.17), it can be verified that

$$P_k (I_{2dN} - K_k H_k)^T = P_k - P_k H_k^T (H_k P_k H_k^T + R)^{-1} H_k P_k \quad (\text{A.26})$$

which is symmetric, and applying the matrix inversion lemma, we get

$$P_k (I_{2dN} - K_k H_k)^T = (P_k^{-1} H_k^T R^{-1} H_k)^{-1} > 0 \quad (\text{A.27})$$

because  $P_k^{-1} > 0$ . Additionally, from (A.17), and since  $P_k > 0$  and  $R > 0$ ,

$$K_k H_k = P_k H_k^T (H_k P_k H_k^T + R)^{-1} H_k \geq 0 \quad (\text{A.28})$$

From (A.27) and (A.28), it can be seen that

$$K_k H_k P_k (I_{2dN} - K_k H_k)^T \geq 0 \quad (\text{A.29})$$

Therefore, from (A.25) and (A.29), the inequality

$$P_{k+1} \geq (\sqrt{W} \otimes A) \left[ (I_{2dN} - K_k H_k) P_k (I_{2dN} - K_k H_k)^T + (I_N \otimes B Q B^T) \right] (\sqrt{W} \otimes A)^T \quad (\text{A.30})$$

holds, and can be rewritten as

$$\begin{aligned} P_{k+1} &\geq (\sqrt{W} \otimes A) (I_{2dN} - K_k H_k) \times \\ &\quad \left[ P_k + (I_{2dN} - K_k H_k)^{-1} (I_N \otimes B Q B^T) (I_{2dN} - K_k H_k)^{-T} \right] \\ &\quad \times (I_{2dN} - K_k H_k)^T (\sqrt{W} \otimes A)^T \end{aligned} \quad (\text{A.31})$$

From (A.17), and the assumed bounds (A.18)–(A.23), it is easy to see that

$$\|K_k\| \leq \frac{\bar{p}\bar{h}}{\sigma_v^2} \quad (\text{A.32})$$

which leads to

$$P_{k+1} \geq (\sqrt{W} \otimes A) (I_{2dN} - K_k H_k) \times \left[ P_k + \frac{\delta \sigma_w^2}{\left(1 + \frac{\bar{p}\bar{h}}{\sigma_v^2}\right)^2} I_{2dN} \right] (I_{2dN} - K_k H_k)^T (\sqrt{W} \otimes A)^T$$

Taking the inverse of both sides, and multiplying from the left by  $(I_{2dN} - K_k H_k)^T (\sqrt{W} \otimes A)^T$  and from the right by  $(\sqrt{W} \otimes A)(I_{2dN} - K_k H_k)$  we get

$$(I_{2dN} - K_k H_k)^T (\sqrt{W} \otimes A)^T P_{k+1}^{-1} (\sqrt{W} \otimes A) \times (I_{2dN} - K_k H_k) \leq \left[ 1 + \frac{\delta \sigma_w^2}{\bar{p} \left( 1 + \frac{\bar{p} \bar{h}}{\sigma_v^2} \right)^2} \right]^{-1} P_k^{-1} \quad (\text{A.33})$$

Since  $W$  is stochastic,

$$\begin{aligned} & (I_{2dN} - K_k H_k)^T (W \otimes A)^T P_{k+1}^{-1} \\ & \times (W \otimes A)(I_{2dN} - K_k H_k) \leq (I_{2dN} - K_k H_k)^T \\ & \times (\sqrt{W} \otimes A)^T P_{k+1}^{-1} (\sqrt{W} \otimes A)(I_{2dN} - K_k H_k) \\ & \leq (1 - \alpha) P_k^{-1} \end{aligned} \quad (\text{A.34})$$

i.e., inequality (A.24) with

$$1 - \alpha = \left( 1 + \frac{\delta \sigma_w^2}{\bar{p} \left( 1 + \frac{\bar{p} \bar{h}}{\sigma_v^2} \right)^2} \right)^{-1} \quad (\text{A.35})$$

■

It is worth noting that conditions (A.18)–(A.20) and (A.22)–(A.23) are easy to satisfy, since we assume knowledge of the system's matrices. Condition (A.21) is specifically addressed in Section III-B.

**Lemma A.1.3** *Let the assumptions in Lemma A.1.2 hold, and assume that there exist positive real numbers  $\kappa_\chi, \epsilon_\chi > 0$ , such that the nonlinear function  $\chi(\xi_1, \xi_2)$  in (A.13) is bounded by*

$$\|\chi(\xi_1, \xi_2)\| \leq \kappa_\chi \|\xi_1 - \xi_2\|^2 \quad (\text{A.36})$$

for  $\xi_1, \xi_2 \in \mathbb{R}^{2dN}$  with  $\|\xi_1 - \xi_2\| < \epsilon_\chi$ , then there is a positive real number  $\kappa_\rho > 0$  such that

$$\rho_k^T (W \otimes I_n)^T P_{k+1}^{-1} [2(W \otimes A)(I_{2dN} - K_k H_k) \tilde{\mathbf{x}}_k + (W \otimes I_{2d}) \rho_k] \leq \kappa_\rho \|\tilde{\mathbf{x}}_k\|^3 \quad (\text{A.37})$$

holds for  $\|\tilde{\mathbf{x}}_k\| \leq \epsilon_\chi$ .

**Proof:** From (A.13) and (A.32), a bound can be established on  $\|\boldsymbol{\rho}_k\|$

$$\|\boldsymbol{\rho}_k\| \leq \frac{\bar{a}\bar{p}\bar{h}}{\sigma_v^2} \|\chi(\mathbf{x}_k, \hat{\mathbf{x}}_k)\| \quad (\text{A.38})$$

For  $\|\tilde{\mathbf{x}}_k\| = \|\mathbf{x}_k - \hat{\mathbf{x}}_k\| \leq \epsilon_\chi$ , using (A.36), one gets

$$\|\boldsymbol{\rho}_k\| \leq \frac{\bar{a}\bar{p}\bar{h}}{\sigma_v^2} \kappa_\chi \|\tilde{\mathbf{x}}_k\|^2 \triangleq \kappa' \|\tilde{\mathbf{x}}_k\|^2 \leq \kappa' \epsilon_\chi \|\tilde{\mathbf{x}}_k^i\| \quad (\text{A.39})$$

which in turn leads to

$$\begin{aligned} & \boldsymbol{\rho}_k^T (W \otimes I_n)^T P_{k+1}^{-1} [2(W \otimes A)(I_{2dN} - K_k H_k) \tilde{\mathbf{x}}_k + (W \otimes I_{2d}) \boldsymbol{\rho}_k] \\ & \leq \kappa' \frac{1}{p} \left[ 2\bar{a} \left( 1 + \frac{\bar{p}\bar{h}^2}{\sigma_v^2} \right) + \kappa' \epsilon_\chi \right] \|\tilde{\mathbf{x}}_k\|^3 \end{aligned} \quad (\text{A.40})$$

i.e., inequality (A.37) with

$$\kappa_\rho = \kappa' \frac{1}{p} \left[ 2\bar{a} \left( 1 + \frac{\bar{p}\bar{h}^2}{\sigma_v^2} \right) + \kappa' \epsilon_\chi \right] \quad (\text{A.41})$$

■

**Lemma A.1.4** *Let the assumptions in Lemma A.1.2 hold, then there is a positive real number  $\kappa_\psi > 0$  such that*

$$E\{\boldsymbol{\psi}_k^T P_{k+1}^{-1} \boldsymbol{\psi}_k\} \leq \kappa_\psi \quad (\text{A.42})$$

for all  $k \geq 0$ .

**Proof:** Using the definition of  $\boldsymbol{\psi}_k$  given by (A.14), and since  $\mathbf{w}_k$  and  $\mathbf{v}_k$  are uncorrelated, we can expand the expectation expression in (A.42) via

$$\begin{aligned} E\{\boldsymbol{\psi}_k^T P_{k+1}^{-1} \boldsymbol{\psi}_k\} &= E\{\mathbf{w}_k^T (I_N \otimes B)^T P_{k+1}^{-1} (I_N \otimes B) \mathbf{w}_k\} \\ &\quad + E\{\mathbf{v}_k^T K_k^T (I_N \otimes A)^T P_{k+1}^{-1} (I_N \otimes A) K_k \mathbf{v}_k\} \end{aligned} \quad (\text{A.43})$$

From the bound in (A.18)–(A.23) and (A.32), equation (A.43) can be converted to an inequality via

$$E\{\boldsymbol{\psi}_k^T P_{k+1}^{-1} \boldsymbol{\psi}_k\} \leq \frac{1}{p} E\{\mathbf{w}_k^T (I_N \otimes B)^T (I_N \otimes B) \mathbf{w}_k\} + \frac{1}{p} \left( \frac{\bar{a}\bar{p}\bar{h}}{\sigma_v^2} \right)^2 E\{\mathbf{v}_k^T \mathbf{v}_k\} \quad (\text{A.44})$$

Because both sides of (A.44) are scalars, we can take the trace of the right-hand side without changing its value

$$\begin{aligned} E\{\boldsymbol{\psi}_k^T P_{k+1}^{-1} \boldsymbol{\psi}_k\} &\leq \frac{1}{\underline{p}} \text{tr} \left( (I_N \otimes B) E\{\mathbf{w}_k \mathbf{w}_k^T\} (I_N \otimes B)^T \right) + \frac{1}{\underline{p}} \left( \frac{\bar{a} \bar{p} \bar{h}}{\sigma_v^2} \right)^2 \text{tr} \left( E\{\mathbf{v}_k \mathbf{v}_k^T\} \right) \\ &= \frac{2dN\delta\sigma_w^2}{\underline{p}} + \frac{\mathcal{N}\bar{a}^2 \bar{p}^2 \bar{h}^2}{\underline{p}\sigma_v^2} \end{aligned} \quad (\text{A.45})$$

Defining

$$\kappa_\psi \triangleq \frac{2dN\delta\sigma_w^2}{\underline{p}} + \frac{\mathcal{N}\bar{a}^2 \bar{p}^2 \bar{h}^2}{\underline{p}\sigma_v^2} \quad (\text{A.46})$$

leads to  $E\{\boldsymbol{\psi}_k^T P_{k+1}^{-1} \boldsymbol{\psi}_k\} \leq \kappa_\psi$ . ■

With the above results, we can now present the following theorem regarding the stochastic stability of the averaged EKF.

**Theorem A.1.5** *Consider the movement model for the target given by (4.5) and the nonlinear measurement model for each agent given by (4.2), along with the averaged EKF in (A.1)–(A.3), and let the assumptions of Lemmas A.1.2 and A.1.3 hold. then the network-wide estimation error  $\tilde{\mathbf{x}}_k$  given by (A.12) is exponentially bounded in mean square with probability one.*

**Proof:** We choose

$$V_k(\tilde{\mathbf{x}}_k) = \tilde{\mathbf{x}}_k^T P_k^{-1} \tilde{\mathbf{x}}_k \quad (\text{A.47})$$

From (A.21), we have

$$\frac{1}{\bar{p}} \leq V_k(\tilde{\mathbf{x}}_k) \leq \frac{1}{\underline{p}} \quad (\text{A.48})$$

which satisfies the first condition of Lemma A.1.1 with  $\underline{v} = \frac{1}{\bar{p}}$  and  $\bar{v} = \frac{1}{\underline{p}}$ . What remains is to establish an upper bound on  $E\{V_{k+1}(\tilde{\mathbf{x}}_{k+1})|\tilde{\mathbf{x}}_k\}$ . Inserting (A.12) into (A.47) yields

$$\begin{aligned} V_{k+1}(\tilde{\mathbf{x}}_{k+1}) &= [(W \otimes A)(I_{2dN} - K_k H_k) \tilde{\mathbf{x}}_k + \\ &\quad (W \otimes I_{2d}) \boldsymbol{\rho}_k + (W \otimes I_{2d}) \boldsymbol{\psi}_k]^T P_k^{-1} \\ &\quad \times [(W \otimes A)(I_{2dN} - K_k H_k) \tilde{\mathbf{x}}_k \\ &\quad + (W \otimes I_{2d}) \boldsymbol{\rho}_k + (W \otimes I_{2d}) \boldsymbol{\psi}_k] \end{aligned} \quad (\text{A.49})$$

Taking the conditional expectation  $E\{V_{k+1}(\tilde{\mathbf{x}}_{k+1})|\tilde{\mathbf{x}}_k\}$  and applying Lemmas A.1.2, A.1.3, and A.1.4 for  $\|\tilde{\mathbf{x}}_k\| \leq \epsilon_\chi$  we obtain

$$\begin{aligned} E\{V_{k+1}(\tilde{\mathbf{x}}_{k+1})|\tilde{\mathbf{x}}_k\} &\leq (1 - \alpha)V_k(\tilde{\mathbf{x}}_k) \\ &\quad + \kappa_\rho \epsilon_\chi \|\tilde{\mathbf{x}}_k\| + \kappa_\psi \end{aligned} \quad (\text{A.50})$$

Defining  $\epsilon = \min\left(\epsilon_\chi, \frac{\alpha}{2\bar{\rho}\kappa_\rho}\right)$ , then for  $\|\tilde{\mathbf{x}}_k\| \leq \epsilon$

$$\kappa_\rho \|\tilde{\mathbf{x}}_k\| \|\tilde{\mathbf{x}}_k\|^2 \leq \frac{\alpha}{2\bar{\rho}} \|\tilde{\mathbf{x}}_k\|^2 \leq \frac{\alpha}{2} V_k(\tilde{\mathbf{x}}_k) \quad (\text{A.51})$$

Applying inequality (A.51) to (A.50) yields

$$E\{V_{k+1}(\tilde{\mathbf{x}}_{k+1}) - V_k(\tilde{\mathbf{x}}_k)\} \leq -\frac{\alpha}{2} V_k(\tilde{\mathbf{x}}_k) + \kappa_\psi \quad (\text{A.52})$$

which satisfies the second condition of Lemma A.1.1, ensuring that the network-wide estimation error  $\tilde{\mathbf{x}}_k$  remains bounded in mean square.  $\blacksquare$

## A.2 Boundedness of Averaged Covariance Matrix

The boundedness of the covariance matrix in inequality (A.21) under the proposed method must be addressed. To that end, consider the operator originally presented in [70].

**Lemma A.2.1** *Let  $\mathbf{P}$  denote the set of matrices  $\{P^1, \dots, P^N\}$  and  $\mathbf{M}$  denote the set of matrices  $\{M^1, \dots, M^N\}$ . Define the following operator*

$$f_{n+1}^i(\mathbf{M}, \mathbf{P}) = \sum_{j=1}^N w_{ij} M^j f_n^j(\mathbf{M}, \mathbf{P}) M^{jT} \quad (\text{A.53})$$

with

$$f_1^i(\mathbf{M}, \mathbf{P}) = \sum_{j=1}^N w_{ij} M^j P^j M^{jT} \quad (\text{A.54})$$

*If there exist positive-definite matrices  $\mathbf{X} = \{X^1, \dots, X^N\}$  such that  $X^i > f_1^i(\mathbf{M}, \mathbf{X})$ , then the following statements hold for all  $i = 1, \dots, N$ :*

1. *For all bounded positive semi-definite matrices  $P^i \geq 0$ ,  $\lim_{n \rightarrow \infty} f_n^i(\mathbf{M}, \mathbf{P}) = 0$ .*
2. *For all bounded positive semi-definite matrices  $P_0^i \geq 0$ , and  $U^i \geq 0$ , the sequences  $P_{k+1}^i = f_1^i(\mathbf{M}, \mathbf{P}_k) + U^i$  are bounded.*

**Proof:**

1. Since  $P^i \geq 0$  and  $X^i > 0$ , then there exists a constant  $\alpha > 0$  such that  $P^i \leq \alpha X^i, \forall i$ . Then it is clear that  $f_n^i(\mathbf{M}, \mathbf{P}) \leq \alpha f_n^i(\mathbf{M}, \mathbf{X})$ . Additionally, since  $f_1^i(\mathbf{M}, \mathbf{X}) < X^i$ , then there exists a constant  $r \in (0, 1)$  such that  $f_1^i(\mathbf{M}, \mathbf{X}) \leq r X^i$ . Then,  $f_2^i(\mathbf{M}, \mathbf{X}) \leq r f_1^i(\mathbf{M}, \mathbf{X}) \leq r^2 X^i$ , and sequentially,  $f_n^i(\mathbf{M}, \mathbf{X}) \leq r^n X^i$ . Therefore,  $f_n^i(\mathbf{M}, \mathbf{P}) \leq \alpha r^n X^i$  and  $\lim_{n \rightarrow \infty} f_n^i(\mathbf{M}, \mathbf{P}) = 0$ .

2. From the definition of  $P_{k+1}^i$ , we have

$$\begin{aligned} P_2^i &= \sum_{j=1}^N w_{ij} M^j P_1^j M^{jT} + U^i \\ &= \sum_{j=1}^N w_{ij} M^j f_1^j(\mathbf{M}, \mathbf{P}_0) M^{jT} \\ &\quad + \sum_{j=1}^N w_{ij} M^j U^j M^{jT} + U^i \\ &= f_2^i(\mathbf{M}, \mathbf{P}_0) + f_1^i(\mathbf{M}, \mathbf{U}) + U^i \end{aligned}$$

and by induction, it can be shown that

$$P_{k+1}^i = f_{k+1}^i(\mathbf{M}, \mathbf{P}_0) + \sum_{l=1}^k f_l^i(\mathbf{M}, \mathbf{U}) + U^i$$

From the proof of Part 1, there exist constants  $\alpha, \mu > 0$  and  $0 < r < 1$  such that  $f_k^i(\mathbf{M}, \mathbf{P}_0) \leq \alpha r^k X^i$  and  $U^i \leq \mu X^i$ , which is used to show that

$$P_k^i \leq \left( \alpha + \frac{\mu}{1-r} \right) X^i$$

■

**Corollary A.2.2** For given matrices  $A, B, Q, \mathbf{R} = \{R^1, \dots, R^N\}$ , and time varying matrices  $\mathbf{H}_k = \{H_k^1, \dots, H_k^N\}$ , define the operator

$$g_k^i(\mathbf{P}) = \sum_{j=1}^N w_{ij} \left[ A(I - K_k^j H_k^j) P^j (I - K_k^j H_k^j)^T A^T \right] + \sum_{j=1}^N w_{ij} \left[ A K_k^j R^j K_k^{jT} A^T \right] + B Q B^T \quad (\text{A.55})$$

where

$$K_k^i = P^i H_k^{iT} \left( H_k^i P^i H_k^{iT} + R^i \right)^{-1}$$

If there exist positive-definite matrices  $\mathbf{X} = \{X^1, \dots, X^N\}$  such that  $X^i > f_1^i(A(I - \mathbf{K}_k \mathbf{H}_k), \mathbf{X})$  for all  $k \geq 0$ , where  $f_1^i(\cdot, \cdot)$  is defined in Lemma A.2.1, then for all positive semi-definite matrices  $P_0^i \geq 0$ , the sequences  $P_{k+1}^i = g_k^i(\mathbf{P}_k)$  are bounded.

**Proof:** This corollary can be proven by directly applying the results in Lemma A.2.1, defining  $M^i = A(I - K_k^i H_k^i)$  and  $U^i = \sum_{j=1}^N w_{ij} \left[ A K_k^j R^j K_k^{jT} A^T \right] + B Q B^T$ . ■

Examining (A.2), it can be seen that the error covariance matrix under the averaged scheme takes the form  $P_{k+1}^i = g_k^i(\mathbf{P}_k)$ . Therefore, by Corollary A.2.2,  $P_k^i$  remains bounded under the proposed scheme if the conditions of Lemma A.2.1 are satisfied.

## APPENDIX B

### SUPPLEMENTAL RESULTS FOR TDOA-BASED DISTRIBUTED LOCALIZATION AND TRACKING OF A MOVING TARGET

#### B.1 Cases (a), (b), and (c) in Theorem 4.2.3

We show that  $\text{rank}(O_1) = 6$  for the remaining three cases in Fig. 4.3.

##### Case (a)

This case is the easiest to examine, as agent 1 has a sufficient number of neighbors. The measurement matrix  $H_1(k)$  has the following structure

$$H_1(\lambda) = \begin{bmatrix} \lambda_1 & \lambda_2 & \lambda_3 & 0 & 0 & 0 \\ \lambda_4 & \lambda_5 & \lambda_6 & 0 & 0 & 0 \\ \lambda_7 & \lambda_8 & \lambda_9 & 0 & 0 & 0 \end{bmatrix}, \quad (\text{B.1})$$

and from the discussion on decentralized approach, the pair  $(A, H_1(\lambda))$  is generically observable.

It immediately follows that  $\text{rank}(O_1) = 6$ , since

$$\text{rank}(O_1) = \text{rank} \left( \begin{bmatrix} [W]_{11} H_1(\lambda) A \\ [W^2]_{11} H_1(\lambda) A^2 \\ \vdots \\ [W^7]_{11} H_1(\lambda) A^7 \end{bmatrix} \right) = 6,$$

for almost all values of  $T$  and  $\lambda$ .

**Case (b)**

The structure of  $H_i(k)$  for  $i = 1, \dots, 4$  is

$$\begin{aligned} H_1(\lambda) &= \begin{bmatrix} \lambda_1 & \lambda_2 & \lambda_3 & 0 & 0 & 0 \end{bmatrix}, \\ H_2(\lambda) &= \begin{bmatrix} -\lambda_1 & -\lambda_2 & -\lambda_3 & 0 & 0 & 0 \\ \lambda_4 & \lambda_5 & \lambda_6 & 0 & 0 & 0 \\ \lambda_7 & \lambda_8 & \lambda_9 & 0 & 0 & 0 \end{bmatrix}, \\ H_3(\lambda) &= \begin{bmatrix} -\lambda_4 & -\lambda_5 & -\lambda_6 & 0 & 0 & 0 \end{bmatrix}, \\ H_4(\lambda) &= \begin{bmatrix} -\lambda_7 & -\lambda_8 & -\lambda_9 & 0 & 0 & 0 \end{bmatrix}. \end{aligned}$$

We first note that the pair

$$\left( A, \begin{bmatrix} H_1(\lambda) \\ H_2(\lambda) \end{bmatrix} \right),$$

is generically observable, which can be shown following the same analysis in the discussion for the decentralized approach. This in turn, ensures that

$$\text{rank} \begin{pmatrix} \begin{bmatrix} H_1(\lambda) \\ H_2(\lambda) \\ \vdots \\ H_1(\lambda)A^6 \\ H_2(\lambda)A^6 \end{bmatrix} \end{pmatrix} = 6,$$

for almost all values of  $T$  and  $\lambda$ , and it immediately follows that  $\text{rank}(O_1) = 6$ .

### Case (c)

The structure of  $H_i(k)$  for  $i = 1, \dots, 4$  follows

$$\begin{aligned} H_1(\lambda) &= \begin{bmatrix} \lambda_1 & \lambda_2 & \lambda_3 & 0 & 0 & 0 \\ \lambda_4 & \lambda_5 & \lambda_6 & 0 & 0 & 0 \end{bmatrix}, \\ H_2(\lambda) &= \begin{bmatrix} -\lambda_1 & -\lambda_2 & -\lambda_3 & 0 & 0 & 0 \end{bmatrix}, \\ H_3(\lambda) &= \begin{bmatrix} -\lambda_4 & -\lambda_5 & -\lambda_6 & 0 & 0 & 0 \\ \lambda_7 & \lambda_8 & \lambda_9 & 0 & 0 & 0 \end{bmatrix}, \\ H_4(\lambda) &= \begin{bmatrix} -\lambda_7 & -\lambda_8 & -\lambda_9 & 0 & 0 & 0 \end{bmatrix}. \end{aligned}$$

Following similar procedures to those presented in the decentralized approach discussion, it can be shown that the pair

$$\left( A, \begin{bmatrix} H_1(\lambda) \\ H_3(\lambda) \\ H_4(\lambda) \end{bmatrix} \right),$$

is generically observable, and that

$$\text{rank} \begin{pmatrix} H_1(\lambda) \\ H_2(\lambda) \\ H_3(\lambda) \\ \vdots \\ H_1(\lambda)A^6 \\ H_2(\lambda)A^6 \\ H_3(\lambda)A^6 \end{pmatrix} = 6,$$

for almost all values of  $T$  and  $\lambda$ . Therefore,  $\text{rank}(O_1) = 6$  for almost all values of  $T$  and  $\lambda$ .

## B.2 Formation Control

In this section, we provide the details for the dynamic feedback linearization controller for the system shown in (4.44). We first augment the system dynamics with another integrator on the  $a_i$

input channel

$$\dot{a}_i = u_{i,1}, \quad (\text{B.2})$$

with  $u_{i,1}$ ,  $u_{i,2}$ , and  $u_{i,3}$  constituting the new control inputs to the  $i$ th robot.

Then we define the position coordinates of agent  $i$  as the outputs to perform feedback linearization

$$\begin{bmatrix} z_{i,1} \\ z_{i,2} \\ z_{i,3} \end{bmatrix} = \begin{bmatrix} q_1(r_i) \\ q_2(r_i) \\ q_3(r_i) \end{bmatrix} = \begin{bmatrix} p_i^x \\ p_i^y \\ p_i^z \end{bmatrix}. \quad (\text{B.3})$$

The augmented robot model in (4.44), (B.2) and output (B.3) can be written in compact form

$$\begin{aligned} \dot{r}_i &= f(r_i) + g(r_i)u_i, \\ z_i &= q(r_i), \end{aligned} \quad (\text{B.4})$$

where

$$r_i = \begin{bmatrix} p_i^x \\ p_i^y \\ p_i^z \\ v_i \\ \phi_i \\ \gamma_i \\ a_i \\ \omega_{i,\phi} \\ \omega_{i,\gamma} \end{bmatrix}, \quad f(r_i) = \begin{bmatrix} v_i \cos(\phi_i) \cos(\gamma_i) \\ v_i \sin(\phi_i) \cos(\gamma_i) \\ v_i \sin(\gamma_i) \\ a_i \\ \omega_{i,\phi} \\ \omega_{i,\gamma} \\ 0 \\ 0 \\ 0 \end{bmatrix}, \quad (\text{B.5})$$

and  $g(r_i) = \begin{bmatrix} g_1 & g_2 & g_3 \end{bmatrix}$ , with

$$g_1 = \begin{bmatrix} 0 \\ 0 \\ 0 \\ 0 \\ 0 \\ 0 \\ 1 \\ 0 \\ 0 \end{bmatrix}, \quad g_2 = \begin{bmatrix} 0 \\ 0 \\ 0 \\ 0 \\ 0 \\ 0 \\ 0 \\ 1 \\ 0 \end{bmatrix}, \quad g_3 = \begin{bmatrix} 0 \\ 0 \\ 0 \\ 0 \\ 0 \\ 0 \\ 0 \\ 0 \\ 1 \end{bmatrix}. \quad (\text{B.6})$$

Noting that  $L_{g_1} L_f^k q_j(r_i) = L_{g_2} L_f^k q_j(r_i) = L_{g_3} L_f^k q_j(r_i) = 0$  for  $k = 0, 1$  and for all  $j = 1, 2, 3$ , and that  $L_{g_1} L_f^2 q_j(r_i) \neq 0$ ,  $L_{g_2} L_f^2 q_j(r_i) \neq 0$ , and  $L_{g_3} L_f^2 q_j(r_i) \neq 0$ , the decoupling matrix  $\mathcal{A}(x_i)$ , defined as

$$\mathcal{A}(r_i) = \begin{bmatrix} L_{g_1} L_f^2 q_1(r_i) & L_{g_2} L_f^2 q_1(r_i) & L_{g_3} L_f^2 q_1(r_i) \\ L_{g_1} L_f^2 q_2(r_i) & L_{g_2} L_f^2 q_2(r_i) & L_{g_3} L_f^2 q_2(r_i) \\ L_{g_1} L_f^2 q_3(r_i) & L_{g_2} L_f^2 q_3(r_i) & L_{g_3} L_f^2 q_3(r_i) \end{bmatrix}, \quad (\text{B.7})$$

is nonsingular as long as  $v_i \neq 0$ , and  $\gamma_i \neq \pm \frac{\pi}{2}$ . Now, we define  $\zeta_i$  as  $\zeta_i = T(x_i)$ , where

$$\begin{aligned} \zeta_{i,1} &= q_1(r_i) \\ \zeta_{i,2} &= L_f q_1(r_i) \\ \zeta_{i,3} &= L_f^2 q_1(r_i) \\ \zeta_{i,4} &= q_2(r_i) \\ \zeta_{i,5} &= L_f q_2(r_i) \\ \zeta_{i,6} &= L_f^2 q_2(r_i) \\ \zeta_{i,7} &= q_3(r_i) \\ \zeta_{i,8} &= L_f q_3(r_i) \\ \zeta_{i,9} &= L_f^2 q_3(r_i) \end{aligned} \quad (\text{B.8})$$

The model can then be written in terms of the transformed state  $\zeta_i$

$$\begin{aligned}
\dot{\zeta}_{i,1} &= \zeta_{i,2} \\
\dot{\zeta}_{i,2} &= \zeta_{i,3} \\
\dot{\zeta}_{i,3} &= L_f^3 q_1(r_i) + \sum_{j=1}^3 L_{g_j} L_f^2 q_1(r_i) \\
\dot{\zeta}_{i,4} &= \zeta_{i,5} \\
\dot{\zeta}_{i,5} &= \zeta_{i,6} \\
\dot{\zeta}_{i,6} &= L_f^3 q_2(r_i) + \sum_{j=1}^3 L_{g_j} L_f^2 q_2(r_i) \\
\dot{\zeta}_{i,7} &= \zeta_{i,8} \\
\dot{\zeta}_{i,8} &= \zeta_{i,9} \\
\dot{\zeta}_{i,9} &= L_f^3 q_3(r_i) + \sum_{j=1}^3 L_{g_j} L_f^2 q_3(r_i)
\end{aligned} \tag{B.9}$$

Combining the equations for  $\dot{\zeta}_{i,3}$ ,  $\dot{\zeta}_{i,6}$  and  $\dot{\zeta}_{i,9}$ ,

$$\begin{bmatrix} \dot{\zeta}_{i,3} \\ \dot{\zeta}_{i,6} \\ \dot{\zeta}_{i,9} \end{bmatrix} = \begin{bmatrix} L_f^3 q_1(r_i) \\ L_f^3 q_2(r_i) \\ L_f^3 q_3(r_i) \end{bmatrix} + \mathcal{A}(r_i) u_i, \tag{B.10}$$

allows for the selection of linearizing control

$$u_i = \mathcal{A}^{-1}(r_i) \left( \rho_i - \begin{bmatrix} L_f^3 q_1(r_i) \\ L_f^3 q_2(r_i) \\ L_f^3 q_3(r_i) \end{bmatrix} \right). \tag{B.11}$$

Substituting (B.11) into (B.10), allows us to rewrite (B.9) as

$$\dot{\zeta}_i = \begin{bmatrix} \bar{A} & 0 & 0 \\ 0 & \bar{A} & 0 \\ 0 & 0 & \bar{A} \end{bmatrix} \zeta_i + \begin{bmatrix} \bar{B} & 0 & 0 \\ 0 & \bar{B} & 0 \\ 0 & 0 & \bar{B} \end{bmatrix} \rho_i, \tag{B.12}$$

where

$$\bar{A} = \begin{bmatrix} 0 & 1 & 0 \\ 0 & 0 & 1 \\ 0 & 0 & 0 \end{bmatrix}, \quad \bar{B} = \begin{bmatrix} 0 \\ 0 \\ 1 \end{bmatrix}, \quad (\text{B.13})$$

generating a linear map from the agent's virtual control  $\rho_i$  to its 3D position.

The estimated position of the moving target is fed into a feedback linearization control strategy to drive each agent to its desired position. The desired state for agent  $i$  can be obtained from its estimate of target's state:

$$p_i^\star = \hat{p}_i + d_i \quad (\text{B.14})$$

$$v_i^\star = \|\hat{p}_i\| \quad (\text{B.15})$$

$$\phi_i^\star = \tan^{-1} \left( \frac{\hat{p}_i^y}{\hat{p}_i^x} \right) \quad (\text{B.16})$$

$$\gamma_i^\star = \sin^{-1} \left( \frac{\hat{p}_i^z}{\|\hat{p}_i\|} \right) \quad (\text{B.17})$$

$$(\text{B.18})$$

where  $d_i$  is a constant vector that defines the position of agent  $i$  relative to the target. Additionally, since the model used for estimation is that of a point particle moving in space, we assume that the target follows a straight line, and set  $a_i^\star = \omega_{i,\phi}^\star = \omega_{i,\gamma}^\star = 0$ . In order to drive the transformed state of agent  $i$ ,  $\zeta_i$ , to its desired value  $\zeta_i^\star = T(r_i^\star)$ , we can design a gain matrix  $K$ , such that

$$\begin{bmatrix} \bar{A} & 0 & 0 \\ 0 & \bar{A} & 0 \\ 0 & 0 & \bar{A} \end{bmatrix} - \begin{bmatrix} \bar{B} & 0 & 0 \\ 0 & \bar{B} & 0 \\ 0 & 0 & \bar{B} \end{bmatrix} K$$

is stable, driving  $\zeta_i$  to  $\zeta_i^\star$ , and therefore driving agent  $i$  to its desired location.

## APPENDIX C

### SUPPLEMENTAL RESULTS FOR THE DISTRIBUTED KALMAN FILTER

In this appendix, we provide the proofs for Lemma 5.2.3, the derivation for the sub-optimal filtering gains in (5.8), and show that the results in Chapter 5 hold when the order of the filtering steps is reversed.

#### C.1 Proof of Lemma 5.2.3

**Remark C.1.1 (From [29])** *Given a set of  $N$  nonnegative scalars  $s_i$  summing up to one, a set of  $N$  vectors  $x_i$ , and a set of  $N$  matrices  $A_i$ , the following holds*

$$\left( \sum_{i=1}^N s_i A_i x_i \right) \left( \sum_{i=1}^N s_i A_i x_i \right)' \leq \sum_{i=1}^N s_i A_i x_i x_i' A_i'.$$

For the noise-free case, the matrix  $\Xi_i(k+1)$  can be explicitly written as

$$\begin{aligned} \Xi_i(k+1) = & \left( (A - L_i C_i) \sum_{j=1}^N w_{ij} \epsilon_j \right) \times \\ & \left( (A - L_i C_i) \sum_{j=1}^N w_{ij} \epsilon_j \right)'. \end{aligned}$$

Using Remark C.1.1, it follows that

$$\Xi_i(k+1) \leq (A - L_i C_i) \sum_{j=1}^N w_{ij} \Xi_j(k) (A - L_i C_i)'.$$

Defining  $\Xi(k) \in \mathbb{H}^{n_0}$ , with  $\Xi_i(k)$  shown above, we have

$$\Xi(k+1) \leq \mathcal{L}(\Xi(k))$$

with  $\Gamma_i = (A - L_i C_i)$ , and the first statement can then be proved by induction.

The second statement can be proved in a similar manner. Since the noises have zero mean and are independent with respect to themselves and  $x(0)$ , using Remark C.1.1 it can be checked that

$$\begin{aligned}\Sigma_i(k+1) &= E \left\{ \epsilon_i(k+1) \epsilon_i(k+1)' \right\} \\ &\leq \mathcal{L}_i(\Sigma(k)) + Q + L_i R_i L_i',\end{aligned}$$

with  $\Sigma(k) = (\Sigma_1(k), \dots, \Sigma_N(k)) \in \mathbb{H}^{n+}$  and  $\Gamma_i = (A - L_i C_i)$ . The second statement can then be proved by induction.

## C.2 Sub-optimal Filtering Gains

From Lemma 5.2.3, it immediately follows that

$$J(k) \leq \bar{J}(k)$$

where  $J(k)$  is defined in (5.6), and  $\bar{J}(k)$  is defined as

$$\bar{J}(k) = \sum_{t=0}^k \sum_{i=1}^N \text{tr}(P_i(k)), \quad (\text{C.1})$$

with  $P_i(k)$  defined in (5.15). In what follows, we will show that the optimal cost  $\bar{J}^*(k)$  is obtained using the gains

$$L_i^*(k) = A \mathcal{E}_i(P^*(k)) C_i' (R_i + C_i \mathcal{E}_i(P^*(k)) C_i')^{-1}, \quad (\text{C.2})$$

with  $P^*(0) = \Sigma(0)$ , and  $P^*(k) \in \mathbb{H}^{n+}$  is computed using (5.15) with the gains  $L_i^*(k)$ .

Let  $\bar{J}(k)$  denote the cost when an arbitrary set of gains  $L_i(k)$  is used, and let  $P(k) \in \mathbb{H}^{n+}$  denote the matrices obtained when these arbitrary gains are used in (5.15).

To show the desired result, we need to show that

$$\bar{J}(k) - \bar{J}^*(k) = \sum_{t=0}^k \sum_{i=1}^N \text{tr}(P_i(k) - P_i^*(k)) \geq 0$$

We do that by induction, and assuming  $P(k) \geq P^*(k)$  for  $k \geq 0$ . It can be shown through matrix manipulation (see [30]) that

$$\begin{aligned} P_i^*(k+1) - P_i(k+1) &= (A - L_i^* C_i) \mathcal{E}_i(P^*(k) - P(k)) (A - L_i^* C_i)' \\ &\quad - (L_i - L_i^*) (R_i + C_i \mathcal{E}_i(P(k)) C_i') (L_i - L_i^*). \end{aligned}$$

Since  $P(k) \geq P^*(k)$  and  $(R_i + C_i \mathcal{E}_i(P(k)) C_i') > 0$ , it immediately follows that  $P_i(k+1) \geq P_i^*(k+1)$  and  $\bar{J}(k) - \bar{J}^*(k) \geq 0$ . Finally, we show that these sub-optimal gains and the matrices  $P^*(k)$  can be computed in the distributed manner as in (5.7)–(5.9). Indeed, substituting  $L_i^*(k)$  in (5.15), and after performing some matrix manipulation, we can write

$$\begin{aligned} P_i^*(k+1) &= A \mathcal{E}_i(P^*(k)) A' + Q - A \mathcal{E}_i(P^*(k)) C_i' \times \\ &\quad (C_i \mathcal{E}_i(P^*(k)) C_i' + R_i)^{-1} C_i \mathcal{E}_i(P^*(k)) A', \end{aligned} \tag{C.3}$$

which is the same expression obtained when substituting (5.7) into (5.8) and (5.9).

### C.3 Reversing Order of Consensus and Filtering Steps

When the order in which the consensus and filtering steps is reversed as in [29], the noise-free estimation error dynamics are given by

$$\epsilon_i(k+1) = \sum_{j=1}^N w_{ij} (A - L_j C_j) \epsilon_j(k). \tag{C.4}$$

First we show that the dynamics in (C.4) are asymptotically stable *iff* the dynamics in (5.5) are asymptotically stable. From (C.4), the network-wide error dynamics can be expressed as

$$\epsilon(k+1) = \mathcal{B}_2 \epsilon(k), \tag{C.5}$$

where  $\mathcal{B}_2 \triangleq (W \otimes I_n) \text{diag}[A - L_i C_i] \in \mathbb{B}(\mathbb{R}^{Nn})$ . Since  $(W \otimes I_n) \in \mathbb{B}(\mathbb{R}^{Nn})$  and  $\text{diag}[A - L_i C_i] \in \mathbb{B}(\mathbb{R}^{Nn})$ , it follows that  $r_\sigma(\mathcal{B}) = r_\sigma(\mathcal{B}_2)$  and (5.11) is asymptotically stable *iff* (C.5) is asymptotically stable.

The notion of S-detectability in Definition 5.2.4 implies that there exist certain gain matrices such that the dynamics of the upper bounds for the noise-free covariances in (5.14) are asymptotically stable. To show that notion holds regardless of the order of the consensus and filtering steps, we need to consider the upper bounds of the noise-free covariances for (C.5). Define the operator  $\mathcal{J}(\cdot) \in \mathbb{B}(\mathbb{H}^n)$  as

$$\mathcal{J}_i(V) \triangleq \sum_{j=1}^N w_{ij} \Gamma_j V_j \Gamma_j' \in \mathbb{B}(\mathbb{R}^n).$$

The upper bound for the noise-free covariances  $\Xi_i(k)$  can be written in a compact form as

$$P(k+1) = \mathcal{J}(P(k)), \quad P(0) = \Xi(0), \quad (\text{C.6})$$

with  $\Gamma_i = (A - L_i C_i)$ .

It has been shown in [30] that  $r_\sigma(\mathcal{J}) = r_\sigma(\mathcal{L})$ . Therefore, the dynamics in (5.14) are asymptotically stable *iff* (C.6) is asymptotically stable, and the notion of S-detectability in Definition 5.2.4 does not depend on the order in which the steps are taken. Furthermore, it has been shown in [30] that the coupled Riccati equations presented in [29], which are used to calculate the sub-optimal filtering gains for this case, converge to a stabilizing solution *iff* the equations in (C.3) converge to a stabilizing solution. Therefore, the necessary conditions we derive in Section 5.2 for the stability of the distributed Kalman filter do not depend on the order of the consensus and filtering steps.

## **BIBLIOGRAPHY**

## BIBLIOGRAPHY

- [1] F. Zhang, “Modeling, design and control of gliding robotic fish,” Ph.D. dissertation, Michigan State University, 2014.
- [2] C. C. Eriksen, T. J. Osse, R. D. Light, T. Wen, T. W. Lehman, P. L. Sabin, J. W. Ballard, and A. M. Chiodi, “Seaglider: A long-range autonomous underwater vehicle for oceanographic research,” *IEEE Journal of Oceanic Engineering*, vol. 26, no. 4, pp. 424–436, 2001.
- [3] D. C. Webb, P. J. Simonetti, and C. P. Jones, “SLOCUM: An underwater glider propelled by environmental energy,” *IEEE Journal of Oceanic Engineering*, vol. 26, no. 4, pp. 447–452, 2001.
- [4] D. W. Welch, G. W. Boehlert, and B. R. Ward, “POST—the Pacific ocean salmon tracking project,” *Oceanologica Acta*, vol. 25, no. 5, pp. 243–253, 2002.
- [5] M. Heupel, J. M. Semmens, and A. Hobday, “Automated acoustic tracking of aquatic animals: scales, design and deployment of listening station arrays,” *Marine and Freshwater Research*, vol. 57, no. 1, pp. 1–13, 2006.
- [6] S. J. Cooke, S. J. Iverson, M. J. Stokesbury, S. G. Hinch, A. T. Fisk, D. L. VanderZwaag, R. Apostle, and F. Whoriskey, “Ocean tracking network Canada: a network approach to addressing critical issues in fisheries and resource management with implications for ocean governance,” *Fisheries*, vol. 36, no. 12, pp. 583–592, 2011.
- [7] C. C. Krueger, C. M. Holbrook, T. R. Binder, C. S. Vandergoot, T. A. Hayden, D. W. Hondorp, N. Nate, K. Paige, S. C. Riley, A. T. Fisk, *et al.*, “Acoustic telemetry observation systems: challenges encountered and overcome in the Laurentian Great Lakes,” *Canadian Journal of Fisheries and Aquatic Sciences*, vol. 75, no. 10, pp. 1755–1763, 2018.
- [8] N. E. Hussey, S. T. Kessel, K. Aarestrup, S. J. Cooke, P. D. Cowley, A. T. Fisk, R. G. Harcourt, K. N. Holland, S. J. Iverson, J. F. Kocik, *et al.*, “Aquatic animal telemetry: a panoramic window into the underwater world,” *Science*, vol. 348, no. 6240, p. 1255642, 2015.
- [9] R. K. O’Dor and M. J. Stokesbury, “The ocean tracking network—adding marine animal movements to the global ocean observing system,” in *Tagging and Tracking of Marine Animals With Electronic Devices*. Springer, 2009, pp. 91–100.
- [10] M. J. Oliver, M. W. Breece, D. E. Haulsee, M. A. Cimino, J. Kohut, D. Aragon, and D. A. Fox, “Factors affecting detection efficiency of mobile telemetry Slocum gliders,” *Animal Biotelemetry*, vol. 5, no. 1, p. 14, 2017.
- [11] M. Cimino, M. Cassen, S. Merrifield, and E. Terrill, “Detection efficiency of acoustic biotelemetry sensors on wave gliders,” *Animal Biotelemetry*, vol. 6, no. 1, p. 16, 2018.

- [12] M. J. Oliver, M. W. Breece, D. A. Fox, D. E. Haulsee, J. T. Kohut, J. Manderson, and T. Savoy, "Shrinking the haystack: using an AUV in an integrated ocean observatory to map Atlantic Sturgeon in the coastal ocean," *Fisheries*, vol. 38, no. 5, pp. 210–216, 2013.
- [13] M. W. Breece, D. A. Fox, K. J. Dunton, M. G. Frisk, A. Jordaan, and M. J. Oliver, "Dynamic seascapes predict the marine occurrence of an endangered species: Atlantic Sturgeon *Acipenser oxyrinchus oxyrinchus*," *Methods in Ecology and Evolution*, vol. 7, no. 6, pp. 725–733, 2016.
- [14] D. Haulsee, M. Breece, D. Miller, B. M. Wetherbee, D. Fox, and M. Oliver, "Habitat selection of a coastal shark species estimated from an autonomous underwater vehicle," *Marine Ecology Progress Series*, vol. 528, pp. 277–288, 2015.
- [15] C. M. Clark, C. Forney, E. Manii, D. Shinzaki, C. Gage, M. Farris, C. G. Lowe, and M. Moline, "Tracking and following a tagged leopard shark with an autonomous underwater vehicle," *Journal of Field Robotics*, vol. 30, no. 3, pp. 309–322, 2013.
- [16] T. M. Grothues, J. Dobarro, J. Ladd, A. Higgs, G. Niezgod, and D. Miller, "Use of a multi-sensored AUV to telemeter tagged atlantic sturgeon and map their spawning habitat in the hudson river, usa," in *2008 IEEE/OES Autonomous Underwater Vehicles*. IEEE, 2008, pp. 1–7.
- [17] R. Carlon, "Tracking tagged fish using a wave glider," in *OCEANS 2015-MTS/IEEE Washington*. IEEE, 2015, pp. 1–5.
- [18] D. Shinzaki, C. Gage, S. Tang, M. Moline, B. Wolfe, C. G. Lowe, and C. Clark, "A multi-AUV system for cooperative tracking and following of leopard sharks," in *2013 IEEE International Conference on Robotics and Automation*. IEEE, 2013, pp. 4153–4158.
- [19] X. Tan, "Autonomous robotic fish as mobile sensor platforms: Challenges and potential solutions," *Marine Technology Society Journal*, vol. 45, no. 4, pp. 31–40, 2011.
- [20] F. Zhang, J. Wang, J. Thon, C. Thon, E. Litchman, and X. Tan, "Gliding robotic fish for mobile sampling of aquatic environments," in *Proceedings of the 11th IEEE International Conference on Networking, Sensing and Control*. IEEE, 2014, pp. 167–172.
- [21] F. Zhang, O. Ennasr, E. Litchman, and X. Tan, "Autonomous sampling of water columns using gliding robotic fish: Algorithms and harmful-algae-sampling experiments," *IEEE Systems Journal*, vol. 10, no. 3, pp. 1271–1281, 2016.
- [22] M. Espinoza, T. J. Farrugia, D. M. Webber, F. Smith, and C. G. Lowe, "Testing a new acoustic telemetry technique to quantify long-term, fine-scale movements of aquatic animals," *Fisheries Research*, vol. 108, no. 2-3, pp. 364–371, 2011.
- [23] D.-H. Shin and T.-K. Sung, "Comparisons of error characteristics between TOA and TDOA positioning," *IEEE Transactions on Aerospace and Electronic Systems*, vol. 38, no. 1, pp. 307–311, 2002.

- [24] R. Olfati-Saber, “Distributed Kalman filtering for sensor networks,” in *2007 46th IEEE Conference on Decision and Control*, Dec 2007, pp. 5492–5498.
- [25] U. A. Khan and A. Jadbabaie, “On the stability and optimality of distributed Kalman filters with finite-time data fusion,” in *Proceedings of the 2011 American Control Conference*, June 2011, pp. 3405–3410.
- [26] S. Park and N. C. Martins, “Design of distributed LTI observers for state omniscience,” *IEEE Transactions on Automatic Control*, vol. 62, no. 2, pp. 561–576, Feb 2017.
- [27] V. Ugrinovskii, “Conditions for detectability in distributed consensus-based observer networks,” *IEEE Transactions on Automatic Control*, vol. 58, no. 10, pp. 2659–2664, 2013.
- [28] A. Mitra and S. Sundaram, “Distributed observers for LTI systems,” *IEEE Transactions on Automatic Control*, vol. 63, no. 11, pp. 3689–3704, Nov 2018.
- [29] I. Matei and J. S. Baras, “Consensus-based linear distributed filtering,” *Automatica*, vol. 48, no. 8, pp. 1776–1782, 2012.
- [30] O. L. V. Costa, M. D. Fragoso, and R. P. Marques, *Discrete-time Markov Jump Linear Systems*. Springer Science & Business Media, 2006.
- [31] D. L. Rudnick, R. E. Davis, C. C. Eriksen, D. M. Fratantoni, and M. J. Perry, “Underwater gliders for ocean research,” *Marine Technology Society Journal*, vol. 38, no. 2, pp. 73–84, 2004.
- [32] E. Garcia, M. A. Jimenez, P. G. De Santos, and M. Armada, “The evolution of robotics research,” *IEEE Robotics & Automation Magazine*, vol. 14, no. 1, pp. 90–103, 2007.
- [33] D. Coleman, M. Castaño, O. Ennasr, and X. Tan, “Backstepping-based trajectory tracking for underwater gliders,” in *ASME 2019 Dynamic Systems and Control Conference*. American Society of Mechanical Engineers Digital Collection, 2019.
- [34] Global Forecast System (GFS), National Oceanic and Atmospheric Administration (NOAA). [Online]. Available: <https://www.ncdc.noaa.gov/data-access/model-data/model-datasets/global-forecast-system-gfs>
- [35] A. Zuur, E. N. Ieno, N. Walker, A. A. Saveliev, and G. M. Smith, *Mixed effects models and extensions in ecology with R*. Springer Science & Business Media, 2009.
- [36] S. N. Wood, “Fast stable restricted maximum likelihood and marginal likelihood estimation of semiparametric generalized linear models,” *Journal of the Royal Statistical Society: Series B (Statistical Methodology)*, vol. 73, no. 1, pp. 3–36, 2011.
- [37] R. C. Team *et al.*, “R: A language and environment for statistical computing,” 2013.
- [38] S. Kessel, S. Cooke, M. Heupel, N. Hussey, C. Simpfendorfer, S. Vagle, and A. Fisk, “A review of detection range testing in aquatic passive acoustic telemetry studies,” *Reviews in Fish Biology and Fisheries*, vol. 24, no. 1, pp. 199–218, 2014.

- [39] S. T. Kessel, N. E. Hussey, D. M. Webber, S. H. Gruber, J. M. Young, M. J. Smale, and A. T. Fisk, "Close proximity detection interference with acoustic telemetry: the importance of considering tag power output in low ambient noise environments," *Animal Biotelemetry*, vol. 3, no. 1, p. 5, 2015.
- [40] J. Chakraborty, G. Ottoy, M. Gelaude, J. P. Goemaere, and L. D. Strycker, "Acoustic localization of unknown sources with wireless sensor nodes," in *Computer and Information Technology (ICCIT), 2014 17th International Conference on*, Dec 2014, pp. 488–493.
- [41] S. Liu, C. Zhang, and Y. Huang, "Research on acoustic source localization using time difference of arrival measurements," in *Measurement, Information and Control (MIC), 2012 International Conference on*, vol. 1, May 2012, pp. 220–224.
- [42] J. Smith and J. Abel, "The spherical interpolation method of source localization," *IEEE Journal of Oceanic Engineering*, vol. 12, no. 1, pp. 246–252, Jan 1987.
- [43] A. Mahajan and M. Walworth, "3D position sensing using the differences in the time-of-flights from a wave source to various receivers," *IEEE Transactions on Robotics and Automation*, vol. 17, no. 1, pp. 91–94, Feb 2001.
- [44] B. Leng and T. Gao, "A passive method of positioning indoor target based on TDOA," in *2014 IEEE International Conference on Signal Processing, Communications and Computing (ICSPCC)*, Aug 2014, pp. 563–566.
- [45] R. Sriram and D. Jalihal, "TDoA based EKF localization for LTE," in *2016 Twenty Second National Conference on Communication (NCC)*, March 2016, pp. 1–6.
- [46] J. Bordoy, P. Hornecker, F. Höflinger, J. Wendeberg, R. Zhang, C. Schindelhauer, and L. Reindl, "Robust tracking of a mobile receiver using unsynchronized time differences of arrival," in *International Conference on Indoor Positioning and Indoor Navigation*, Oct 2013, pp. 1–10.
- [47] W. Meng, L. Xie, and W. Xiao, "Decentralized TDOA sensor pairing in multihop wireless sensor networks," *IEEE Signal Processing Letters*, vol. 20, no. 2, pp. 181–184, Feb 2013.
- [48] —, "Optimal TDOA sensor-pair placement with uncertainty in source location," *IEEE Transactions on Vehicular Technology*, vol. 65, no. 11, pp. 9260–9271, Nov 2016.
- [49] R. Agniel and E. Jury, "Almost sure boundedness of randomly sampled systems," *SIAM Journal on Control*, vol. 9, no. 3, pp. 372–384, 1971.
- [50] T.-J. Tarn and Y. Rasis, "Observers for nonlinear stochastic systems," *Automatic Control, IEEE Transactions on*, vol. 21, no. 4, pp. 441–448, 1976.
- [51] M. Doostmohammadian and U. A. Khan, "On the genericity properties in distributed estimation: Topology design and sensor placement," *IEEE Journal of Selected Topics in Signal Processing*, vol. 7, no. 2, pp. 195–204, April 2013.
- [52] —, "Graph-theoretic distributed inference in social networks," *IEEE Journal of Selected Topics in Signal Processing*, vol. 8, no. 4, pp. 613–623, 2014.

- [53] J.-M. Dion, C. Commault, and J. Van Der Woude, “Generic properties and control of linear structured systems: a survey,” *Automatica*, vol. 39, no. 7, pp. 1125–1144, 2003.
- [54] E. Davison and S. Wang, “Properties and calculation of transmission zeros of linear multi-variable systems,” *Automatica*, vol. 10, no. 6, pp. 643 – 658, 1974.
- [55] A. B. Alexandru, S. Pequito, A. Jadbabaie, and G. J. Pappas, “Decentralized observability with limited communication between sensors,” in *2016 IEEE 55th Conference on Decision and Control (CDC)*, Dec 2016, pp. 885–890.
- [56] K. Reif, S. Günther, E. Yaz, and R. Unbehauen, “Stochastic stability of the discrete-time extended Kalman filter,” *IEEE Transactions on Automatic Control*, vol. 44, no. 4, pp. 714–728, 1999.
- [57] R. E. Kalman and R. S. Bucy, “New results in linear filtering and prediction theory,” *Journal of Basic Engineering*, vol. 83, no. 1, pp. 95–108, 1961.
- [58] L. El Ghaoui, F. Oustry, and M. AitRami, “A cone complementarity linearization algorithm for static output-feedback and related problems,” *IEEE Transactions on Automatic Control*, vol. 42, no. 8, pp. 1171–1176, 1997.
- [59] M. Pajic, S. Sundaram, J. Le Ny, G. J. Pappas, and R. Mangharam, “The wireless control network: Synthesis and robustness,” in *49th IEEE Conference on Decision and Control (CDC)*. IEEE, 2010, pp. 7576–7581.
- [60] I. Matei and J. S. Baras, “A linear distributed filter inspired by the Markovian jump linear system filtering problem,” *Automatica*, vol. 48, no. 8, pp. 1924–1928, 2012.
- [61] M. Mesbahi and M. Egerstedt, *Graph Theoretic Methods in Multiagent Networks*. Princeton University Press, 2010.
- [62] B. Yang and J. Scheuing, “Cramer-Rao bound and optimum sensor array for source localization from time differences of arrival,” in *Acoustics, Speech, and Signal Processing, 2005. Proceedings.(ICASSP’05). IEEE International Conference on*, vol. 4. IEEE, 2005, pp. iv–961.
- [63] Y. T. Chan and K. Ho, “A simple and efficient estimator for hyperbolic location,” *IEEE Transactions on Signal Processing*, vol. 42, no. 8, pp. 1905–1915, 1994.
- [64] E. F. Costa and J. B. Do Val, “On the detectability and observability of discrete-time Markov jump linear systems,” *Systems & Control Letters*, vol. 44, no. 2, pp. 135–145, 2001.
- [65] —, “Weak detectability and the linear-quadratic control problem of discrete-time Markov jump linear systems,” *International Journal of Control*, vol. 75, no. 16-17, pp. 1282–1292, 2002.
- [66] J. B. do Val, J. C. Geromel, and O. L. Costa, “Uncoupled Riccati iterations for the linear quadratic control problem of discrete-time Markov jump linear systems,” *IEEE Transactions on Automatic Control*, vol. 43, no. 12, pp. 1727–1733, 1998.

- [67] E. Gurarie, “Models of movement and migration: from individual tracks to mass dispersal (early draft),” Ph.D. dissertation, University of Washington, 2008.
- [68] X. Zhong and J. R. Hopgood, “Particle filtering for TDOA based acoustic source tracking: Nonconcurrent multiple talkers,” *Signal processing*, vol. 96, pp. 382–394, 2014.
- [69] M. B. Rhudy and Y. Gu, “Online stochastic convergence analysis of the Kalman filter,” *International Journal of Stochastic Analysis*, vol. 2013, 2013.
- [70] Y. Zhang, Y. P. Tian, and Y. Chen, “Distributed filtering based on weighted average strategy in unreliable sensor networks,” in *2015 54th IEEE Conference on Decision and Control (CDC)*, Dec 2015, pp. 6251–6256.